Forschungszentrum Jülich GmbH

Institute of Bio- and Geosciences

Agrosphere (IBG-3)

Modeling the impact of biopores in the soil on root growth and root water uptake

Dissertation

zur Erlangung des Grades

Doktorin der Agrarwissenschaften (Dr. agr.)

der Landwirtschaftlichen Fakultät der

Rheinischen Friedrich-Wilhelms-Universität Bonn

von

Magdalena Landl

aus Schwaz, Österreich

Bonn 2019

Referent: Prof. Dr. Andrea Schnepf
Korreferent: Prof. Dr. Jan Vanderborght
Tag der mündlichen Prüfung: 29.01.2019

Angefertigt mit Genehmigung der Landwirtschaftlichen Fakultät der Universität Bonn

Abstract

Background and Motivation Biopores are tubular shaped cavities in the soil formed by biological activity that enable plant roots to reach water and nutrient reservoirs at greater depths. Especially during prolonged drought periods or when the topsoil is nutrient depleted, biopores play an important role in plant nutrition and can help to reduce the required amount of irrigation and fertilization. Direct measurements of the impact of biopores on root growth, root water and nutrient uptake are difficult. 3D root architecture models can help to systematically investigate the influence of different environmental conditions on root system development, to interpret experimental data and to test hypotheses on root–soil interaction processes on different scales. However, parameterization of such models is challenging due to the large effort of measuring root system traits.

Methods We developed a new model approach for the simulation of root system development in soil with biopores, which is based on the analogy between root growth and water flow in porous media and which determines the direction of root growth as a function of soil penetration resistance. This model approach was implemented into the mechanistic 3D model R-SWMS, which allows the simulation of root growth and water flow in the soil- root continuum. To improve the parameterization of the root growth module, we evaluated distributions of different root architecture traits from 2D root images of various wheat varieties. Using data from a field experiment, we then applied the coupled simulation model to evaluate the impact of biopores on root growth and root water uptake under realistic environmental and soil physical conditions.

Results We tested our new model approach on the single root and the root system scale using data from literature. Root trait analysis allowed us to quantify gravitropism and tortuosity parameters and showed the influence of parameter distribution on root foraging performance. Simulations under field conditions and evaluation with extensive field data confirmed that biopores mitigate transpiration deficits in times of water scarcity by allowing roots to take up water from deeper, less dry soil regions. This benefit

persisted even under the assumption of reduced root water uptake in biopores due to limited root-soil contact.

Conclusions The good agreement between simulated and observed root growth patterns in structured soil confirmed the new model approach for modelling root growth in soils with biopores. 2D image analysis allowed us to systematically and efficiently analyze root system architectures and to identify model parameters. Plot-scale simulations with different scenarios of environmental and soil physical conditions provided new insights into the influence of biopores on plant transpiration.

Zusammenfassung

Hintergrund und Motivation Bioporen sind röhrenförmige Hohlräume im Boden, welche durch abgestorbene Pflanzenwurzeln oder Regenwurmaktivität geformt wurden. Sie werden von Pflanzenwurzeln als Wachstumspfade mit geringem Widerstand genutzt, um Wasser und Nährstoffressourcen in größerer Tiefe zu erreichen. Während Trockenperioden oder bei Nährstoffmangel im Oberboden können Bioporen auf diese Weise dazu beitragen, den Bedarf an Bewässerung und Düngemitteln kleinzuhalten. Aufgrund der Schwierigkeit direkter Messungen des Einflusses von Bioporen auf Wurzelentwicklung verwenden wir Simulationsmodelle, welche dabei helfen, experimentelle Messungen zu interpretieren, den Einfluss unterschiedlicher Umweltbedingungen auf Wurzelentwicklung zu untersuchen sowie das Prozessverständnis von Wechselwirkungen zwischen Wurzel und Boden zu testen. Die Parametrisierung solcher Modelle ist jedoch eine Herausforderung, weil die Messung von Wurzelarchitekturmerkmalen sehr aufwändig ist.

Methoden Wir entwickelten einen neuen Modellansatz zur Simulation von Wurzelentwicklung in Boden mit Bioporen, welcher auf der Analogie zwischen Wurzelwachstum und Wasserfluss im Boden basiert und welcher die Wachstumsrichtung der Wurzeln in Abhängigkeit von Bodenfestigkeit bestimmt. Dieser Modellansatz wurde in das mechanistische, 3-dimensionale Boden-Wurzel-Modell R-SWMS implementiert. Um die Parametrisierung des Wurzelwachstumsmoduls zu verbessern, evaluierten wir Verteilungen unterschiedlicher Wurzelarchitekturmerkmale mithilfe von 2D-Wurzelbildern verschiedener Weizensorten. Im Anschluss verwendeten wir das gekoppelte Simulationsmodell, um mithilfe von experimentellen Felddaten den Einfluss von Bioporen auf Wurzelwachstum sowie Wurzelwasseraufnahme unter realistischen Boden- und Klimabedingungen zu analysieren.

Ergebnisse Wir testeten unseren neuen Modellansatz mithilfe von Literaturdaten zu Einzelwurzel- und Topfexperimenten. Die Analyse der Wurzelarchitekturmerkmale ermöglichte es uns, Parameter zur Beschreibung von Gravitropismus und Tortuosität zu bestimmen und zeigte den Einfluss der Parameterverteilung auf das Nährstoffaufnahmepotential der Wurzel. Simulationen unter Feldbedingungen bestätigten, dass Bioporen im Fall von Trockenheit Transpirationsdefizite lindern können, indem sie Wurzelwasseraufnahme aus weniger trockenen Bodenregionen ermöglichen. Dieser

positive Effekt war sogar unter Annahme verminderter Wurzelwasseraufnahme aufgrund von verringertem Wurzel-Boden-Kontakt in Bioporen klar erkennbar.

Schlussfolgerungen Die gute Übereinstimmung zwischen simulierten und beobachteten Wurzelsystemen bestätigte die Tauglichkeit unseres neuen Modellansatzes Wurzelwachstum in Boden mit Bioporen zu modellieren. 2D-Bildanalyse erwies sich als geeignete Methode, um Wurzelarchitekturen systematisch und effizient zu analysieren sowie Wurzelparameter zu identifizieren. Simulationen im Parzellenmaßstab mit unterschiedlichen Boden- und Klimaszenarien lieferten neue Erkenntnisse zum Einfluss von Bioporen auf die Transpiration von Pflanzen.

Table of Contents

List of Abbreviations

α	Azimuth angle of a root segment	-
α	Inverse of air entry suction	L^{-1}
BBCH-scale	Plant development scale according to "Biologische Bundesanstalt, Bundessortenamt und Chemische Industrie"	
BP	Biopore	
β	Polar angle of a root segment	-
CT	Computed tomography	
γ	Deflection angle of the azimuth of a root segment	-
d	Root tip movement vector	-
dl	Length of a root segment	L
DA	Degree of anisotropy	-
DAS	Days after sowing	
D_e	Diffusion coefficient of a solute in soil	$L^2 T^{-1}$
DWD	German weather service	
δ	Deflection angle of the polar angle of a root segment	-
E_r	Root elongation rate	$L T^{-1}$
ET_0	Potential evapotranspiration	$L T^{-1}$
fp	Focus parameter	
F	Driving force that influences root growth direction	
HC	Hydraulic conductivity	
ibd	Inter-branch distance	L
IRC	Inter-root competition	

ISSR	International society of root research	
k	Soil mechanical conductance	P^{-1}
k	Constant that governs the radiation extinction by the canopy	-
k_c	Crop coefficient	-
k_{comp}	Compensatory rot water uptake	$L^3P^{-1}T^{-1}$
k_{rs}	Equivalent conductance of the root system	$L^3P^{-1}T^{-1}$
k_{macro}	Conductance in the macropore	P^{-1}
K	Unsaturated hydraulic conductivity	LT^{-1}
K_s	Saturated hydraulic conductivity	LT^{-1}
LAI	Leaf area index	-
m	Shape parameter of the van Genuchten equation	-
MP	Macropore	
M_{rot}	Rotation matrix	
μ	Mean value	
n	Shape parameter of the van Genuchten equation	-
ψ	Soil water potential (matric and gravitational)	P
Ψ_{col}	Water potential at the root collar	P
Ψ_{lim}	Threshold water potential	P
ψ_m	Soil matric potential	P
$\Psi_{s,\,eq}$	Equivalent soil water potential sensed by the plant	P
r	Root radius	L
rRSME	Relative root mean square error	-
R	Soil penetration resistance	P

R	Correlation coefficient	-
R_{rhiz}	Radius of the rhizosphere	L
RLD	Root length density	$L\ L^{-3}$
R^2	Coefficient of determination	-
ρ_b	Bulk density	$M\ L^{-3}$
sg	Sensitivity to gravitropism	-
std	Standard deviation	
S	Sink term	$L^3\ L^{-3}\ T^{-1}$
S_e	Effective saturation	-
SE_{est}	Standard error of the estimate	
SSF	Standard sink fraction	-
SWP	Soil water potential	
σ	Unit standard deviation of the random deflection angle (tortuosity)	-
t	Time	T
T_{act}	Actual transpiration rate from the root collar	$L^3\ T^{-1}$
T_{pot}	Potential transpiration rate from the root collar	$L^3\ T^{-1}$
θ	Branching angle in the vertical plane	-
θ	Volumetric water content	$L^3\ L^{-3}$
θ_r	Residual volumetric water content	$L^3\ L^{-3}$
θ_s	Saturated volumetric water content	$L^3\ L^{-3}$
zSSF	Mean depth of the standard sink fraction	L

Chapter I

General Introduction

Water shortage is one of the primary factors limiting global crop production and will become an even more serious problem with regard to global warming (Alcamo et al. 2017; Schlaepfer et al. 2017). The ability of plants to take up water from the soil is strongly connected to root system architecture, whose development is determined by both genetic and environmental factors (Lynch 2013; Manschadi et al. 2008). Environmental impacts on root system development include different physical, biological and chemical factors, among which soil compaction is of particular significance (Bengough et al. 2011; Topp 2016). Soil compaction leads to less extended root systems with reduced ability to take up water from deeper soil layers (Chen et al. 2014). A possibility for roots to overcome compact soil layers and to grow into greater depths is the use of biopores as preferential growth pathways (Kautz 2015). Biopores are tubular shaped cavities in the soil originating from biological activity. The importance of biopores for root proliferation in the subsoil has been acknowledged since more than 150 years (Thiel 1865). In recent times, biopores have regained attention as a sustainable measure to improve crop performance in organic agriculture. However, many questions regarding the impact of biopores on crop yield are unanswered and more research is needed (Kautz 2015). The main research challenge is the difficulty to directly measure the influence of biopores on root growth, root water and nutrient uptake. Simulation models that explicitly take into account root system development and root water uptake in three dimensions can thereby help to test hypotheses on root– soil interaction processes on different scales and to interpret experimental results. The development of such a model approach, its parameterization and application is the main focus of this thesis.

1.1. The Root system, the Soil and their Interactions

1.1.1. Root system development

The shape and spatial configuration of a root system is commonly referred to as root architecture (Lynch 1995). Up to a certain extent, root architecture is genetically determined, however, plants can also adjust their root systems to the surrounding environmental conditions to make optimal use of available water and nutrient resources (Malamy 2005). This adjustment is commonly referred to as root plasticity. According to the nomenclature of the International Society of Root Research (ISSR) (Gregory 2008; Zobel and Waisel 2010), root systems are made up of different physiological types of roots, which vary for monocotyledonous (e.g. wheat, maize, rice) and dicotyledonous plants (e.g. pea, beans, lentils) (Fig. 1.1). The first root emerging from the seed is called tap root. Further roots evolving from the hypocotyl respectively the mesocotyl are commonly referred to as basal roots. Monocotyledonous plants (Fig. 1.1b) can furthermore develop shoot-born roots, which emerge from shoot nodes above the radicle and are in some literature sources also called adventitious, nodal or crown roots. Lateral roots of varying orders are produced by all these different root types. Environmental stress factors that affect the development of root systems include soil compaction, nutrient and water deficiency, low/high soil temperature, salinity and limited oxygen availability among others (Waisel et al. 2002). Soil compaction is of particular importance, because it directly hampers root elongation and leads to small and shallow root systems (Bengough et al. 2011; Potocka and Szymanowska-Pułka 2018). Such root systems cannot reach subsoil water resources, which is a problem especially in times of drought (Kirkegaard et al. 2007).

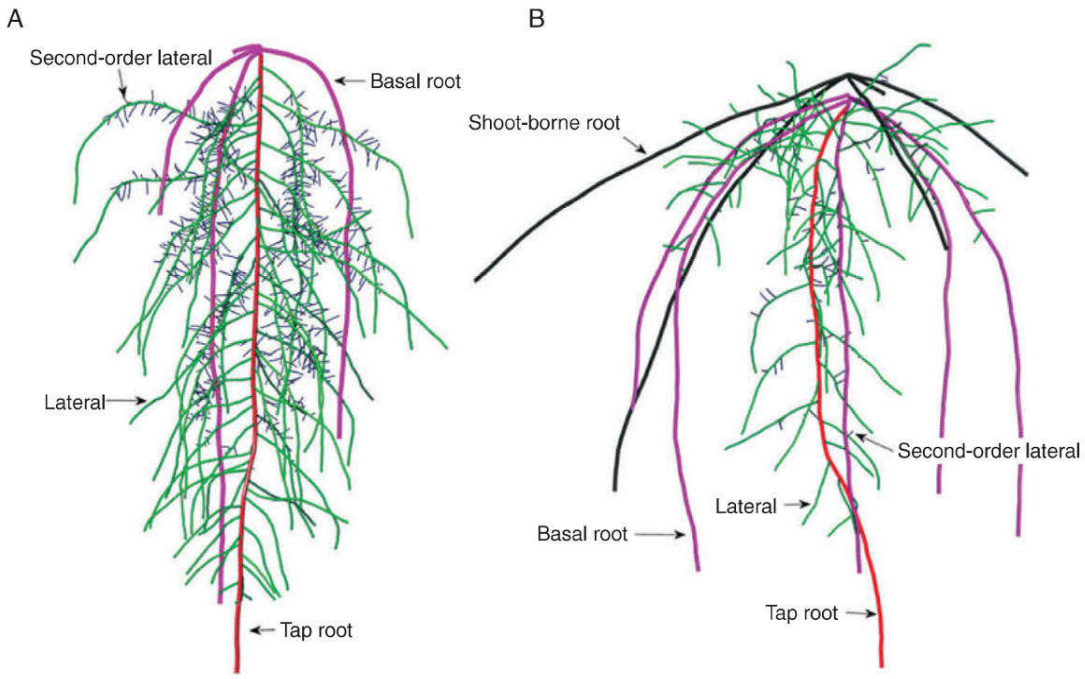

Fig. 1.1: Physiological root types of dicotyledonous and monocotyledonous plants specified according to the ISSR nomenclature; different colors represent different root types [reprint from Schnepf et al. (2018), Figure 2]

1.1.2. Soil – the root growth medium

Soil is an extremely complex growth medium with immense biodiversity and widely differing mineral structure, organic composition and pore space. It serves plants as a source of water and nutrients and provides anchorage. The part of the soil profile affected by plant communities is called the unsaturated or vadose zone, in which water contents are generally less than soil porosity. This unsaturated zone is characterized by large spatial and temporal variations in water content caused by precipitation, evaporation, groundwater recharge and plant water uptake. Water flow in the vadose zone is affected by soil hydraulic properties and is driven by gradients in soil water potential. Soil hydraulic properties describe the relationship between soil water content and soil water potential (expressed by the water retention curve) as well as soil water potential and soil hydraulic conductivity (expressed by the unsaturated conductivity curve). They depend on soil inherent features such as soil texture and bulk

density as well as on external characteristics such as hysteresis effects due to wetting/drying cycles, soil temperature and salinity, which makes them hard to estimate (Durner 1994; Nielsen and Biggar 1986). Two soil characteristics, which strongly impact root growth, are soil penetration resistance and soil pore space. Soil penetration resistance and thus soil compaction is positively correlated with soil bulk density and negatively with soil water potential (Gao et al. 2012; Whalley et al. 2007). Soil porosity typically amounts to 30%-60% of the total soil volume (Hillel 2013). Soil pores are created, destroyed and modified by different natural and artificial soil processes such as shrinkage, swelling and biological activity. Most of the pore space in soils is covered by small-sized pores with diameters <2mm. Macropores with diameters >2mm typically comprise only between 1 and 3% of the total soil volume (Asare et al. 1999). Nevertheless, these macropores play an important role by allowing roots to gain access to water and nutrient resources located in deeper soil horizons (Kautz 2015; McKenzie et al. 2009; White and Kirkegaard 2010). Macropores are furthermore a key component for preferential flow (Wiekenkamp et al. 2016); in this thesis, however, we do not consider this aspect.

1.1.3. Root water uptake

Only about 3% of total plant water uptake is actually used for growth and metabolism. The remaining 97% of absorbed water is lost by transpiration through open stomata in exchange for CO_2 uptake during the process of photosynthesis (Sinha 2004). To obtain sufficient water supply, plants invest a substantial amount of their resources in the development of water uptake and transport tissue (i.a. the root system), which cannot fix CO_2 (Waisel et al. 2002). Water flow from the soil to the atmosphere through the plant is driven by potential gradients. When water evaporates from the cell wall of the leaves, a negative pressure is applied on the water in the wall pores. This capillary suction is transmitted through the wall pores to the xylem conduits and further to the water in the soil. The root system therefore serves as a conduit between soil and atmosphere (Waisel et al. 2002). The flow rate is affected by root hydraulic properties, which differ significantly for different plant species and also depend on root type and root age (Steudle 2000).

1.2. Root system observation techniques

Due to the opaque nature of the soil, observation of root architecture development and measurement of individual root traits still remains a challenge. Over the years, different observation techniques have been developed. The first methods include destructive root excavations as well as hand drawings of excavated root systems in their natural environment (Gregory et al. 1978; Kutschera 1960; Weaver et al. 1922) (Fig. 1.2a). Both techniques allow measuring mature root systems, but are extremely time-consuming when dealing with large root systems and cannot be used to study the temporal dynamics of root systems (Judd et al. 2015). Another well established and simple technique is the use of soil-filled rhizoboxes or rhizotrons, whose transparent front plate allows the observation of dynamic changes of root architecture development (Cahn et al. 1989; Nagel et al. 2012; Nagel et al. 2015) (Fig. 1.2b). While rhizotrons permit non-invasive observation of root system architecture as well as close surveillance of environmental influences, they spatially constrict root growth and guarantee only partial visibility of the root system (Nagel et al. 2012; Nagel et al. 2015; Wenzel et al. 2001). A more recent technique to efficiently analyze root architecture development of large numbers of young plants is represented by roots growing in hydroponics or on germination paper (rhizoslides) (Atkinson et al. 2017; Keller et al. 2015; Le Marié et al. 2014)(Fig. 1.2c). The major limitation of this method is the absence of the soil environment, which makes comparisons with soil-grown roots difficult (Clark et al. 2011; Hargreaves et al. 2009). Novel and promising techniques, which allow the analysis of root architecture development in 3D, are magnetic resonance imaging (MRI) and X-ray computed tomography (CT) (Pohlmeier et al. 2013; Tracy et al. 2015) (Fig. 1.2d). At the moment, however, the application of these techniques is still quite elaborate and can only be used on relatively small and young root systems (Mairhofer et al. 2012; Nagel et al. 2012).

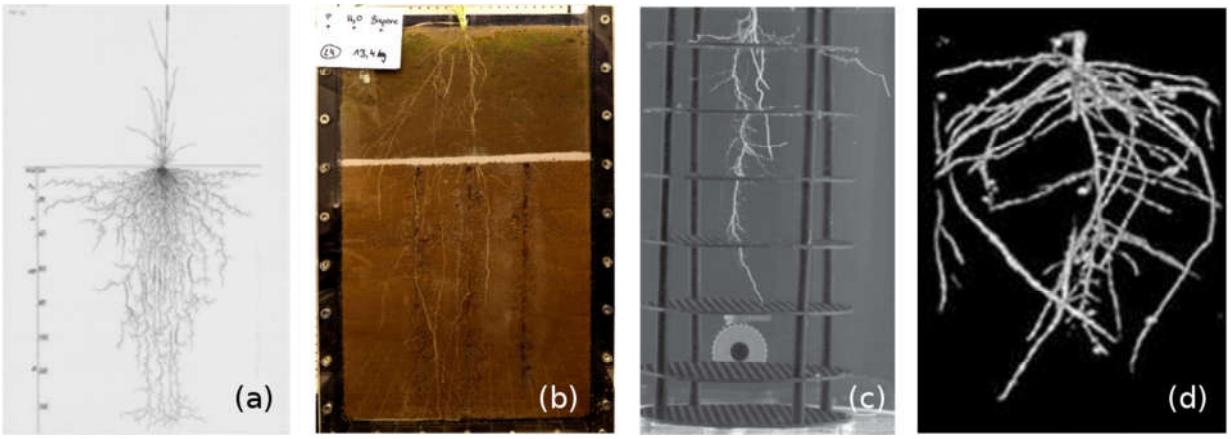

Fig. 1.2: (a) Hand drawing of a wheat root system [reprint from Kutschera and Lichtenegger (2010), Figure 4d], (b) Wheat root system grown in a rhizotron (Bauke et al. 2017), (c) Root system of Azucena Rice grown in hydroponics [reprint from Piñeros et al. (2016), Figure 4d], (d) CT-scan of a bean root system grown in a container [reprint from Koebernick et al. (2015), Figure 2a]

1.3. Mathematical Modeling of the Soil-Root Continuum

1.3.1. Modeling approaches

Simulation models have been used extensively since many years to evaluate the performance of agricultural plants under variable climate conditions and management practices with regard to productivity and profitability (Wang and Smith 2004). For a long time, however, the main focus of these models was the simulation of growth and development of the above-ground part of the plant; influences of root growth and function have either been neglected or taken into account in a very simplified way (Van Keulen and Seligman 1987; Van Laar et al. 1992). The growing interest in the development of more sustainable and resource-efficient farming practices has raised the need to get a better understanding of water and nutrient dynamics in the soil as influenced by plant root systems (Wang and Smith 2004).

Depending on modeling purpose and scale, 1D, 2D, or 3D root architecture models are available. While 1D models can only describe root system variation with depth, 2D and 3D models are able to explicitly represent root system architectures as a complex net of interconnected nodes (Pages et al. 2000). Due to the steady increase in computing power over the last years, a strong focus was put on the evolution of 3D root architecture models. In these models, the dynamic root system development both influences

and is influenced by the surrounding environment (Dunbabin et al. 2013). Such environmental impacts include soil temperature (e.g. Jones et al. (1991)), soil strength (e.g. Clausnitzer and Hopmans (1994)) and soil water and nutrient content (e.g. Somma et al. (1998)), which affect both size and shape of a root system. Significant progress in extending the functionality of 3D root architecture models was made by Doussan et al. (1998), who coupled the root growth model RootTyp (Pages et al. 1989) with the root water uptake model by Alm et al. (1992) to compute water uptake of 3D branched root architectures. This approach was followed up by Javaux et al. (2008) with the model R-SWMS (root-soil water movement and solute transport), which combines the soil water flow model by Šimůnek et al. (2005) with the root growth model by Clausnitzer and Hopmans (1994) and the root water uptake model by Doussan et al. (1998). This structural-functional model approach has been developed further to models that include the above-ground part of the plant (Lobet et al. 2014), root nutrient and carbon allocation (Postma et al. 2017) or rhizosphere gradients around each root segment (Schnepf et al. 2012). Our newly developed simulation model for root growth and root water uptake in soil with biopores (Landl et al. 2017) also ranks alongside these 3D structural-functional models.

1.3.2. 3D root architecture modeling

Most 3D root architecture models use simple rules to describe the development of complex root system architectures (Pagès 2002). It was shown that a limited number of branching rules, which is applied repeatedly in space and time, is sufficient to create a large variety of different root systems (Fitter et al. 1991; Leitner et al. 2010a). In the simplest case, these branching rules include the following processes: (1) root emission from the seed, (2) root branching and development of higher-order roots and (3) root growth. To take into account varying developmental characteristics of individual roots, branching parameters (e.g. root growth speed, inter-branch distance and preferential growth direction) are generally defined separately for different root orders (e.g. Clausnitzer and Hopmans 1994; Postma et al. 2017; Schnepf et al. 2018). Some models, however, (e.g. Pagès et al. (2014)) combine individual branching parameters (e.g. diameter of root tip and elongation rate) to obtain root architecture models that can be parameterized more easily and integrated into larger crop models. Coding principles are similar among the different root architecture models: The root system consists of a multitude of straight root segments. At each root growth time step, a new segment emerges from the tip of a growing branch and moves the root apex to a new position.

1.3.3. Modeling the influence of environmental stress conditions on root system development

Root systems are known for their plasticity towards various environmental influences, which can be of physical, chemical or biological nature (Topp 2016). In 3D root architecture models, this plasticity is considered on the root segment scale, where newly emerging root segments are affected in length and/ or orientation by surrounding environmental conditions. The root growth and soil water flow model R-SWMS, which is used in this thesis, includes empirical functions that account for the effects of soil strength, soil temperature and soil nutrient concentration on root architecture development. We further extended its functionality by considering the deviation from intrinsic root growth direction due to soil penetration resistance anisotropy caused by biopores (Landl et al. 2017).

1.3.4. Modeling soil water flow and root water uptake

In coupled 3D root growth and soil water flow models such as R-SWMS, the soil domain is frequently made up of a regular cubic grid of nodes in which the root system is embedded. The representation of the root system differs for the different simulation models: While explicit models consider root systems as 3D objects (e.g. Leitner et al. (2010b)), implicit models regard them as line sources, which are not physically present in the soil domain (e. g. Javaux et al. (2008)). Each grid node contains information on soil properties as well as temporally variable soil moisture data. Water flow in the soil domain is described by the Richards' equation (Richards 1931), in which temporal variations in soil water content are computed as a function of unsaturated hydraulic conductivity, soil water potential and a sink term that accounts for root water uptake. Root water uptake can be computed at different levels of complexity and dimensionalities, depending on the problem. 1D models (e.g. Jarvis (1989), Feddes et al. (2001)), which compute root water uptake as a function of root length density as well as a depth-dependent stress term that accounts for low soil water availability, are less computationally expensive and are thus often used to simulate root water uptake over longer time periods. 3D models (e.g. Doussan et al. (1998), Roose and Fowler (2004)), which consider 3D branched root architecture and compute water uptake based on pressure differences in root and soil, typically focus on the single plant or single root scale. Another distinction must be made between explicit and implicit 3D root water uptake models: While implicit models assume that root water uptake is equal across the whole root surface and thereby neglect soil moisture heterogeneity in the rhizosphere, explicit models allow visualizing the spatial distribution of water around the root system as well as calculating water fluxes

into the root (Daly et al. 2018). The advantage of 3D models is their ability to consider the effect of lateral variations in root density on root water uptake as well as compensatory root water uptake and soil water redistribution (hydraulic lift) (Couvreur et al. 2014a; Meunier et al. 2017). Couvreur et al. (2012) recently developed a model that combines 3D and 1D approach and represents a promising way to efficiently and accurately solve root water uptake for large root system architectures. The root growth and soil water flow model R-SWMS includes three model approaches of different complexity for the computation of root water uptake: for simple 1D solutions, the approach by Feddes et al. (2001) can be used, for 3D water uptake of simple root systems, the 'hydraulic tree model approach' by Doussan et al. (1998) is available and 3D water uptake of complex root architectures can be tackled with the approach by Couvreur et al. (2012).

1.4. Objectives

The objective of this thesis was to get a better understanding of the influence of biopores on root system development and root water uptake. We firstly aimed to develop a 3D root architecture model, which is capable of reproducing observed root growth patterns in soil with macropores using data from literature as well as from 2D root-images. Our second objective was then to combine the simulation model with extensive experimental field data and evaluate the impact of soil structure on root growth and root water uptake under different soil physical and environmental conditions.

1.4.1. Thesis outline

Chapters 2-4 in this thesis refer to publications that have already been accepted by scientific journals or have been prepared for submission.

The first paper, described in chapter 2, addresses model development. Most 3D root architecture models consider the impact of soil heterogeneities in a simplified way. In these models the gradient of soil mechanical resistance defines the direction of root growth, i.e. roots grow in the direction in which soil resistance decreases most rapidly (Clausnitzer and Hopmans 1994; Pagès et al. 2004). However, using this approach, we were not able to simulate root growth along the macropore wall or to simulate the way that roots appear to 'find' macropores in deeper soil layers and grow into them. We therefore developed a new model approach for the simulation of root growth in structured soil. This alternative

approach is based on the analogy between root growth and water flow in porous media and was implemented into the three-dimensional numerical soil and root water flow model, R-SWMS. We tested the new model approach using data from literature with the aim to reproduce observed root growth patterns in soil with artificial macropores on the single root and on the root system scale. Qualitative and quantitative comparisons between simulated and experimentally observed root systems showed good agreement in the response of root system development to structured soil.

The second paper, which is described in chapter 3, deals with model parameterization. Due to the difficulty of observing and measuring root system traits, the parameterization of 3D root architecture models remains challenging. Root system architecture influences in particular the ability of roots to forage the soil and thus root water and nutrient uptake capacity. A simple method to recover parameters that can be used in 3D root architecture models is the analysis of 2D root images. 2D root images can be obtained from various sources such as drawings (Kutschera and Lichtenegger 2010), rhizotrons (Bauke et al. 2017) or rhizoslides (Atkinson et al. 2017). To facilitate their analysis, automated root tracking systems have been developed (e.g. Delory et al. (2016), Leitner et al. (2014)). In our study, we used 2D wheat root images from various sources to recover the root traits inter-branch distance, branching angle and axial root trajectories, which are three of the main parameters that determine shape and distribution of a root system. We evaluated parameter distributions as well as parameter patterns that were common on the different images. Using simulation studies, we linked the observed root traits with model input parameters, evaluated errors due to the 2D (versus 3D) nature of image sources and investigated the effect of model parameter distributions on root foraging performance.

The third paper, which is described in chapter 4, deals with model application. Direct measurements of the impact of biopores on root growth and root water uptake are difficult. Simulation models that are calibrated with measured field data can thereby help to find relations between experimental measurements and to get a better understanding of the processes governing root growth and root water uptake in soil with biopores. In this study, we combined our previously developed simulation model (chapter II) with data from an extensive experimental field trial. X-ray CT scans of soil columns from the field site were used to create a biopore network that could be integrated into the model soil domain. Spring wheat root architecture as well as water flow in the root-soil continuum were simulated with the 3D numerical R-SWMS model, which was extended to include root growth in structured soil. The model

was calibrated against observed root length densities in both bulk soil and biopores by optimizing root growth model input parameters. By implementing known interactions between root growth and soil penetration resistance into our model, we could simulate root systems whose response to biopores corresponded well to experimental observations described in literature such as increased total root length and increased maximum rooting depth. We found biopores to substantially mitigate transpiration deficits in times of drought by allowing roots to take up water from deeper, less dry soil regions. This effect persisted even under the assumption of reduced root water uptake in biopores due to limited root-soil contact and was stronger for more compact soil and soil with low hydraulic conductivity at low soil water potential[1].

[1] In this thesis, the terms ‘macropore‘ and ‘biopore‘ are both used to describe tubular shaped voids in the soil. Throughout chapter 2, we use the term ‘macropore’ because our model can also be applied on root growth in pores of non-biological origin. In chapter 4, we use the term ‘biopore’ because the biopores in the field originate from earthworms or decayed plant roots.

Chapter II

A new model for root growth in soil with macropores

Based on a journal article published as

Landl M, Huber K, Schnepf A, Vanderborght J, Javaux M, Bengough AG, Vereecken H 2017 A new model for root growth in soil with macropores. Plant and Soil 415: 99-116

2.1. Introduction

Due to high bulk densities in the subsoil, roots preferentially grow in the topsoil layer, where soil penetration resistance is low (Ehlers et al. 1983; Gregory 2008). There is, however, evidence that a significant amount of plant available nutrients as well as water supplies are stored in the subsoil. Especially during drought periods or when the topsoil layer is nutrient depleted these subsoil resources play an important role in plant nutrition and can help to reduce the amount of irrigation water and fertilizer needed (Gaiser et al. 2013; Kautz et al. 2013a; Kirkegaard et al. 2007).

The extent to which plants take up nutrients and water from the subsoil essentially depends on the fraction of roots that are able to penetrate this hard soil layer (Kuhlmann and Baumgärtel 1991). A possibility for roots to gain access to deeper, highly dense soil horizons is to use large sized macropores (diameters > 2 mm) as preferential pathways (Ehlers et al. 1983; Gaiser et al. 2013; McKenzie et al. 2009; Stewart et al. 1999; Stirzaker et al. 1996). The probability of roots to grow in macropores depends on the abundance of pores in the soil (Hatano et al. 1988) and on the penetration resistance of the bulk soil (Hirth et al. 2005). While some studies (Stewart et al. 1999; Stirzaker et al. 1996) observed that significantly more roots encountered macropores than what would be expected if root growth was purely random, others (Dexter 1986; McKenzie et al. 2009) assume that roots locate macropores only by chance. Gaiser et al. (2013) observed that roots use macropores to overcome hard soil layers, but then again re-enter the bulk soil. This is in line with the results by Hirth et al. (2005) who found roots to grow more frequently in macropores when the bulk density is higher. Dexter and Hewitt (1978), Stirzaker et al. (1996) and Hirth et al. (2005) observed that roots tend to grow over a longer distance in macropores that are aligned more vertically. Hatano et al. (1988), Stirzaker et al. (1996) and Valentine et al. (2012) have shown that root elongation in macropores is higher than in the surrounding bulk soil.

Roots do not only use macropores as preferential pathways, but also take up nutrients from the pore walls, which were observed to be rich in nutrients (Athmann et al. 2014). Due to the generally low water content inside macropores when soil is dry (Laloy et al. 2010), root water uptake from the pore walls is vital (White and Kirkegaard 2010). Knowledge about the root – macropore – soil contact is thus essential. Athmann et al. (2013) have shown that the way roots connect to the pore wall depends on the plant genotype. White and Kirkegaard (2010) and Kautz and Köpke (2009) found most roots to grow straight

through the pore and connect to the pore wall by the help of root hairs respectively lateral branches if they do not have direct contact. Athmann et al. (2013) observed that barley roots spiral down in large coils inside the pore wall. Field studies have shown that 85 % of the roots of a barley and oilseed rape crop, which were found in macropores established contact to the pore wall (Athmann et al. 2013).

These plant scale observations converge with our current understanding how environmental stimuli influence root growth. Toyota and Gilroy (2013) physiologically analyzed the mechanisms of gravitropic and mechanical signaling in roots. Shkolnik et al. (2016) state the importance of hydrosensing, where roots grow away from low water potential towards higher water potential. Bao et al. (2014) observed that the formation of lateral roots depends on the availability of water in the vicinity of the root.

The influence of macropores on root growth as well as on root water and nutrient uptake from the subsoil is hard to measure directly. Simulation models that describe root development in structured soils and water and nutrient fluxes in the root zone are therefore useful tools to interpret measurements that provide indirect information about uptake processes, e.g. soil water contents, plant nutrient contents and water and nutrient isotopic profiles in the soil and in the plant. Until now, only few models exist, which include the responses of roots to macropores (Vereecken et al. 2016). Gaiser et al. (2013) modeled the effect of macropores on root development at the plot scale and Jakobsen and Dexter (1986) investigated the influence of macropores on root growth and water uptake in a water balance model. In these model simulations, the amount of roots that grow into macropores was prescribed or parameterized. But how this parameterization changes with changing soil properties (e.g. matric bulk density, amount and orientation of macropores) and root growth parameters (e.g. root growth responses to soil penetration resistance, gravity) cannot be predicted by these models but is required model input. Such predictions require explicit simulation of root growth and development on both the single root and the root system scale.

In recent years, several different simulation models for the description of growing root systems have been developed. While the early models merely focused on the representation of the root system architecture, the later models are more complex and also include the influence of the surrounding soil. Most of these later models (Clausnitzer and Hopmans 1994; Pagès et al. 2004) calculate the rate and direction of root growth as the vector sum of various root segment length and direction-affecting components. Root growth models frequently use the concept of tropisms to represent the influence of

plant physiological properties on the direction of root growth. The gradient of the environmental stimulus that triggers a certain tropism defines the direction in which the root tip will grow. Most root growth models include the influence of gravitropism (Clausnitzer and Hopmans 1994; Leitner et al. 2010a; Pagès et al. 2004) and some also take into account chemotropism and hydrotropism (Leitner et al. 2010a; Tsutsumi et al. 2003). The effect of soil heterogeneities on the direction of root growth is typically implemented similarly to the concept of tropisms: The gradient of soil mechanical resistance defines the direction of root growth, i.e. roots grow in the direction in which the soil resistance decreases most rapidly (Clausnitzer and Hopmans 1994; Pagès et al. 2004). The influence of soil mechanical resistance on the root growth direction is controlled by a sensitivity factor. However, using this 'tropism approach', we were not able to simulate root growth along the macropore wall or to simulate the way that roots appear to 'find' macropores in deeper soil layers and grow into them. Whilst the approach is logical and attractive in simulating root growth in bulk soil, it needs to be modified to enable the simulation of root growth in, along, and out of macropores. This is primarily due to large gradients in strength, geometry, and matric potential that change rapidly adjacent to macropore walls. Therefore, a more mechanistic description of root growth to determine the root growth direction seems necessary.

This study presents a new method for computing root growth in soils with macropores. It distinguishes between the driving forces for root growth and anisotropy of soil strength, which is similar to the description of water flow in a soil with anisotropic hydraulic conductivity. The new 'anisotropy approach' is illustrated by the simulation of an experimental study by Stirzaker et al. (1996) on root growth in artificial macropores. Experimental and simulation results using both the tropism and anisotropy approach to model changes in root growth direction are compared visually and quantitatively. The potential of the anisotropy approach to simulate the effects of different macropore inclination angles, bulk soil penetration resistances, and gravitropism on root growth in structured soil are demonstrated by comparing simulation results with experimental data from Hirth et al. (2005). To evaluate its performance on root growth in a multi – layered soil domain containing macropores, we carried out a simulation study that was inspired by an experimental study by Dexter (1986).

2.2. Material and Methods

2.2.1. Model description

In our new approach, we draw an analogy between the movement of a root tip and water flow in porous media (Bear 2013). The root tip is pushed by a root inherent driving force into the soil. The direction of this driving force depends on the direction of the previous root segment and on a gravitational component that is directed downwards. This driving force is counteracted by soil mechanical forces and friction. If the friction force depends on the direction of the movement, i.e. when the friction or soil resistance is anisotropic, the movement of the root tip will deviate from the direction of the driving force.

In analogy with soil water flow, the direction of the root tip movement corresponds to the water flux vector, while the driving force represents the gradient of the water potential. Soil mechanical forces can be seen as the viscous friction forces that counteract water flow and thus the driving force. In the Darcy equation, the effect of these viscous forces on energy dissipation is represented by the hydraulic conductance tensor, which may show anisotropy. Analogous to the Darcy flow equation, we express the movement of the root tip by the following equation:

$$\mathrm{d} = \mathrm{k} \cdot \mathrm{F}, \tag{2.1}$$

where d is the root tip movement vector, k is the soil mechanical conductance tensor that represents the ease with which the root can penetrate the soil and F is the driving force that influences the root growth direction.

The soil mechanical conductance tensor k is a symmetric, second rank tensor with nine entry values defining conductances in the three principal directions:

$$\mathrm{k} = \begin{pmatrix} \mathrm{k_{xx}} & \mathrm{k_{xy}} & \mathrm{k_{xz}} \\ \mathrm{k_{yx}} & \mathrm{k_{yy}} & \mathrm{k_{yz}} \\ \mathrm{k_{zx}} & \mathrm{k_{zy}} & \mathrm{k_{zz}} \end{pmatrix}. \tag{2.2}$$

For an isotropic soil domain, where soil penetration resistance, or conductance as its inverse, is uniform in each direction, the conductance tensor k can be reduced to a diagonal matrix in which all diagonal entry values are identical. The direction of movement of the root tip then merely depends on the driving force. The simplest example of soil heterogeneity is a stratified soil domain where each layer has a different conductance. In accordance with soil hydraulic conductivity, the soil mechanical conductance in direction of the soil layering equals the arithmetic mean whereas the conductance perpendicular to the soil layering is equal to the harmonic mean of the individual soil layer conductances. If the direction of the soil layers, i.e. the axis of anisotropy, coincides with one of the axes of the Cartesian coordinate system, the conductance tensor is a diagonal matrix with three different entry values. If the layering or the axes of anisotropy are not aligned with the Cartesian coordinate system, the conductance tensor k is fully occupied with nine entry values. In an anisotropic medium, the root tip movement deviates from the direction of the driving force and is oriented towards the axis of anisotropy in which the conductance is largest and resistance is smallest. Anisotropy in the soil domain can be caused by macropores, soil aggregation or differently compacted soil layers. Furthermore, local differences in soil water content e.g. due to root water uptake, also lead to anisotropy and affect the direction of root growth. Unlike the approaches by Clausnitzer and Hopmans (1994) and Pagès et al. (2004), no sensitivity factor is needed to weigh the influence of penetration resistance on the root growth direction.

The driving force F could comprise several factors. We chose here the direction vector of the previous root segment and gravitropism. The direction of the previous root segment is expressed by the azimuth angle α and the polar angle β. To account for small scale variations in the soil matrix and to represent a random behavior of the root tip, random deflection angles γ and δ are added to α and β (Fig. 2.1).

$$F = \begin{pmatrix} dx_{(\alpha,\beta,\gamma,\delta)} \\ dy_{(\alpha,\beta\gamma,\delta)} \\ dz_{(\alpha,\beta\gamma,\delta)} \end{pmatrix} + sg \begin{pmatrix} 0 \\ 0 \\ -1 \end{pmatrix}; \tag{2.3}$$

While the first term on the right hand side of equation (2.3) represents the previous growth direction vector of F, the second term expresses the gravitropism component with sg as gravitropism sensitivity factor.

While the deflection of the azimuth angle γ is a uniformly distributed random angle between [0 2π], the deflection of the polar δ is a normally distributed random angle with mean zero and standard deviation σ_{dl}, which is calculated following the approach by Leitner et al. (2010a). The standard deviation σ_{dl} is derived from the user defined unit standard deviation σ of a root segment of 1 cm length and the maximum root segment length dl, which is reached when soil penetration resistance equals zero. In probability theory, standard deviation decreases by the square root of the number of trials. If 1/dl (segments per cm) is regarded as the number of trials, the standard deviation σ_{dl} (° $cm^{1/2}$) can be given as

$$\sigma_{dl} = \sqrt{dl} \times \sigma. \tag{2.4}$$

In this way, the deflection from the original root tip location does not depend on the spatial resolution of the root growth model. By using the maximum root segment length as normalization factor for the standard deviation of the random deflection angle, we create a dependency between σ_{dl} and soil penetration resistance. In this way, experimental observations of higher root tortuosity in more compact soil (Tracy 2013) are taken into account.

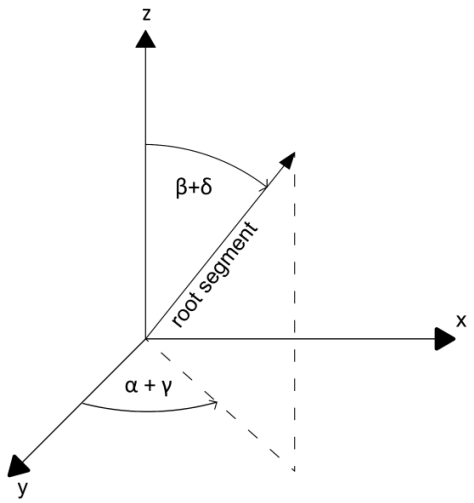

Fig. 2.1: Direction of the root segment expressed by the azimuth angle α with random deflection γ and the polar angle β with random deflection δ

2.2.2. Mathematical formulation of the anisotropy approach to model changes in root growth direction

We implemented our new model approach in the three dimensional numerical R-SWMS model (Javaux et al. 2008). This model couples the root growth model by Clausnitzer and Hopmans (1994) with a model that simulates water flow in the soil domain and in the root system (Doussan et al. 1998; Richards 1931). For the numerical solution of the water flow equation, the soil domain is discretized in a regular cubic grid of nodes. Initial soil hydraulic properties and soil bulk density are user defined input values and given explicitly for each node of the grid. The system of root branches consists of straight root segments. At each root growth time step, a new root segment emerges from the tip of a growing branch and moves the root apex to a new position. Length and orientation of the newly developed root segment are influenced by a soil mechanical conductance tensor and a root inherent driving force (equation (2.1)).

Soil penetration resistance in the bulk soil is calculated for each grid node as a function of soil bulk density, soil water potential and effective saturation using the pedotransfer function developed by Whalley et al. (2007):

$$\log_{10}(R) = 0.35 \times \log_{10}(|\psi_m| \times S_e) + 0.93 \times \rho_b + 1.26, \tag{2.5}$$

where R is the soil penetration resistance (kPa), ψ_m the matric potential (kPa), S_e the effective saturation (-) and ρ_b the soil bulk density (g cm^{-3}). This pedotransfer function is based on the analysis of 12 different soils with varying bulk density and organic carbon, sand, silt and clay contents and can thus be assumed to be valid for a wide range of soils. Soil mechanical conductance k (kPa^{-1}) is then determined as the inverse of soil penetration resistance R:

$$\mathrm{k} = \frac{1}{\mathrm{R}}. \tag{2.6}$$

Soil penetration resistances respectively soil mechanical conductances are specified at each node of a grid cell. We assume that these nodal soil mechanical conductances are direction independent or isotropic properties. The eight nodal conductances of the grid cell in which the root tip is located are used to determine an average or grid cell conductance tensor (equation (2.2)), which is assumed to be

constant within the grid cell. Homogeneous nodal root conductances lead to an isotropic soil mechanical conductance.

In a regular cubic soil grid, macropores are designed in a stepwise structure by arranging grid cells on top or next to each other (Fig. 2.2). For whichever inclination angle of the macropore, the principal axes of anisotropy then either coincide with or stand at an angle of 45 ° to one of the three axes of the Cartesian coordinate system. If macropores are the cause of soil anisotropy, it is thus sufficient to only consider four possible orientations of the axes of anisotropy. Rotating the Cartesian coordinate system by 45° around each one of its main axes gives us three local coordinate systems of anisotropy (Fig. 2.3). For each root tip, we then calculate four different conductance tensors and choose the one for which the contrast between the main axes of anisotropy is largest.

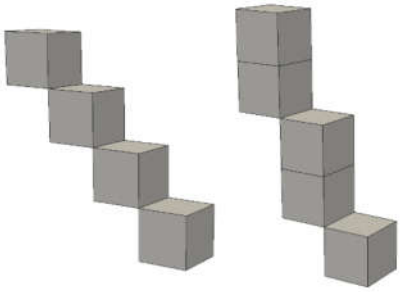

Fig. 2.2: Stepwise structure of a 45 ° and a 60° inclined macropore

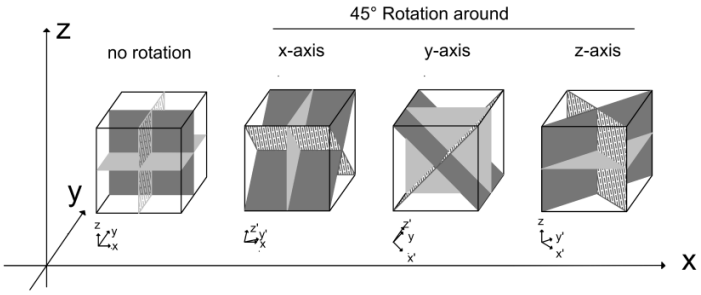

Fig. 2.3: Four local coordinate systems are sufficient to describe all possible main axes of anisotropy in a regular cubic grid. The planes perpendicular to the local coordinate axes are used to divide one cubic soil element in two half-spaces that are used to compute local average conductances (e.g. Fig. 2.5)

In the simplest case where the main axes of anisotropy coincide with the axes of the Cartesian coordinate system, the conductance tensor is calculated as follows: In all three directions of the Cartesian coordinate system, the grid cell is virtually cut into two halves, which are regarded as two separate soil layers with different conductances. The average soil conductance of each half space of one grid cell is calculated as the arithmetic mean of the conductance values of the four corner nodes located within this half (Fig. 2.4, equation (2.7)):

$$\mathrm{kh}_{x1} = \frac{\mathrm{k}_1 + \mathrm{k}_2 + \mathrm{k}_3 + \mathrm{k}_4}{4}. \tag{2.7}$$

Each axis of the Cartesian coordinate system is aligned perpendicular to two half spaces of a grid cell. In line with hydraulic conductivity, the average conductance for each direction is calculated as the harmonic mean of the conductances of two opposing half spaces of a grid cell (Fig. 2.5, equation (2.8)).

$$\mathrm{k}_{xx} = \frac{2}{\frac{1}{\mathrm{kh}_{x1}} + \frac{1}{\mathrm{kh}_{x2}}}. \tag{2.8}$$

In case that the main axes of anisotropy do not coincide with axes of the Cartesian coordinate system, we calculate the average soil conductance for each grid cell half perpendicular to the axes of the rotated coordinate system. The average soil conductance of the half space on either side of a rotated plane is the arithmetic mean of six weighted conductances: While the conductances of the two corner nodes, which lie within one half are given the weight 1, the conductances of the four corner nodes lying on the separating plane between two halves have the weight 0.5. The average conductance for each direction is then once again calculated as the harmonic mean of the conductances of two opposing grid cell halves. Fig. 2.6 and equations (2.9), (2.10) and (2.11) give an example for the calculation of the conductance in y' – direction of the coordinate system that was rotated around the x-axis.

$$k'_{y1} = \frac{k_1 + k_2 + \frac{k_3}{2} + \frac{k_4}{2} + \frac{k_5}{2} + \frac{k_6}{2}}{4}, \tag{2.9}$$

$$k'_{y2} = \frac{k_7 + k_8 + \frac{k_3}{2} + \frac{k_4}{2} + \frac{k_5}{2} + \frac{k_6}{2}}{4}, \tag{2.10}$$

$$\mathrm{k}'_{yy} = \frac{2}{\frac{1}{k_{y'1}} + \frac{1}{k_{y'2}}}, \tag{2.11}$$

where k'_{y1} and k'_{y2} are the average conductances of the rotated halves of a grid cell in y' direction, k_1 to k_8 are the conductance values of the corner nodes of the grid cell and k'_{yy} is the conductance vector of the local coordinate system, which was rotated around the x-axis in y' direction.

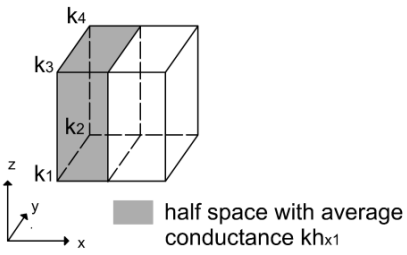

Fig. 2.4: Average conductance of one half space of a grid element perpendicular to the x-axis

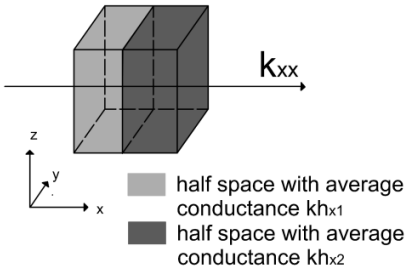

Fig. 2.5: Conductance perpendicular to the conductances of the two half spaces

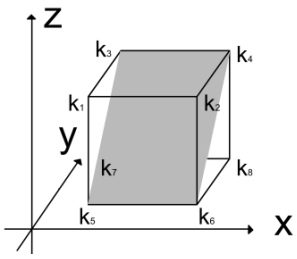

Fig. 2.6: Separating plane between two halves perpendicular to the y'–direction of the local coordinate system which was rotated around the x–axis

The three conductance tensors in their local coordinate systems are then mapped back onto the Cartesian coordinate system by the help of a rotation matrix (equation (2.12)) following the approach by Lust (2001):

$$\mathrm{k} = \mathrm{M}_{\mathrm{rot}} \times \mathrm{k}' \times \mathrm{M}'_{\mathrm{rot}}, \tag{2.12}$$

where k is the conductance tensor in the Cartesian coordinate system, k' is the conductance tensor in the local coordinate system, $\mathrm{M_{rot}}$ is the rotation matrix and $\mathrm{M'_{rot}}$ is the conjugated rotation matrix.

The length of a newly developed root segment is calculated as the product of root elongation rate and a user defined root growth time step. The root elongation rate E_r (cm d^{-1}) is assumed to be a function of soil strength. Bengough et al. (2011) observed that the soil penetration resistance sufficient to stop root elongation completely (R_{max}, kPa) is a function of matric potential (ψ_m, kPa) and can be calculated as

$$R_{max} = 4000 + 2.33 \times |\psi_m|, \tag{2.13}$$

In the bulk soil, R_{max} corresponds approximately to the soil penetration resistance at the permanent wilting point (ψ_m = -1500 kPa).The root elongation rate is assumed to decrease linearly between zero and maximum soil penetration resistance. The actual root elongation rate can thus be calculated based on the fraction of the maximum root elongation rate by

$$E_r = E_{max} \times \left(1 - \frac{R_{eff}}{R_{max}}\right), \tag{2.14}$$

where E_r (cm d^{-1}) is the actual root elongation rate, E_{max} (cm d^{-1}) is the maximum root elongation rate and R_{eff} is the effective soil penetration resistance in the direction of the root tip growth. R_{eff} is by definition the inverse of an effective conductance in the direction of root growth k_{eff}:

$$R_{eff} = \frac{1}{k_{eff}}; \tag{2.15}$$

k_{eff} is a function of both the average conductance of the grid cell and the root inherent growth direction and is calculated as:

$$k_{eff} = \left|\mathrm{k} \times \hat{F}\right|, \tag{2.16}$$

where $\hat{F}$ is the unit length vector of the driving force. In this way, E_r is reduced stronger if the root grows perpendicular to a hard soil layer than if it grows along a hard soil layer. This approach corresponds to

observations by Kolb et al. (2012) who found that radial constrictions applied to roots did not significantly reduce root elongation rates, while axial constrictions did have a significant impact.

2.2.3. Model assumptions for root growth in macropores

In the case of a root growing within a grid cell at the interface between bulk soil and macropore, soil domain and macropore are regarded as two soil regions with different soil mechanical conductances that influence the direction in which the root will grow. The intensity with which a root is forced to grow towards the direction of higher conductance depends on both the conductances in the bulk soil and in the macropore. While the conductance in the bulk soil is calculated as the inverse of soil penetration resistance, the conductance in the macropore (k_{macro}) is unknown. To identify plausible values of k_{macro}, we analyzed the anisotropy of one single grid cell with four bulk soil and four macropore nodes. We define the degree of anisotropy (DA) according to Dal Ferro et al. (2014) as

$$DA = 1 - \frac{k_{perp}}{k_{long}}, \tag{2.17}$$

where k_{perp} and k_{long} are the conductances perpendicular and along the macropore – bulk soil grid cell half spaces (Fig. 2.7). A Da of 0 signifies perfect isotropy, while a DA of 1 represents maximum anisotropy. Fig. 2.8 shows the influence of different parametrizations of k_{macro} on anisotropy for typical minimum and maximum values of soil penetration resistance. Assuming that the conductance in the macropore is much higher than in the bulk soil, anisotropy shall be well above 0. If the degree of anisotropy approaches 1, however, the influence of different soil conductances is no longer perceptible. We therefore assume macropore conductance values of $1e4 \leq k_{macro} \leq 2e5$ kPa^{-1} as most plausible. The conductance in the macropore can be regarded as a sensitivity factor, which influences the probability of a root to continue growing within the macropore or to re-enter the bulk soil.

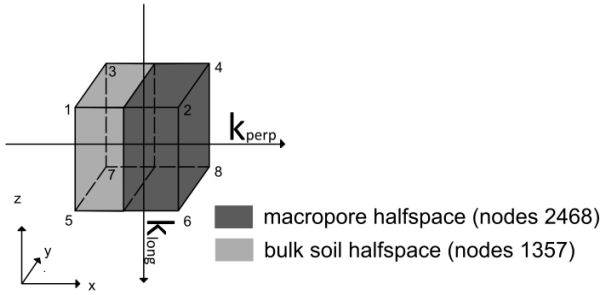

Fig. 2.7: The degree of anisotropy is one minus the ratio between the conductance perpendicular to (k_{perp}) and along (k_{long}) the plane that separates macropore from bulk soil and the bulk soil plane

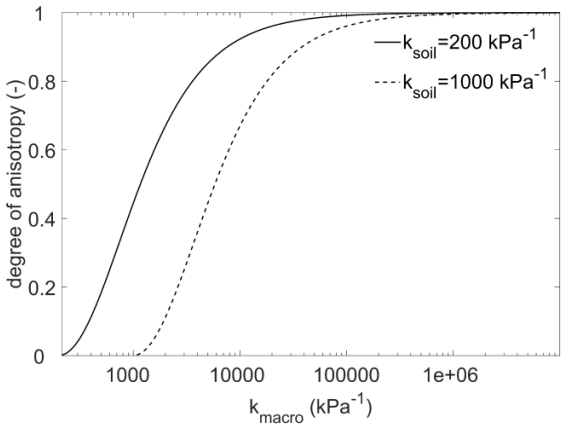

Fig. 2.8: Influence of k_{macro} on the degree of anisotropy for typical minimum and maximum values of k_{soil}

2.2.4. Model setup

Using experimental model setups from literature, we built three simulation scenarios to assess the performance of our new model approach.

Scenario 1: Visual comparison of simulation results with observed root growth patterns in structure soil

For our first simulation scenario, we used an experimental study by Stirzaker et al. (1996) on root growth of barley (*Hordeum vulgare cv.* Yagan) in soil containing macropores at the plant root scale. The setup of the simulation model was designed according to the descriptions by Stirzaker et al. (1996). Undescribed model parameters were either taken from literature or approximated. The soil domain was a rectangular cuboid with a surface area of 8.7 x 8.7 cm^2 and a depth of 20.1 cm, which we discretized to cubic grid elements of 0.1 cm side length. The bulk density of the boundary grid cells of the sides and the base of the soil domain were set to a virtual density of 4 g cm^{-3} in order to simulate the impenetrable pot walls. Eight vertical macropores with a diameter each of 0.4 cm were arranged symmetrically around the center of the soil domain on a circle with a radius of 2.5 cm (Fig. 2.9). We used the soil properties of a

sandy loam (Table 2-1), which was packed to a bulk density of 1.77 g cm^{-3}. We did not consider soil water flow and assumed hydrostatic equilibrium in the soil domain. The simulation runtime was set to 25 days.

The simulated root system consisted of seven axes from which one emerged at day zero, three at day one and three at day three. The initial potential root elongation rate for barley was derived from literature (Materechera et al. 1991) and set to 1.2 cm d^{-1}. Watt et al. (2006) observed the growth rates of roots to decrease with time and branch roots to grow more slowly than their parent axes. We thus reduced the elongation rate for 8 day old first order roots to 0.8 cm d^{-1}. Root images by Stirzaker et al. (1996) show that roots grew in a low angle from the horizontal over the whole width of the pot before they turn downwards (Fig. 2.11a). In order to reproduce these root growth patterns, sensitivity to gravitropism was set to the extremely low value of 0.005 for 1st order roots. Rose (1983) observed roots of higher branching to be less gravitropic. Sensitivity to gravitropism for 2nd and 3rd order roots was thus reduced to 0.001. The root tortuosity as displayed in Fig. 2.11a could be best reproduced with unit standard deviations of the random angle of 45 °. The initial growth angle for axial roots was set to 0 °; the branching angle (relative to the parent roots) to 90 °. Branch spacing was estimated and set to a value of 0.6 days for 1st order roots and 0.4 days for 2nd order roots.

Root water uptake was not considered in the simulations. Soil water potentials were set so that simulated soil penetration resistances matched experimentally measured ones. We chose a whole pot matrix potential of -100 kPa, which resulted in soil penetration resistances of 2500 kPa and corresponded approximately to the experimentally observed values by Stirzaker et al. (1996), which lay between 2000 and 4000 kPa. The complete parameter set is presented in Table 2-2.

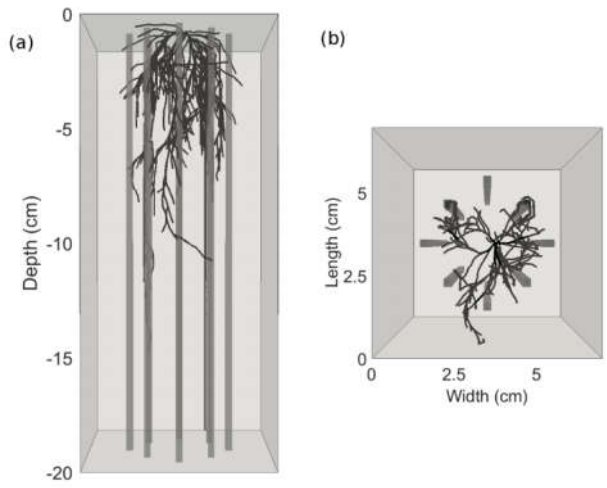

Fig. 2.9: Side (a) and top (b) view of the soil domain with a 25–day old barley root, scenario 1; the bulk soil is displayed in light grey, while the macropores are presented in dark grey and the root in black

Table 2-1: Texture of soils used in the simulation scenarios 1, 2 and 3

Simulation scenario	FAO soil classification	Sand (%)	Silt (%)	Clay (%)
Scenario 1	Sandy loam	74	12	14
Scenario 2 and 3	Silty loam	55.8	26.6	12.3

Table 2-2: Model parametrizations for simulation scenarios 1, 2 and 3

	Geometry of the soil domain					Root growth parameters								Simulation runtime
	L (cm)	W (cm)	D (cm)	ρ_b (g cm^{-3})	ψ_m (kPa)	E_{max} (cm d^{-1})	nbas (-)	basang (°)	brnang (°)	brspac (d^{-1})	σ (°)	sg (-)	k_{macro} (kPa^{-1})	(d)
Scenario1	8.7	8.7	20.1	1.77	-100	1.2 (0.8)	6	0	90	0.6 (0.4)	45	0.005 (0.001)	2x10^5	25
Scenario2	3	1	3	Table 2-3	-5	0.68	-	-	-	-	Table 2-3	Table 2-3	Table 2-3	7
Scenario3	3	3	3	1.25 resp. 3	-15	0.68	-	-	-	-	45	0.05	1x10^5	10

Values in parentheses indicate parametrizations for 2nd and 3rd order roots, *L* Length, *W* Width, *D* Depth, ρ_b bulk density, ψ_m soil matric potential, E_{max} maximum elongation rate, *nbas* number of basal roots, *basang* basal root angle, *brnang* branching angle, *brspac* branch spacing, σ unit standard deviation of the random angle, *sg* sensitivity to gravitropism, k_{macro} conductance in the macropore

Scenario 2: Quantitative comparison of simulation and experimental results on single root growth in inclined macropores

For our second simulation scenario, we used an experimental study by Hirth et al. (2005) on the ability of seedling roots of rye grass (*Lolium perenne L.)* to penetrate the soil from artificial macropores under varying soil bulk densities and macropore inclination angles. The setup of the simulation model was designed according to the descriptions by Hirth et al. (2005). Undescribed model parameters were either taken from literature or approximated. The rectangular-shaped soil domain had a surface area of 3 x 1 cm^2 and a depth of 3 cm, which we discretized to cubic grid cells of 0.1 cm side length. One single macropore with an angle of 40 ° respectively 90 ° was inserted into the soil domain. Macropore and interface had a horizontal cross section area of 0.09 cm^2. The seed (starting point of the root tip) was placed at the edge of the macropore (Fig. 2.10). We used the soil properties of a silty loam with the texture indicated in Table 2-1. The soil was packed to uniform bulk densities of 1.25, 1.38 and 1.50 g cm^{-3}. In accordance with the experimental setup, macropore wall compaction was not considered. Hirth et al. (2005) kept the matric potential in the soil cores at a constant value of -5 kPa by connecting them to 0.5 m hanging columns of water. We therefore assumed that root water uptake does not significantly affect the surrounding soil and performed simulations without root water uptake. We did not consider soil water flow and assumed hydrostatic equilibrium in the soil domain. The simulation runtime was set to 7 days.

The simulation of only one single root without laterals reduced the required input parameters for root growth to potential root elongation rate, sensitivity to gravitropism, unit standard deviation of the random deflection angle and conductance in the macropore. A potential root elongation rate of 0.49 cm d^{-1}, which we assumed to stay constant over time was best suited to reproduce the actual root lengths measured by Hirth et al. (2005). This value is within the range of the standard error of the mean of the potential root elongation rate for seedlings of annual ryegrass (*L.rigidum*) given by Materechera et al. (1991). The remaining root growth parameters were not experimentally determined and thus unknown. To evaluate the influence of different root growth parametrizations, we performed simulations with different combinations of these parameters (see Table 2-3 for chosen parameter values). Altogether, we carried out 576 different simulations, which were the factorial combinations of three bulk densities, two macropore angles and a control soil domain without macropore, four sensitivities to gravitropism (sg),

four unit standard deviations of the random deflection angle (σ) and four conductances in the macropore (k_{macro}). The complete parameter set is presented in Table 2-2.

To obtain representative simulation results of the stochastic process, which is generated by the random deflection angle, we performed 100 replicates of each simulation using different random seed numbers. Experimental results reported by Hirth et al. (2005) represent the average of 24 replicates, but no information of standard deviations was provided.

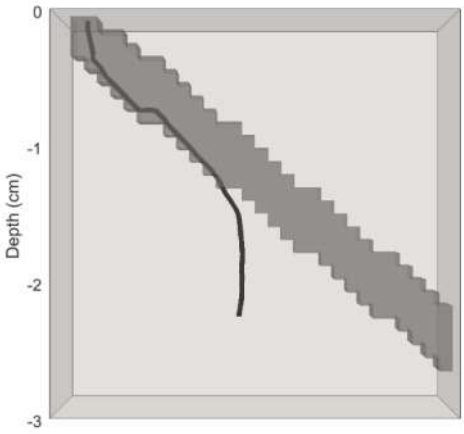

Fig. 2.10: Soil domain, scenario 2; the bulk soil is displayed in light grey, while the macropores are presented in dark grey and the root in black

Table 2-3: Values for different parametrizations of scenario 2

		Root growth parameters		
Inclination angle of the MP (°)	Soil bulk density, ρb (g cm^{-3})	Sensitivity to gravitropism, sg (-)	Unit stdev of the random angle, σ (°)	Conductance in the MP, kmacro (kPa^{-1})
No macropore	1.25	0.005	5	$2x10^4$
40	1.38	0.05	45	$3x10^4$
90	1.50	0.1	90	$5x10^4$
		0.2	180	$8x10^4$

Scenario 3: Virtual simulation experiment on root growth in a compacted subsoil layer that contains macropores

For our third simulation scenario, we carried out a simulation experiment on single root growth in a two-layered soil domain where the compacted subsoil contained macropores. The simulation experiment represents the case of root growth in soil with a plough. The soil domain was a rectangular cuboid of 3 cm side length in each direction, which we discretized to cubic grid cells of 0.1 cm side length. We implemented two different soil layers into this soil cube: a topsoil layer with a bulk density of 1.25 g cm^{-3} in the upper 1.5 cm of the cube and an impenetrable subsoil layer with a bulk density of 3 g cm^{-3} in the lower 1.5 cm of the cube. Additionally, we inserted eight macropores into the compacted subsoil layer. They were aligned symmetrically in a square with a distance of 0.9 cm to the borders of the soil cube (Fig. 2.15). Each macropore was made up of nine grid nodes with macropore properties. We used root growth parameters from the previous example for rye grass (*Lolium perenne L.*) with a sensitivity to gravitropism of 0.05 and a unit standard deviation of the random angle of 45 °. Root water uptake was not included. We did not consider soil water flow and assumed hydrostatic equilibrium in the soil domain. The simulation runtime was set to 10 days. We performed only one simulation. The complete parameter set is presented in Table 2-2.

2.3. Results

2.3.1. Scenario 1: Visual comparison of simulation results with observed root growth patterns in structure soil

We used both the tropism and anisotropy approach in order to simulate the experimental observations by Stirzaker et al. (1996). The quality of the simulation results was evaluated visually by comparing 2D-images of the simulated and the experimental root systems and quantitatively by comparing total root lengths and root length density profiles (RLD profiles).

Both approaches led to simulation results where the roots predominantly did use macropores as preferential growth pathways. The root growth behavior within macropores, however, was different: Using the tropism approach, the roots only slowly grew downwards while spiraling horizontally over the whole cross section of the macropore; using the anisotropy approach, the roots grew straight

downwards along the pore wall, which better captures experimental observations (Fig. 2.11). The simulation results in Fig. 2.11 are displayed in a layout so as to resemble the original figure from Stirzaker et al. (1996). We found a total root length of 750 cm for the simulated root system, which corresponds well to the experimentally observed one of 720 cm.

We determined the RLD profile from the original 2D image from Stirzaker et al. (1996) with the help of the image analysis tool Root System Analyzer (Leitner et al. 2014) and compared it with the RLD profiles of the simulated 3D root systems (Fig. 2.12). It must be noted that the RLD profile obtained from the 2D image from Stirzaker et al. (1996) can only be an approximation of the RLD profile of the real root system due to low image resolution and the two dimensional representation of a three dimensional root system. The RLD profile produced with the anisotropy approach was able to capture the larger root length density in the upper 5 cm of the soil domain, which then decreased sharply. The RLD profile produced with the tropism approach largely overestimated RLD in the upper soil domain, while underestimating it in the lower soil domain. The root length density within macropores (area between the dashed and the solid line) as a percentage of total RLD was similar for the experimental RLD profile (26 %) and the simulated RLD profile produced with the anisotropy approach (21 %).

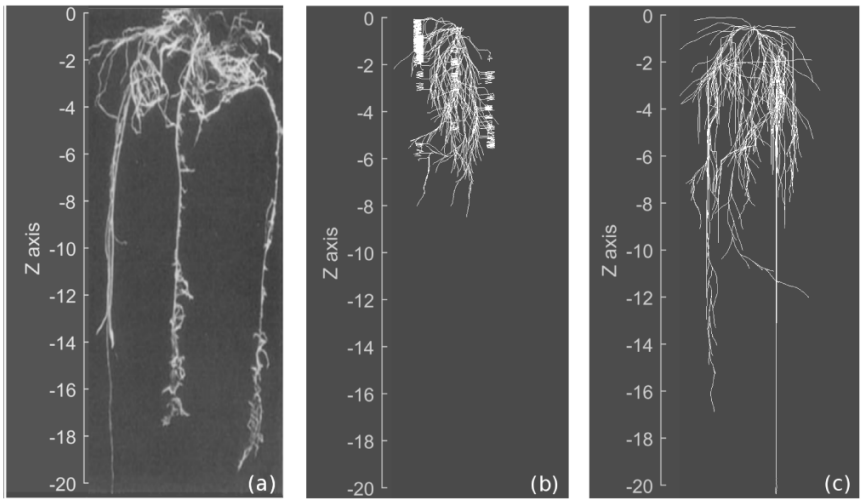

Fig. 2.11: Front view of barley roots growing in dense soil with macropores for 25 days: (a) Experimental results [reprint from Stirzaker et al. (1996), Figure 6c], (b) Simulation results produced with the tropism approach, (c) Simulation results produced with the anisotropy approach

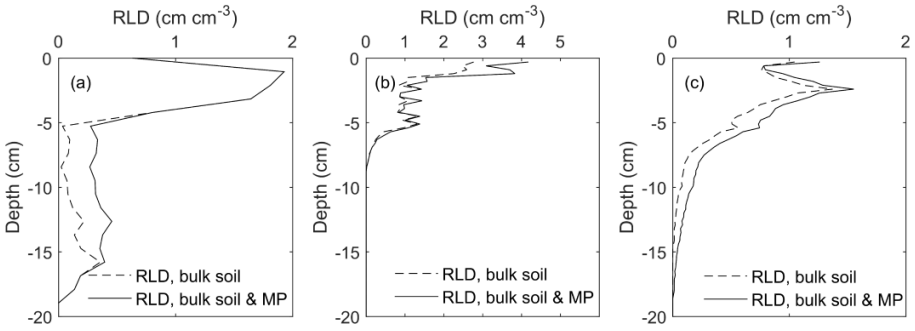

Fig. 2.12: Root length density profiles of barley roots growing in dense soil with macropores for 25 days: (a) RLD profile for original 2D image by Stirzaker et al. (1996), (b) RLD profile for simulated 3D root system produced with the tropism approach, (c) RLD profile for simulated 3D root system produced with the anisotropy approach

2.3.2. Scenario 2: Quantitative comparison of simulation and experimental results on single root growth in inclined macropores

Simulation and experimental results by Hirth et al. (2005) were compared quantitatively. We used the characteristics total root length (cm) and root length fraction that remained within the macropore (%) as a means of comparison between experiment and simulation. The variability of the averaged results of different simulations is caused by different parameter combinations, while the variability of the individual results is the random variation between the 100 replicate simulations.

Influence of different macropore inclination angles and different bulk densities

Fig. 2.13 shows a comparison between the simulation results obtained with a randomly chosen parametrization (sg = 0.05, σ = 45 °, k_{macro} = 8e^4 kPa^{-1}), and the experimental results by Hirth et al. (2005) for a smooth macropore wall. The simulations captured well the experimental observations of increasing root length fractions within the macropore with an increasing macropore inclination angle from the horizontal. In accordance with the experimental observations, different levels of bulk density only had an effect on the roots growing in the 40 ° inclined macropores. Simulations were able to reproduce the experimentally observed increase in root length fractions within the macropore for increasing levels of

bulk density. Due to this increase, total root lengths did not decrease for increasing levels of bulk density. Compared to root growth in a homogeneous soil domain with equal bulk density, the presence of macropores increased total root lengths by 20 % to 40 %.

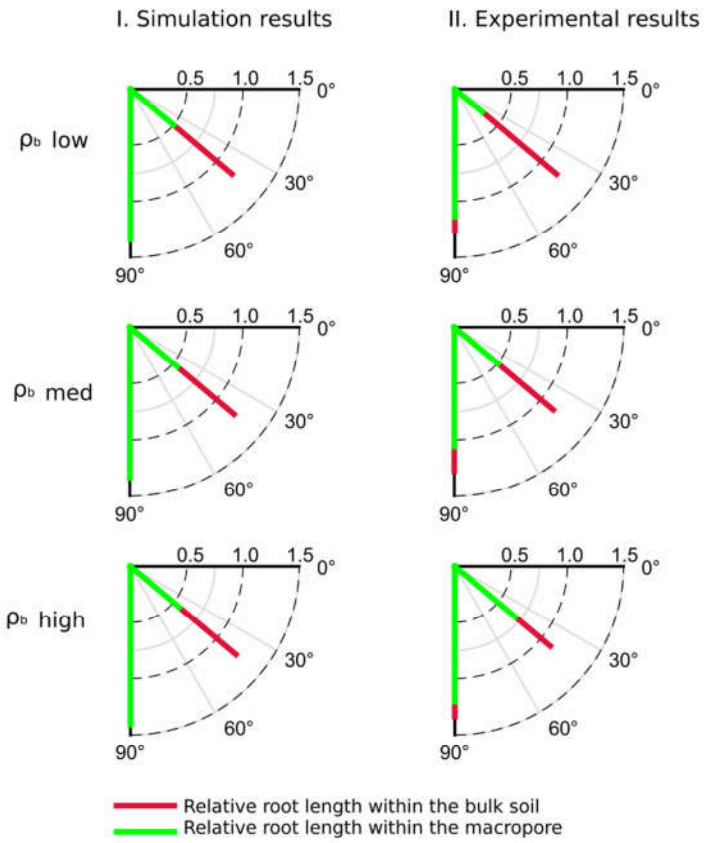

Fig. 2.13: Simulated and experimentally found relative root lengths within macropore and bulk soil; the first column (I) shows the simulation results obtained with a randomly chosen parametrization (sg= 0.05, σ=45 °, k_{macro} = 8e^4 kPa-1), while the second (II) column illustrates the experimental results by Hirth et al. (2005). The different rows show results for different levels of soil bulk density (ρ_b low, ρ_b med, ρ_b high; values are given in Table 2-3). The inclination angles of the colored lines represent the macropore inclination angles (40°, 90°); the different colors indicate the different locations of the root within the soil domain (macropore, bulk soil). The length of the colored lines represents the relative root length which is the total root length normalized with the length of a root growing in a soil domain with equal bulk density, but without macropore. Each line in the first column represents the average of 100 individual

simulations. Each line in the second column represents the average of 24 individual simulations

Quantitative simulation results: 90 °-inclined macropore

In the case of a 90 ° inclined (vertical) macropore, all simulated roots remained within the macropore for all different parameter combinations. They reached average root lengths between 2.8 cm and 3.3 cm and thus grew at 83 % to 98 % of the potential root elongation rate. These results correspond well to the findings by Hirth et al. (2005) who measured average root length fractions in macropores between 83 % and 90 % and total root lengths between 2.9 cm and 3.1 cm.

Quantitative simulation results: 40 °-inclined macropore

In the case of a macropore with 40 ° inclination, the simulated average root length fraction within a macropore reached - depending on the parametrization - values between 18 % and 60 %. Simulated averaged total root lengths ranged from 2.5 cm to 3.0 cm. The root thus grew at 74 % to 89 % of the potential root elongation rate. Hirth et al. (2005) found – depending on the roughness of the macropore walls – root length fractions within macropores between 14 % and 86 % and total root lengths between 1.9 cm and 3.0 cm. Both simulated root length fractions within macropores and total root lengths were thus in acceptable agreement with experimental results.

Influence of different parametrizations on the simulation results of the 40 ° inclined macropore

Fig. 2.14 gives an overview of the influence of different parametrizations (Table 2-3) on simulated root length fractions remaining within a 40 ° inclined macropore. Different parametrizations of bulk density and conductance in the macropore (k_{macro}) were pooled in the parameter 'degree of anisotropy' (Fig. 2.7, equation (2.17)).

To evaluate the influence of different degrees of anisotropy on root length fractions remaining within the macropore, we fitted linear regression lines to the simulation results of each parameter combination. As expected, increasing degrees of anisotropy led to an increase in root length fractions within a macropore for nearly all parameter combinations. The coefficients of determination show that the variability of the simulation results increased both with increasing standard deviations of the random

angle and decreasing sensitivities to gravitropism. For parameter combinations including a sensitivity of gravitropism of 0.005, no regression line could be fitted due to the high variability of the simulation results. There is a trend of increasing root length fractions and decreasing rates of increase both with increasing standard deviations of the random angle and decreasing sensitivities to gravitropism, but the pattern is not consistent. For individual simulations, root length fractions within macropores of up to 100 % could be reached; the maximum value for the intercept of a regression line with a degree of anisotropy of 1, however, was only 50 %.

Influence of the roughness of macropore walls

Hirth et al. (2005) performed experiments with smooth and scarified macropore wall reliefs. They found significant differences in both root length fractions within macropores and total root lengths for the two different treatments. Larger root length fractions remained within the smooth macropore (averaged over all bulk density levels, 68 %) than within the scarified macropore (averaged over all bulk density levels, 38 %). Consequently, total root lengths were larger for roots growing in smooth macropores (on average 2.85 cm) than for roots growing in scarified macropores (on average 2.3 cm). In the simulation model, it is not possible to directly take into account macropore wall roughness. However, the influence of wall roughness can be controlled indirectly via the conductance in the macropore. In the parameterization example from Fig. 2.13, an increase of k_{macro} from $2x10^4$ kPa^{-1} to $8x10^4$ kPa^{-1} led to an increase in the average root length fraction within the macropore from 33 % to 44 % if averaged over all bulk density levels.

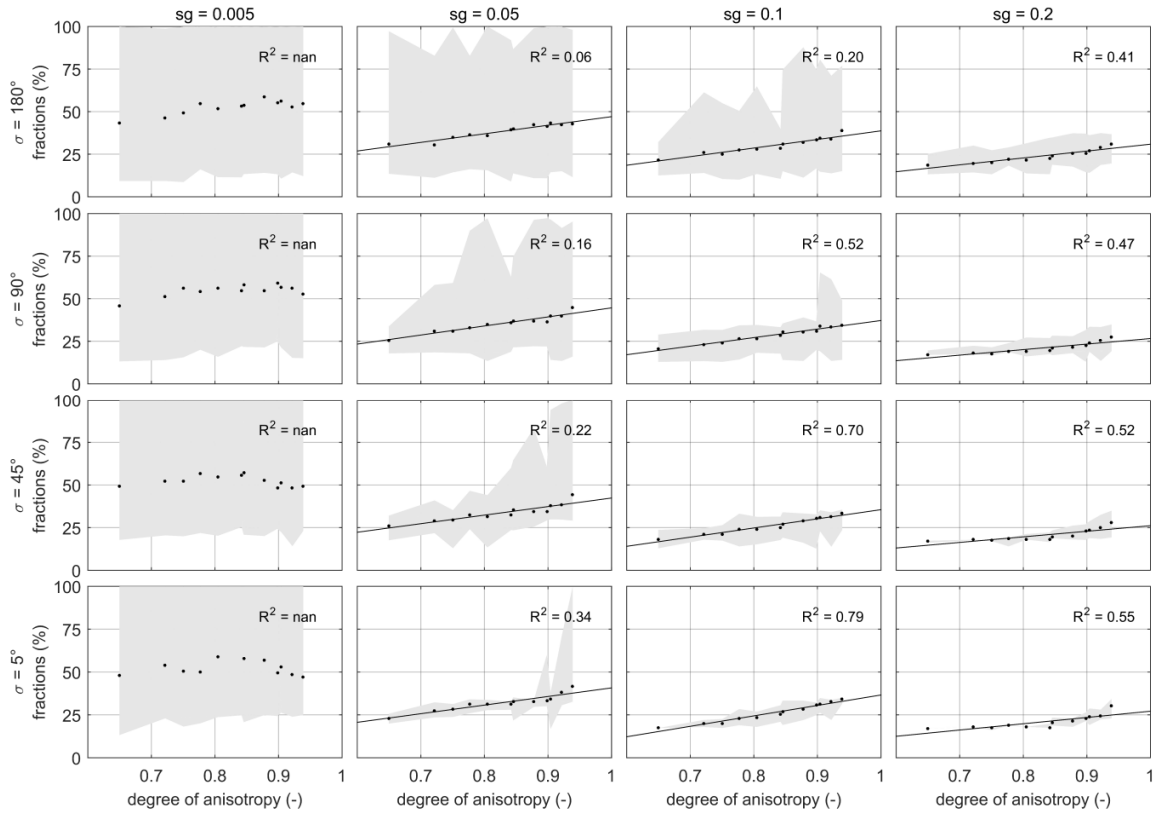

Fig. 2.14: Influence of different parametrizations of sensitivity to gravitropism (sg), unit standard deviation of the random angle (σ) and degree of anisotropy on the fractions of root lengths remaining within a 40° inclined macropore. Each of the 16 figures shows a different combination of sg and σ. The black dots show the averaged root length fraction that remains within the macropore for each degree of anisotropy; the grey shaded area shows the hull of the total range of the simulation results. R^2 specifies the coefficient of determination of the linear regression line that was fitted to the total range of the simulation results

2.3.3. Scenario 3: Virtual simulation experiment on root growth in a compacted subsoil layer that contains macropores

The simulation result produced with the anisotropy approach captured well the expected root growth behavior (Fig. 2.15b). When reaching the compacted subsoil layer, the root grew horizontally along it keeping constant contact to the soil layer until it encountered a macropore. It then entered the pore and

grew straight down along the pore wall. Using the tropism approach (Fig. 2.15a), the root was not able to enter the macropore, but oscillated around its opening without entering it.

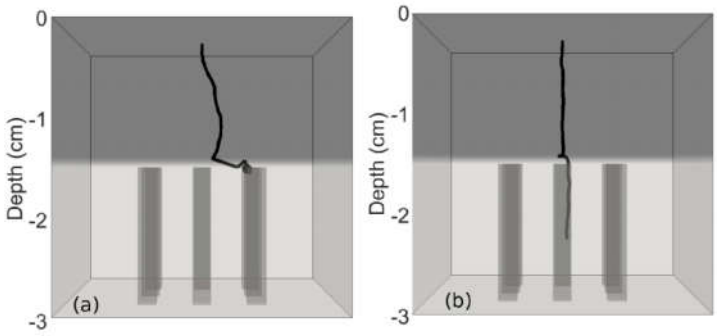

Fig. 2.15: Soil domain and root simulated with the tropism(a) and the anisotropy (b) approach; the topsoil layer is presented in dark grey, the subsoil layer in light grey; the macropores are displayed in light grey and the root in black

2.4. Discussion

Concepts of root growth models and their parameters are difficult or even impossible to validate or derive from direct measurements. However, by comparing simulated root architectures with experimentally observed ones, different concepts can be compared with each other and more appropriate ones can be identified. In this study we demonstrated that our new anisotropy approach to simulate changes in root growth direction due to soil penetration resistance is more appropriate to describe the development of root systems in soil with macropores. Data from experiments in which parameters like the macropore inclination angle and the matric bulk density were systematically varied could be used to constrain parameters of the root growth model. It must be noted that these experiments were not designed with the purpose of calibrating or validating a root growth model. Using a simulation model to design or plan such experiments could be beneficial to measure variables that contain additional information and allow a better determination of model parameters. In this example, the variability of root lengths and root length fractions within macropores could have been an additional source of information since it differed strongly between simulations using different parameter values.

Hirth et al. (2005) showed that the roughness of macropore walls has a significant influence on the probability of a root to continue growing within a macropore or to re-enter the bulk soil. For the simulation of roots growing in natural macropore networks, knowledge about the macropore wall roughness is thus mandatory. Combined information on root growth in macropores and on the roughness of earthworm burrow walls or root channels such as provided by Leue and Gerke (2016) could be used to calibrate the simulation model in that way.

Macropore walls were observed to be richer in nutrients than the surrounding bulk soil (Athmann et al. 2014; Barej et al. 2014; Jiménez et al. 2003). For simulations of root growth in macropores including nutrient uptake, information about the root – macropore wall contact is thus essential.

The new model approach was developed for a simulation domain that is discretized into a regular cubic grid of nodes. If used in a model with a different description of the simulation domain, an alternative approach must be devised for the calculation of soil mechanical conductances. An example for such a model is RootBox (Leitner et al. 2010a), where soil physical properties are not assigned to grid nodes, but implemented in a lattice-free way using signed distance functions.

For simulations of root growth in macropores on a scale larger than the single root scale, we rely on extensive experimental data to parametrize and validate the model. Non – invasive methods such as rhizotron studies (Kuchenbuch and Ingram 2002; Nagel et al. 2012; Tracy et al. 2010) may provide reliable information on root elongation rates and root growth parameters. Imaging methods such as X-ray computed tomography (Rab et al. 2014; Tracy et al. 2010) or magnetic resonance imaging (Gruwel 2014; Stingaciu et al. 2013) can be used to characterize the spatial distribution of both macropore networks and plant roots in 3D and additionally to visualize and quantify soil water dynamics including preferential flow (Sammartino et al. 2015).

Our new anisotropy approach to model the effect of macropores on root growth direction is part of the mechanistic 3D model for water and solute transport in the soil-root system, R-SWMS (Javaux et al. 2008). Thus, it is a contribution to a better understanding of underlying processes and feedback loops of soil -plant interactions on the root system scale.

Chapter III

Measuring root system traits of wheat in 2D images to parameterize 3D root architecture models

This chapter is based on a journal article published as

Landl M, Schnepf A, Vanderborght J, Bengough AG, Bauke SL, Lobet G, Bol R, Vereecken H 2018 Measuring root system traits of wheat in 2D images to parameterize 3D root architecture models. Plant and Soil 425: 457-477

3.1. Introduction

The efficiency of a plant root system to acquire below-ground resources predominantly depends on its root system architecture (Lynch 2007; Rich and Watt 2013; Smith and De Smet 2012). The complex process of root system development and its interaction with the soil matrix is, however, hard to study due to the opaque nature of the soil which makes direct measurements difficult. The use of three-dimensional root architecture models can thereby provide an opportunity to systematically investigate the influence of different environmental conditions and a wide range of crop management regimes on the formation and functionality of root systems, to interpret experimental data and to test hypotheses on root – soil interaction processes at different scales (Dunbabin et al. 2013; Roose and Schnepf 2008). In experimental field studies, such large scale testing approaches are impossible to realize. An important prerequisite for this simulation based investigation is that properties and behavior of the root system that define its functioning in soils under different conditions can be inferred from experimental data.

Over the years, several three-dimensional root architectural models have been developed: RootMap (Diggle 1988), R-SWMS (Javaux et al. 2008), RootBox (Leitner et al. 2010a), SimRoot (Lynch et al. 1997), RootTyp (Pagès et al. 2004), SPACSYS (Wu et al. 2007). This diversity can be explained by the wide range of specific model objectives such as representation of architectural characteristics of different species (Diggle 1988; Pagès et al. 2004), analysis of interactions between root development and water and nutrient uptake (Dunbabin et al. 2002) or investigation of root growth in structured soil (Landl et al. 2017). The gross representation of root systems, however, is comparable in all these models and they use similar root architectural parameter sets: While the total size of a root system is mainly determined by root traits regulating the branching density such as inter-branch distance, the shape or distribution of a root system depends essentially on branching angle and root growth trajectories of the main axes (Bingham and Wu 2011). Root growth trajectories of the main axes are determined by the directional orientation of newly developed root segments. Due to the ability to use both space and time dimensions as well as various model concepts, parameters that are used in models that generate root architectures can be defined in several ways. Table 3-1 gives an overview of the parameterization of the root traits inter-branch distance, branching angle and root growth trajectories of the main axes for several individual root architecture models.

Differences in the parameterization of root traits leads to changes in root system architecture, which significantly affects the ability of roots to forage the soil and thus the root nutrient uptake capacity (Fitter et al. 1991; Pagès 2011). Correct parameterization of 3D root architecture models is thus crucial when evaluating root-soil interaction processes.

Root architecture parameterization techniques always represent a compromise between throughputs, precision, realistic representation of field root architectures and ease of data processing (Kuijken et al. 2015). While 3D imaging techniques such as x-ray computed tomography (Mooney et al. 2012; Tracy et al. 2012; Tracy et al. 2010) and magnetic resonance imaging (Pohlmeier et al. 2013; Rascher et al. 2011) allow non – invasive studying of the spatio – temporal dynamics of root growth, they still require elaborate data processing and are only suitable for relatively small and young root systems scanned at low throughput rate (Mairhofer et al. 2012; Nagel et al. 2012). Destructive sampling allows measurement of the whole root system, however, it is a time consuming and tedious work, natural root positions can hardly be kept and a large loss of fine roots must be accepted (Judd et al. 2015; Pagès and Pellerin 1994; Pellerin and Pagès 1994). In that sense, root parameterization via 2D image analysis represents a good alternative by allowing for various methods of image acquisition, high throughput and – due to recent developments of automated root tracking software – relatively simple processing (Delory et al. 2016; Leitner et al. 2014).

Various methods for the acquisition of 2D root images have been developed over the years: The first 2D representations of root system architecture were hand drawings (Kutschera 1960; Weaver et al. 1922; Weaver et al. 1924). The field grown root systems were thereby gradually excavated and simultaneously traced on sketching paper (Kutschera 1960). A recently-revived method to non-invasively image the development of root system architecture in 2D is that of imaging roots grown in rhizotrons, and specifically rhizotron boxes (Kuchenbuch and Ingram 2002; Nagel et al. 2012). Rhizotron boxes are soil filled containers with a transparent front plate that allows observing dynamic changes in root system architecture. While rhizotrons enable better control of environmental influences on root architecture development, they spatially constrict the root system and allow only partial visibility of roots at the transparent front plate (Nagel et al. 2012; Nagel et al. 2015; Wenzel et al. 2001). A simple method that produces a large number of images with perfect visibility of the root system is represented by roots grown on germination paper (Atkinson et al. 2017; Atkinson et al. 2015). The absence of soil structure

and soil mechanical impedance as well the limited root age, however, cast doubt if the observed root architecture is a valid representation of root systems of field grown plants (Clark et al. 2011; Hargreaves et al. 2009; Nagel et al. 2012).

In this study, we want to recover the root traits inter-branch distance, branching angle and root growth trajectories of the main axes from various 2D root images of different wheat varieties (*Triticum Aestivum).* Model input parameters and common parameter patterns are identified. In a series of simulation studies possible parameterization errors due to the two-dimensionality of image sources as well as the influence of different parameterizations on root foraging performance are evaluated.

Table 3-1: Overview of the parametrization of the root traits inter-branch distance, branching angle and directional orientation of root segments in the different 3D root architecture models; L…length unit, T… time unit

	RootTyp (Pagès et al. 2004)	SimRoot (Lynch et al. 1997)	ROOTMAP (Diggle 1988)	SPACSYS (Wu et al. 2007)	R-SWMS (Javaux et al. 2008)	RootBox Leitner et al. (2010a)
Inter-branch distance	Fixed value or increasing values with depth (L) specified for each root order	Fixed value (L) specified for each root order	Fixed value (L) specified for each root order	Fixed value (L) specified for each root order	Fixed value (T) specified for each root order (inter-branch distance is then also a function of root growth rate)	Drawn from truncated normal distribution (L) with mean and standard deviation specified for each order
Branching angle	Drawn from normal distribution with mean and standard deviation specified for each root order	Fixed value specified for each root order	Fixed at 90° to its parent root	Initial value with random variation within a predefined range	Fixed value specified for each root order	Drawn from normal distribution with mean and standard deviation specified for each order
Directional orientation of root segments	Computed from the direction of the previous root segment, different selectable tropisms and a random deflection angle	Computed from the direction of the previous root segment, gravitropism and a random deflection angle	Stochastically determined with the help of a random deflection angle that is calculated on the basis of a user defined probability and a gravitropism index	Computed from the direction of the previous root segment, gravitropism and a random deflection angle, which is scaled with the maximum root segment length	Computed from the direction of the previous root segment, plagiogravitropism and a random deflection angle, which is scaled with the maximum root segment length	A random angle, which is scaled with the root segment length, is added to the growth direction of the previous root segment; this random angle is selected for its directional proximity to a desired selectable tropism from a specified number of random angle realizations

3.2. Materials and Methods

3.2.1. Image Sources

We used root images from three different sources: hand drawings from literature, images from a rhizotron experiment and images from roots grown on germination paper (Fig. 3.1). The 11 hand drawings with image resolutions between 85 and 270 ppi were selected from three different literature sources and represent root systems of variable age and wheat varieties growing at diverse locations (Table 3-2). The rhizotron images with a resolution of 300 ppi were obtained from an experimental study, in which spring wheat was grown under controlled laboratory conditions in rhizotrons with inner dimensions of 50 x 30 x 3.5 cm. The lower part of the rhizotrons was filled with compacted subsoil, the upper part with lose topsoil (bulk density 1.4 g cm^{-3} and 1 g cm^{-3} respectively). While the experimental setup included different topsoil treatments with regard to phosphorus and water supply, we only used the images of the six control replicates where both phosphorus and water supply was sufficient. The rhizotron images were taken on day 41 after sowing, just before harvest. A detailed description of the experimental setup is given in (Bauke et al. 2017). The images of roots grown on germination paper (24x30 cm) with a resolution of 442 ppi were obtained from an experimental study, where two different winter wheat cultivars (‘Rialto’ and ‘Savannah’) were grown in 41 respectively 39 replicates over a time period of 8 days under controlled lab conditions. A detailed description of the experimental setup is given in Atkinson et al. (2015).

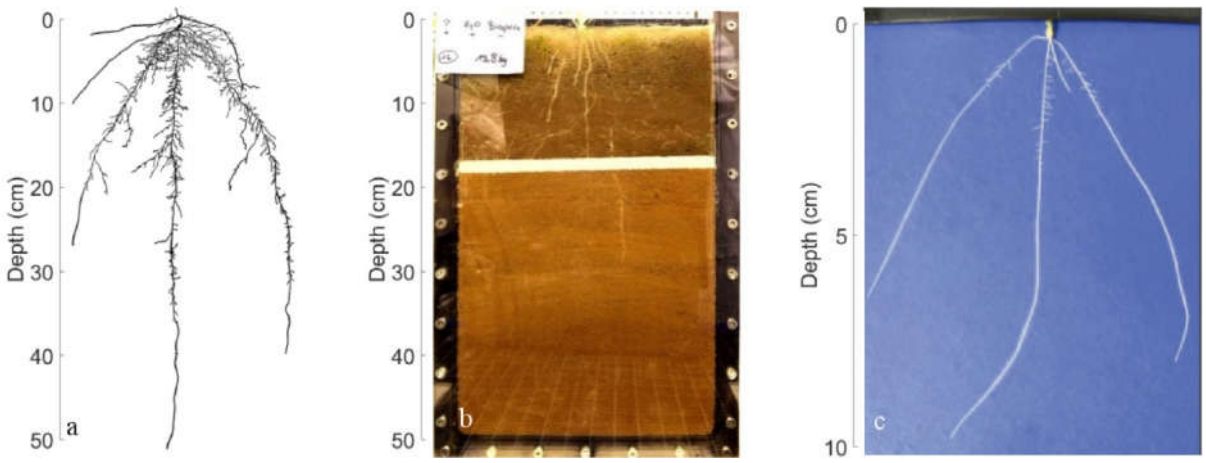

Fig. 3.1: Example images for each data source: (a) root drawing [Adapted from Weaver et al. (1924), Fig.

1], (b) rhizotron image, (c) image of roots grown on germination paper [Reprinted by permission from The Company of Biologist Ltd.: J Exp Bot. Atkinson et al. (2015), Fig. 1c]

Table 3-2: Description of image sources from literature; SW…spring wheat, WW…winter wheat

Image Number	Variety	Root system age (calendar days)	Location	Literature source
1	SW	60	Peru, Nebraska, US	Weaver et al. (1922)
2	SW	70		
3	SW	93		
4	SW	93		
5	WW	20	Lincoln, Nebraska, US	Weaver et al. (1922), Weaver et al. (1924)
6	WW	30		
7	SW	31		
8	SW	45		
9	SW	60		
10	WW	60	St. Donat, Carinthia, Austria	Kutschera and Lichtenegger (2010)
11	WW	60		

3.2.2. Image Analysis

Root system images were processed using the fully automatic root tracking software Root System Analyzer which is based on MATLAB (R2014b) (RSA; Leitner et al. 2014). The RSA saves detailed information on the coordinates of a root system in MATLAB mat-files. Analysis with the RSA requires images with continuous and clearly visible root systems. The rhizotron images, where only part of the total root system is visible at the transparent front plate of the rhizotron, thus had to be pre-processed prior to analysis. We used the open source tool GIMP 2.8 to segment the root systems manually. To keep error propagation from image segmentation to parameter determination at a minimum, we first only segmented those roots, which were clearly visible on the rhizotron image. These root systems were later used for recovering the parameters branching angle and axial trajectories. We then additionally inserted laterals, for which we had to estimate the location of the connection to their parent root. These

extended root systems were later used for recovering the parameter inter-branch distance, which depends on the visibility of all lateral roots.

3.2.3. Root Parameter Analysis

We parameterized the root traits inter-branch distance, branching angle and root growth trajectories of the main axes from the extracted root system coordinates. The inter-branch distance was measured as the distance between two successive branches in centimeters. The branching angle was determined as the angle in the vertical plane between a branch and its parent root in degrees, which is measured at a certain distance from the point where the branch emerges. In one respect, this distance should be minimized to measure the initial branching angle; however, it also needs to be large enough to avoid inaccuracies in the computation process. We performed a small analysis based on artificial root systems with known ground truth and similar root radii, which suggested that a search radius of 0.5 cm distance from the branch point is suitable for correctly computing branching angles. Root growth trajectories of axial roots are determined by their initial growth angle from the horizontal and its dynamic changes from the root base to the root apex which is affected by numerous factors such as soil compaction (Popova et al. 2016), soil temperature (Tardieu and Pellerin 1990) or soil water status (Nakamoto 1994). In a simplified way, the shape of a root trajectory can be described by two features: its overall curvature and its small-scale waviness which is known as tortuosity (Popova et al. 2016). To characterize the axial root trajectories from our data sources, we divided each root into segments of 1 cm length and determined for each segment its angle to the horizontal as well as its reorientation angle with respect to the previous root segment in degrees. We then calculated the relationship between growth angle and reorientation angle of individual root segments, which gives information on the curvature of a trajectory in relation to its inclination as well as on tortuosity.

Root parameters were quantified separately for each of the 11 root drawings. Root parameters derived from the six rhizotron images obtained from replicate experiments were pooled together to one group. Root parameters derived from images of roots grown on germination paper were classified into two groups according to cultivar (‘Rialto’: 39 images, ‘Savannah’: 41 images). Altogether, we analyzed root parameters from 14 different data sources. None of the used image sources allowed differentiating between seminal and shoot-born roots and only one order of lateral roots was identified. We therefore only distinguish between axial roots and first order laterals.

3.2.4. Simulation Studies

Among the different traits describing root architecture, root growth trajectories of axial roots are of particular importance for the shape of a root system. Their correct representation in 3D root architecture models is thus important to obtain plausible simulation results. In a first simulation study, we therefore tested the ability of different model approaches to reproduce our experimental findings on axial root trajectories and quantified model parameters for our analyzed root systems.

The recovery of 3D root architecture parameters from 2D images has the obvious drawback of losing the third dimension. Images respectively drawings of root architectures are created by projecting the 3D root systems onto 2D space. Root system architectures of plants grown in rhizotrons or on germination paper are affected by root deflection due to spatial growth constraints. While this has no influence on the parameter inter-branch distance, both branching angle and axial root growth trajectories are affected. In a second simulation study, we therefore analyzed the effects of projection and deflection, respectively, on the parameters branching angle and axial root growth trajectories.

Root architecture significantly influences root foraging performance by determining the volume of soil that can be explored by roots (Fitter et al. 1991; Pagès 2011). In a third simulation study, we evaluated the effect of different parameterizations of our focus root architecture parameters inter-branch distance, branching angle and axial root growth trajectories on the foraging performance of root systems.

Simulation study 1: Ability of 3D root architecture models to reproduce experimental observations on axial root trajectories

In 3D root architecture models, root growth trajectories are composed of individual root segments. At each root growth time step, a new segment emerges whose directional orientation must be determined with regard to overall curvature and tortuosity. Most root architecture models (SimRoot, RootTyp, SPACSYS, R-SWMS) use a vector-based approach, where the directional orientation of an individual root segment is calculated from a vector expressing tortuosity and a vector expressing gravitropism. 2D root images represent root systems in the xz-plane and thus provide information on root curvature and root tortuosity in vertical, but not in horizontal direction. To test the ability of the vector-based approach to

reproduce observations of axial root trajectories on 2D root images, we thus converted the 3D equation to 2D space:

$$\vec{d} = \begin{pmatrix} dx_{\beta,\delta} \\ dz_{\beta,\delta} \end{pmatrix} + sg \times \begin{pmatrix} 0 \\ -1 \end{pmatrix}. \quad (3.1)$$

The first term on the right hand side represents the growth direction vector of the preceding root segment dx_β with unit length 1 which is deflected by the random angle δ; the second term expresses the gravitropism component with sg as gravitropism sensitivity factor. The random deflection angle δ is a normally distributed random angle with mean zero and unit standard deviation σ. The unknown parameters are thus the sensitivity to gravitropism sg and the standard deviation of the random deflection angle σ (cf. Clausnitzer and Hopmans (1994)). We implemented this formula in MATLAB and computed root trajectories using 7 different parameterizations of sg and 21 different parameterizations of σ (147 parameter combinations altogether, values are given in Table 3-3). For each parameter combination, we simulated 50 axial root trajectories with individual lengths of 50 cm (example in Fig. 3.2).

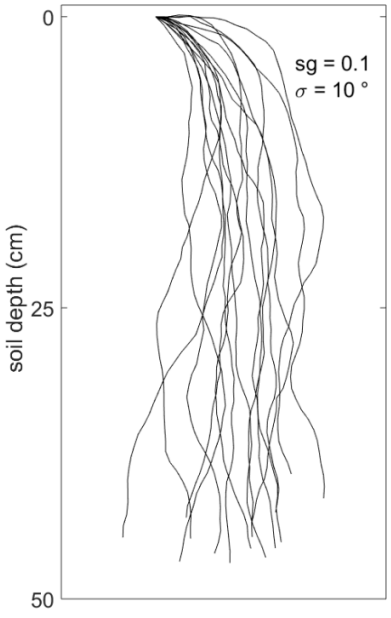

Fig. 3.2: Example of simulated axial

Table 3-3: Parameter values for simulation; sg… sensitivity to gravitropism (-), σ… unit standard deviation of the random angle (°), parameter explanations can be found in Clausnitzer and Hopmans (1994)

Gravitropism component	Tortuosity component
sg = [0.005; 0.01; 0.05; 0.1; 0.15; 0.2; 0.25; 0.3; 0.35; 0.4]	σ = 0 to 20, interval = 1

root trajectories

Simulation study 2: Effects of projection and deflection on the parameters branching angle and axial root growth trajectories.

The objective of this study was to analyze the effects of projection and deflection, respectively, on the parameters branching angle and axial root growth trajectories.

Root system development was simulated using the MATLAB version of the 3D root architecture model RootBox, which is fully described in Leitner et al. (2010a) and shall here only be addressed briefly. RootBox defines each root order by a set of different model parameters. Basal and apical root zone determine the length of the unbranched zone before the first and after the last branch, respectively. Inter-branch distance defines the distance between two successive branches and thereby also affects the maximum root length for a given number of branches. Root growth speed is described by a negative exponential function whose initial slope is determined by the initial elongation rate and whose asymptote depends on the maximum root length. The emergence angle of axial roots respectively the initial angle between a branch and its parent root is defined by a radial angle in the horizontal plane, and an insertion respectively branching angle in the vertical plane. The radial angle is generally drawn at random between 0 and 2π, but can also be set to a specific angle to consider non-independence of branching files. To describe axial root growth trajectories, we implemented the vector-based approach used in most root architecture models (SimRoot, RootTyp, SPACSYS, R-SWMS) into RootBox: In this approach, newly emerged root segments are oriented according to the direction of the previous root segment, sensitivity to gravitropism and random angle deflection.

To evaluate the effect of projection, we mapped the unconstrained 3D root system onto the x-z plane. To evaluate the effect of deflection, we simulated a root system, which was spatially constrained by a rhizotron with dimensions of 20 x 2 x 30 cm (Fig. 3.3). This geometry is implemented based on signed distance functions in which the distance of a given point to the closest boundary is evaluated and given a positive sign if located inside the geometry and a negative sign if located outside. Random optimization ensures that the new position of a growing root tip is always inside the rhizotron domain (Leitner et al. 2010a). Using the coordinates of these root systems, we then computed (1) branching angles between

laterals and their parent roots and (2) relationships between angle to the horizontal and reorientation angle of individual root segments.

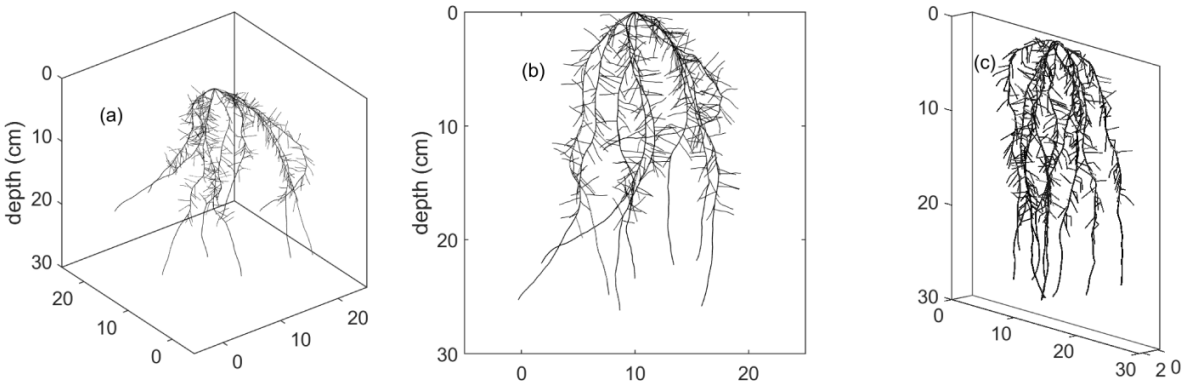

Fig. 3.3: (a) unconstrained root growth in 3D, (b) unconstrained root growth projected onto x-z plane, (c) constrained root growth in a rhizotron

Simulation study 3: Influence of different parameterizations of inter-branch distance, branching angle and axial root trajectories on foraging performance of a root system

Root system development was simulated using the MATLAB version of the 3D root architecture model RootBox with an alternative approach for the simulation of axial root growth trajectories as described in simulation study 2.

The soil volume around a root system available for nutrient uptake, i.e. the rhizosphere, was computed using the approach by Fitter et al. (1991). For this procedure, a very fine 3D grid is overlaid on the root system. The center of every grid cell is then scanned for its distance to the nearest root segment. If the distance is smaller than a specified rhizosphere radius R_{rhiz}, the grid cell volume is counted as rhizosphere volume. The rhizosphere radius R_{rhiz} is determined by the effective diffusion coefficient of a solute in soil and the age of the respective root segment and calculated according to Nye and Tinker (1977) as

$$R_{rhiz} = r + 2\sqrt{D_e\, t}, \tag{3.2}$$

where r is the radius of the root segment (cm), D_e is the effective diffusion coefficient in soil (cm^2s^{-1}) and t is the root segment age (s). To evaluate the influence of different soil diffusion coefficients (D_e) on the rhizosphere volume, we performed simulations with three different D_e values: 10^{-8}, 10^{-7} and $2x10^{-6}$ cm^2 s^{-1}. The first two values are typical effective phosphorus diffusion coefficients in soil, which account for the effect of sorption of phosphorus to soil particles (Schenk and Barber 1979); the latter one is a characteristic nitrate diffusion coefficient of the soil (Volder et al. 2005). While the net rhizosphere volume was defined as the volumetric sum of all unique grid cells, the rhizosphere volume with overlap was specified as the volumetric sum of all - partially multiply assigned - grid cells. The overlap volume is then the difference between rhizosphere volume with overlap and net rhizosphere volume (Fig. 3.4).

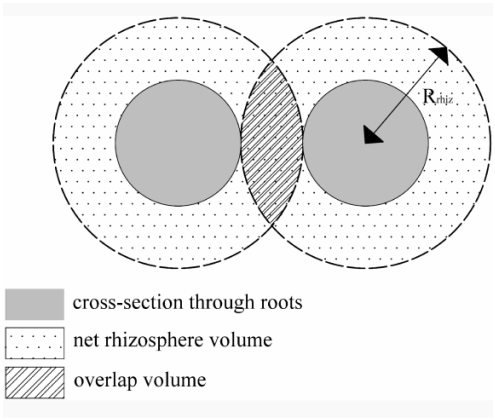

Fig. 3.4: Schematic representation of rhizosphere volume, overlap volume and rhizosphere radius R_{rhiz}: grey circles represent cross-sections through two individual roots, dotted and diagonal hatching show net rhizosphere and overlap volume, respectively

Considering that both rhizosphere and overlap volume are absolute values and depend on the total size of a root system, we introduced the parameter inter-root competition (IRC) as a size-independent measure of comparison following the approach by Ge et al. (2000). IRC is calculated as

$$IRC = \frac{V_{overlap}}{V_{rhizo}} \times 100\%, \tag{3.3}$$

where $V_{overlap}$ is the overlap volume and V_{rhizo} is the net rhizosphere volume. Fig. 3.5 shows an example of a simulated root system and its surrounding rhizosphere volume for different values of D_e.

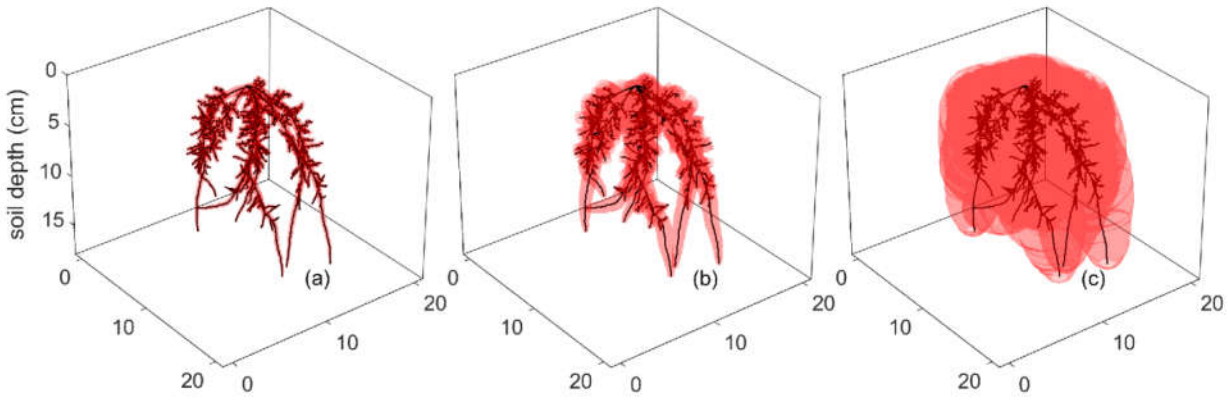

Fig. 3.5: Representation of the computed 3D root system (black) with rhizosphere zone (red) for simulations with $D_e = 10^{-8}$ cm^2s^{-1} (a), $D_e = 10^{-7}$ cm^2s^{-1} (b) and $D_e = 2x10^{-6}$ cm^2s^{-1} (c) at simulation day 30

Using observations from root image analysis, we identified factors that can be used to differently parameterize our three focus parameters. These factors were mean and standard deviation for both inter-branch distance and branching angle and standard deviation of the random angle deflection respectively sensitivity to gravitropism for the parameter axial root growth trajectories. For each of these factors, we defined variation intervals with lower and upper bounds. For the parameter inter-branch distance, we used probability distribution as an additional categorical factor of variation, which was set to either normal or lognormal distribution. Descriptive statistics of the lognormal distribution were calculated by transformation from the parameters of the normal distribution. The domain of the normal distribution was restricted to the positive number range; negative values were set to 10^{-6} cm. We also included a categorical factor of variation for the radial alignment of 1st order laterals around the main axis. In literature, the alignment of lateral roots around the root axis is still unclear. While Abadia-Fenoll et al. (1986) and Barlow and Adam (1988) found lateral roots of onion and tomato to form in acropetal sequence around their parent axis, Pellerin and Tabourel (1995) and Yu et al. (2016) observed an unpredictable radial emergence pattern for lateral roots of maize and wheat. Due to these inconsistencies, we specified the radial angle either as random in the interval [0 2π] or set it to a value of 45 ° (sequential acropetal branching from 8 phloem poles around the axis). Variation intervals for

parameterization factors as well as descriptions of the additional factors are given in Table 3-4. The remaining root growth parameters were set to fixed values, which were either derived from literature or directly from our analyzed root images (Table 3-5). We considered two orders of lateral roots. The simulation time was set to 30 days and each root system consisted of 7 axial roots.

For all possible combinations of categorical factors, we then performed 1000 root system realizations that corresponded with 1000 parameter sets that were randomly drawn from the intervals specified in Table 3-4. This gave a total of 4000 root system realizations (i.e.2^2x1000). For each root system, we then computed inter-root competition as a measure of foraging performance for all three soil diffusion coefficients (D_e) defined above. Relationships between inter-root competition and our focus parameters were explored by means of scatterplots. To visualize the main trends, we fitted linear regression lines. Correlation analyses were then used to quantitatively evaluate the linear relationship between inter-root competition and our focus parameters.

Table 3-4: Variation factor values of focus parameters; detailed parameter explanations can be found in Leitner et al. (2010a)

Parameter	Factor	Unit	Root order	min	max
Inter-branch distance	µ	(cm)	Axial	0.1	0.5
	std	(cm)	Axial	0	0.5
Branching angle	µ	(°)	1st order lateral	60	90
	std	(°)	1st order lateral	0	50
Root growth trajectories	Unit std of random angle	(°)	Axial	9	20
	Deflection / tortuosity				
	Sensitivity to gravitropism	(-)	Axial	0.01	0.3
	Additional factors:	Normally / lognormally distributed inter-branch distance			
		Random / regular radial branching angle			

µ… mean value, std… standard deviation

Table 3-5: Constant parameter values; detailed parameter explanations can be found in Leitner et al. (2010a)

Parameter		Unit	axis	1st order laterals	2nd order laterals
Initial elongation rate		(cm d^{-1})	1.2[a]	0.8[a]	0.8[a]
Root radius		(cm)	0.038[a]	0.027[a]	0.027[a]
Basal root zone		(cm)	2	0.2[c]	0.125
Apical root zone		(cm)	6	0.3[c]	0.125
Inter-branch distance		(cm)	fp	0.25	0
Number of branches per root axis		(-)	50	6[c]	0
Insertion/Branching angle		(°)	70	fp	90
Tropism		(-)	Gravitropism	Exotropism	Exotropism
Tropism sensitivity	sg	(-)	fp	0.1	0.1
Unit std of random angle deflection	σ	(°)	fp	20	20

fp… focus parameter, specified in Table 3-4; std…standard deviation

[a] based on Materechera et al. (1991)

[b] based on Ito et al. (2006)

[c] derived from root lengths of 1st order laterals given by Ito et al. (2006)

3.2.5. Statistics

Statistical analyses were performed with MATLAB (R2014b). To evaluate differences in means with unequal variance, a Welch's t-test was used. To analyze differences in variances, we performed a two-sample F-test. Linear regression relationships were evaluated by means of an F-test. In the following, significant results correspond to $p<0.05$, while highly significant results represent $p<0.01$.

3.3. Results

3.3.1. Inter-branch distance

The relationships between inter-branch distance and distance along the root axis are very scattered for all data sources with values ranging from close to 0 cm to up to 3 cm. An F-test showed a significant increase in inter-branch distance from the base of the branched zone down to the root apex for 11 out of 14 data sets, no trend for two data sets and a decrease for one data set (Fig. 3.6). The large variability of

inter-branch distances observed for the data source from rhizotron images can be explained by the only partial visibility of the root system which has probably obscured some lateral roots. The global distributions show for all data sources a highly asymmetrical shape which can be well described with lognormal distributions (Fig. 3.7). We observed a large percentage of short inter-branch distances with medians ranging between 0.1 and 0.5 cm (Fig. 3.8). No systematic pattern was apparent with regard to the different data sources.

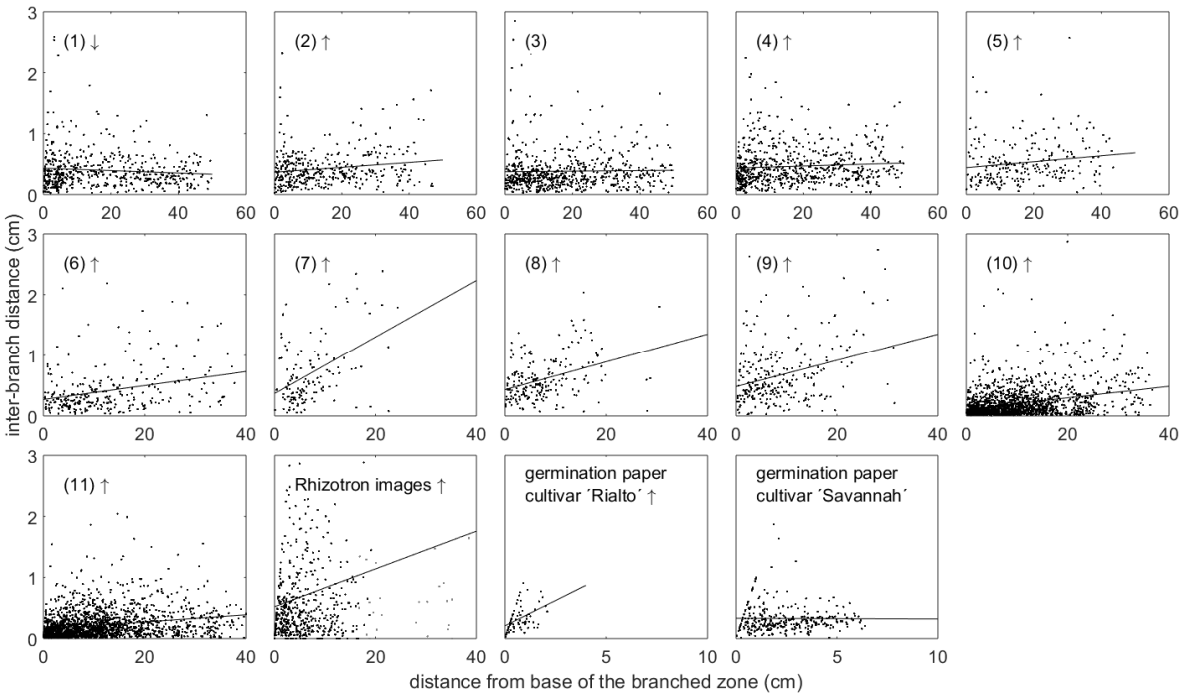

Fig. 3.6: Relationship between inter-branch distance and distance from the base of the branched zone illustrated for each data source; arrows indicate a significant up- respectively downward trend in the data set; the number codes for data sources one to eleven are found in Table 3-2

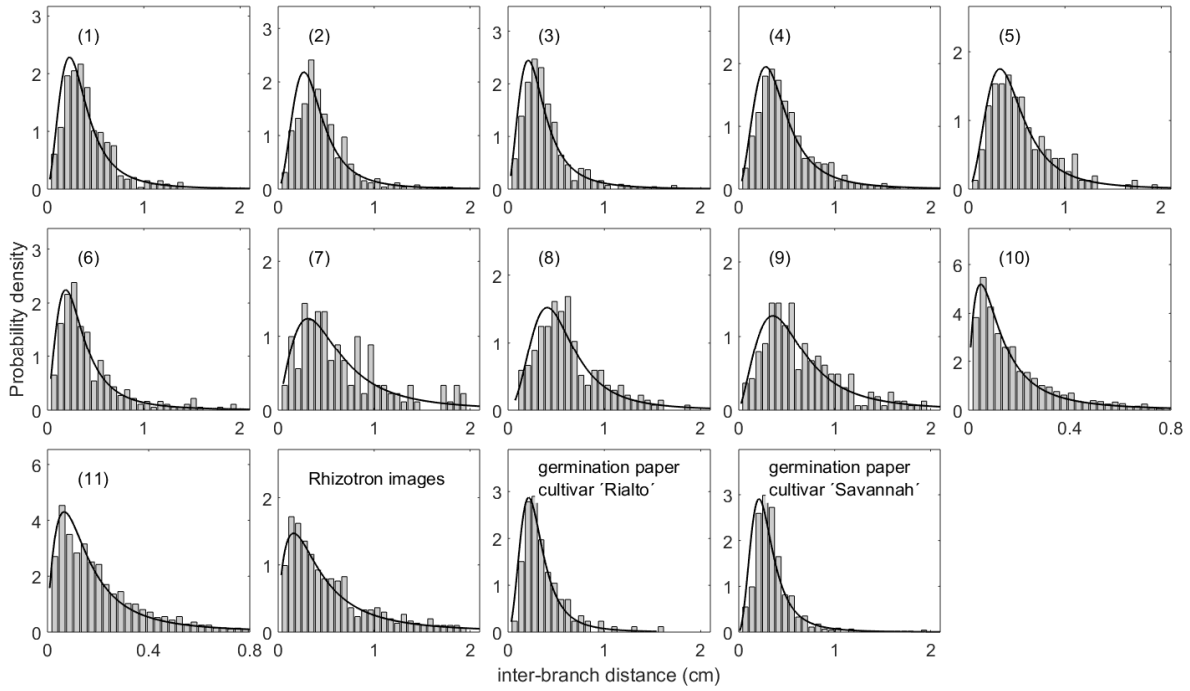

Fig. 3.7: Probability distributions of inter-branch distances with fitted lognormal functions illustrated for each data source; data sets were plotted using different scales for x- and y-axis; the number codes for data sources one to eleven are found in Table 3-2

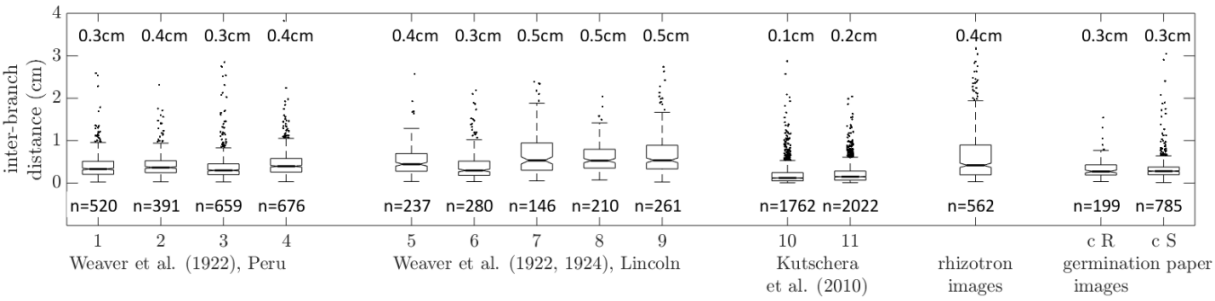

Fig. 3.8: Variation of inter-branch distances, medians and sample sizes (n) for the different data sources; the number codes for data sources one to eleven are found in Table 3-2; cR…cultivar Rialto, cS… cultivar Savannah

3.3.2. Branching angle

The global distribution of branching angles shows a bell shape for the roots grown on germination paper that can be approximated with a normal distribution; for the remaining data sources, the distribution of branching angles is spread more widely and shows positive skewness (Fig. 3.9). Interestingly, branching angles from all data sources show similar medians that range from 59.5° to 79.4° and are well below 90° (Fig. 3.10).

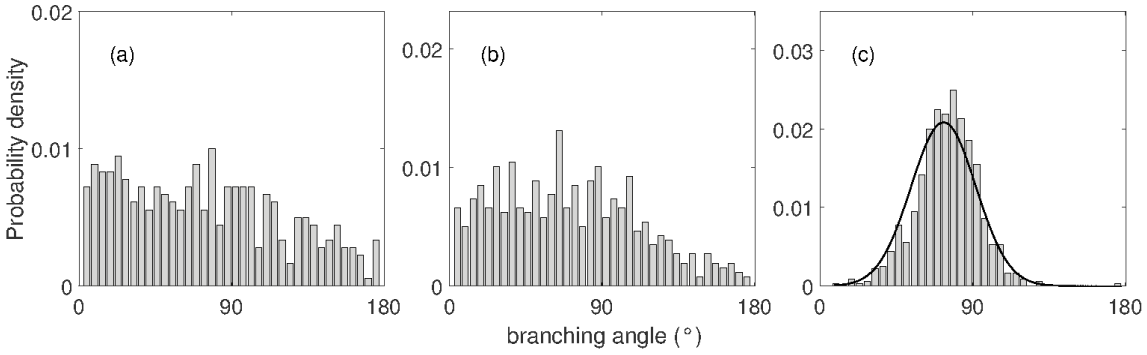

Fig. 3.9: Examples of probability distributions of branching angles for (a) a root drawing, (b) a rhizotron image, (c) an image of roots grown on germination paper with fitted normal function

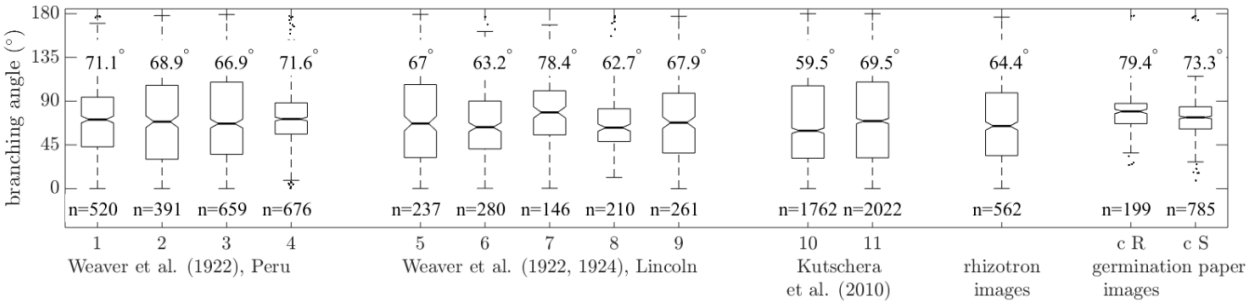

Fig. 3.10: Variation of branching angles, medians and sample sizes (n) for the different data sources; the number codes for data sources one to eleven are found in Table 3-2; cR…cultivar Rialto, cS… cultivar Savannah

3.3.3. Root growth trajectories

Root growth trajectories of axial roots were reconstructed for all root systems of each data source from the extracted root coordinates prior to analysis (Fig. 3.11).

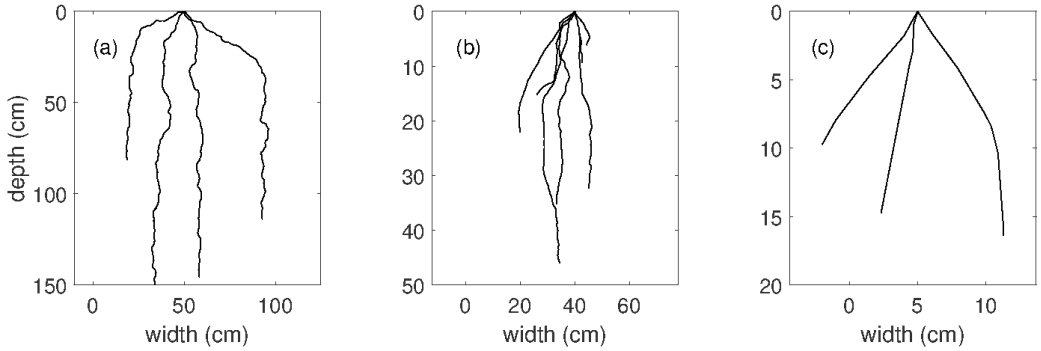

Fig. 3.11: Examples of reconstructed root growth trajectories of the axial roots for (a) a root drawing, (b) a rhizotron image, (c) an image of roots grown on germination paper

There was a negative relationship between reorientation angle and angle of the previous 1 cm long root segment for all but one data source meaning that more horizontally growing roots generally reoriented stronger towards the vertical than more perpendicularly growing ones (Fig. 3.12). An F-test showed that this correlation was highly significant for 3, significant for 5 and not significant for 6 data sources. Not significant relationships can be an indicator for abrupt changes in the growth path (e.g. the rightmost trajectory in Fig. 3.11a), high root tortuosity or liminal growth angles that deviate from the vertical (Nakamoto 1994). The reorientation angle $\Delta\beta$ at a segment angle of β=-90° (vertical root growth) predicted by regression tended for all data sources towards zero suggesting that gravitropism is the predominant influence factor in the formation of trajectory curvature. While the slope of the regression line is a measure of gravitropism, the standard error of the estimate determines the degree of root tortuosity. The slope of the regression lines ranged between 0 and -0.2; the standard error of the estimate between 7.7 ° and 21.8 °. With regard to different data sources, we did not find any systematic pattern of slope; standard errors of the estimate, however, were highest for root drawings of large, mature root systems and lowest for roots grown on germination paper.

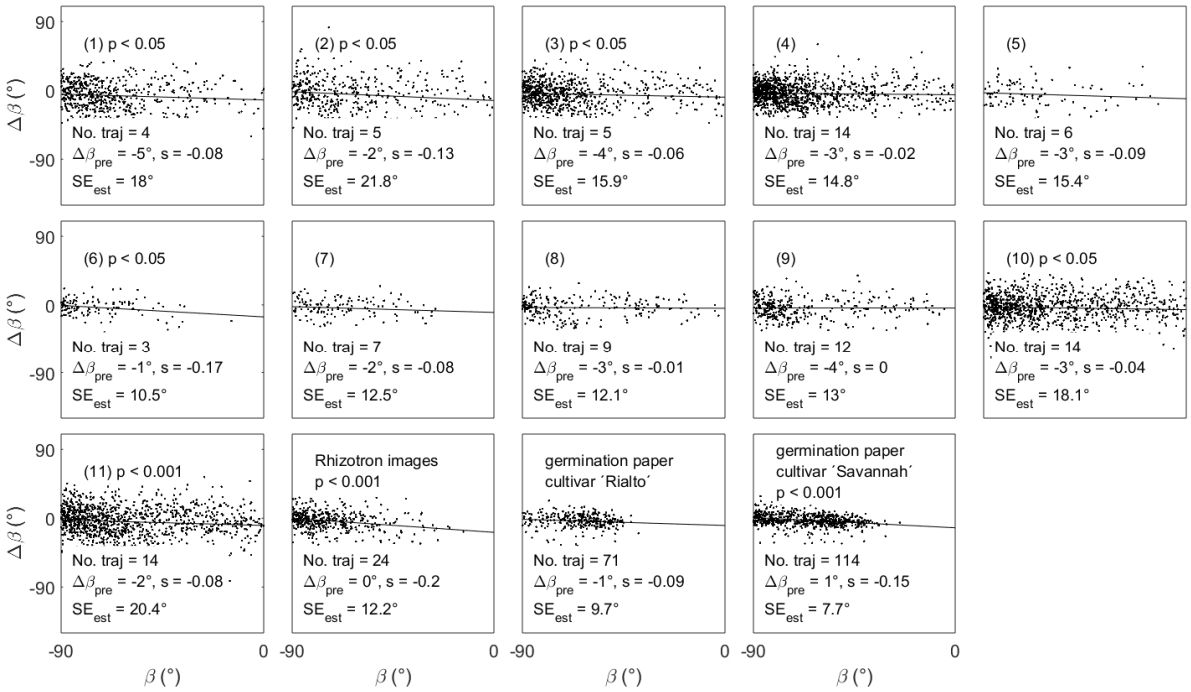

Fig. 3.12: Relationship between reorientation angle Δβ and angle of the previous 1 cm long axial root section β for each data source; $\Delta\beta_{pre}$… Δβ predicted by regression at β=-90°; s…slope, SE_{est}… standard error of the estimate; No. traj … number of analyzed trajectories; the number codes for data sources one to eleven are found in Table 3-2

3.3.4. Simulation studies

Simulation study 1: Ability of 3D root architecture models to reproduce experimental observations on axial root trajectories

For each combination of parameters describing gravitropism and tortuosity, we calculated the relationship between reorientation angle Δβ and angle of the previous 1 cm long root segment β and approximated it with a linear regression line. The results are shown in Fig. 3.13 for 20 selected parameter combinations. The standard deviation of the random deflection angle σ can be seen as a direct measure of the standard error of the estimate and thus tortuosity if the influence of gravitropism is not too strong. Large values of gravitropism force the root tip to grow towards the vertical and result in standard errors of the estimate smaller than σ. The gravitropism parameter sg is inversely proportional to the

slope of the regression line. The prediction with the regression lines, which are close to 0° at β= -90°, reflect the minimum average reorientation of vertically oriented roots. An F-test showed that correlations between reorientation angle and angle of the previous 1 cm long root segment were highly significant for all combinations, except for the combination of the largest root tortuosity and smallest gravitropism value. The relationships between root reorientation and root angle resemble those calculated for our image-derived axial root trajectories (Fig. 3.12). The approach is thus well suited to simulate curvature and tortuosity of wheat root trajectories.

To link the model parameters necessary for the simulation of root trajectories (sensitivity to gravitropism sg and root tortuosity σ) to the relationship between root reorientation and root segment angle, we calculated characteristic curves for the different parameter combinations (Fig. 3.14). The characteristic curves are the smoothed connection lines between the properties of the regression lines (standard error of the estimate and slope) that relate segment angles and reorientation angles of axial root trajectories for each parameter combination. Fig. 3.14 shows that slope and standard error of the regression cannot be mapped linearly to the parameters σ and sg that describe gravitropism and tortuosity. To quantify model parameters for our observed root trajectories, we inserted the regression line properties deduced from Fig. 3.12 into the graphs and located their positions. This gave us values between 0.01 and 0.3 for the sensitivity to gravitropism sg and values between 9° and 20 for the unit standard deviation of the random angle σ.

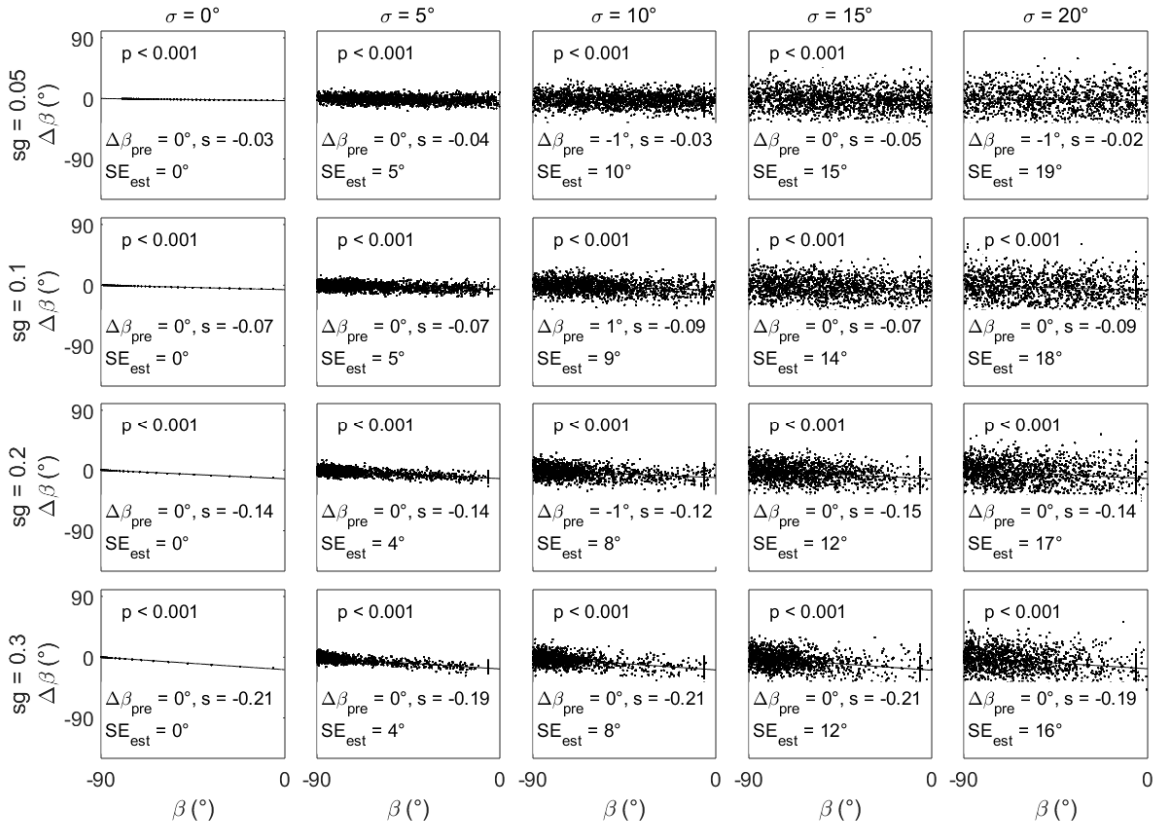

Fig. 3.13: Relationship between reorientation angle Δβ and angle of the previous 1 cm long axial root section β for simulated root systems using different parametrizations of the sensitivity to gravitropism sg and the unit standard deviation of the random angle σ; Δβpre… Δβ predicted by regression at β=-90°, s…slope, SE_{est}… standard error of the estimate

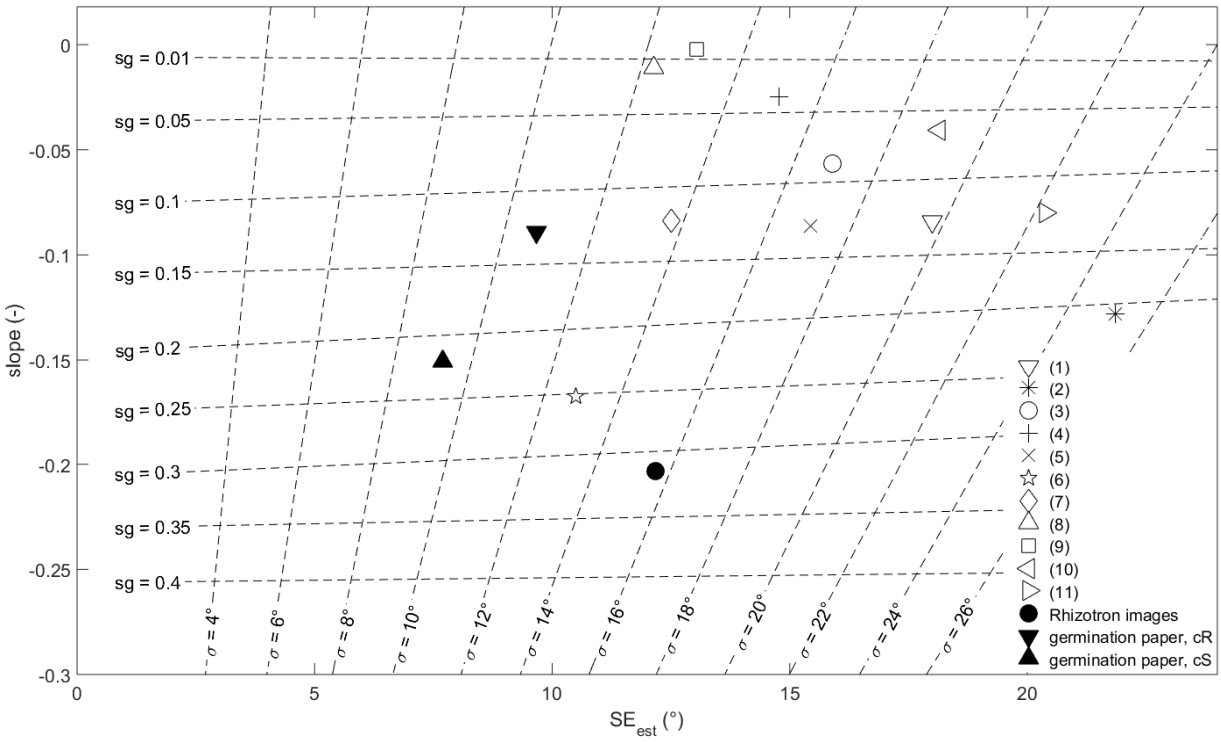

Fig. 3.14: Characteristic curves for the deduction of the gravitropism parameter sg and the tortuosity parameter σ from the properties of the regression line (standard error of the estimate SE_{est} and slope) that relates root reorientation and root angle. The value pair of regression line properties of each data source deduced from Fig. 3.12 is inserted into the graph; the number codes for data sources one to eleven are found in Table 3-2

Simulation study 2: Effects of projection and deflection on the parameters branching angle and axial root growth trajectories.

While mean branching angles of projected and deflected root systems did not differ significantly from branching angles of the unconstrained 3D root system, their variance was significantly higher. This was especially true for the projected root system (Fig. 3.15-1). The similarity in mean branching angles can be explained by the symmetrical alignment of lateral roots around the root axis, which leads to a compensation between positive and negative angle deviations due to projection or deflection. Relationships between reorientation angle and angle of the previous 1 cm long root segment differed

significantly between projected and deflected root systems and the unconstrained 3D root system with regard to slope and thus gravitropic root growth. With regard to standard deviation of the estimate and thus tortuosity, only the projected, but not the deflected root system showed a significantly higher value than the unconstrained 3D root system (Fig. 3.15-2). Considering that absolute deviations are rather small, these discrepancies in gravitropism and tortuosity are negligible in terms of model parameterization.

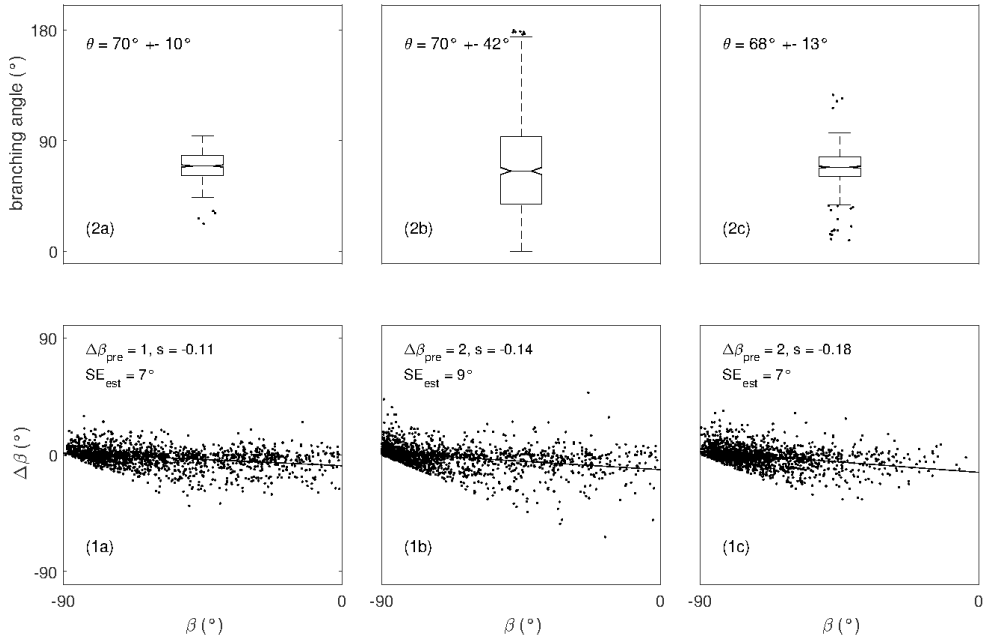

Fig. 3.15: (1) Branching angle θ (mean +- standard deviation) and (2) relationship between reorientation angle Δβ and angle of the previous 1 cm long axile root section β with Δβpre… Δβ predicted by regression at β=-90°, s…slope, SE_{est}… standard error of the estimate for (a) unconstrained root growth in 3D, (b) unconstrained root growth projected onto the x-z plane and (c) constrained root growth in a rhizotron (Fig. 3.3)

Simulation study 3: Influence of different parameterizations of inter-branch distance, branching angle and axial root trajectories on foraging performance of a root system

We found clear relationships between inter-root competition and different parameterizations. These relationships are illustrated for $D_e = 10^{-8}$ cm^2s^{-1} in Fig. 3.16. In each plot, all simulation results were plotted against the specific parameter. In Table 3-6, correlation coefficients show the significance of linear relationships between inter-root competition and parameters. As expected, IRC decreased with increasing mean inter-branch distance. If mean inter-branch distance was low, IRC was significantly higher for lognormally than for normally distributed inter-branch distances. Regular alignment of laterals around the main axis tended to less IRC than random alignment, however, not significantly. The relationship between IRC and mean inter-branch distance was significantly weaker for the largest soil diffusion coefficient. The effect of varying standard deviation of inter-branch distance on IRC was surprising: For lognormally distributed inter-branch distances IRC increased with increasing standard deviation; for normally distributed inter-branch distances, it decreased. These relationships remained nearly constant for all soil diffusion coefficients. IRC decreased with increasing mean branching angle. This effect, however, was only significant for the lowest soil diffusion coefficient. Larger standard deviations of the branching angle led to a significant increase in IRC for the lower two soil diffusion coefficients. This effect was larger for regularly aligned laterals than for randomly aligned ones. Greater values of standard deviation of the random angle deflection led to lower IRC. This effect, however, was only significant for the largest soil diffusion coefficient. As expected, larger values of sensitivity to gravitropism led to more IRC. This effect was stronger for larger soil diffusion coefficients and also for root systems with normally distributed inter-branch distances as compared with lognormally distributed ones.

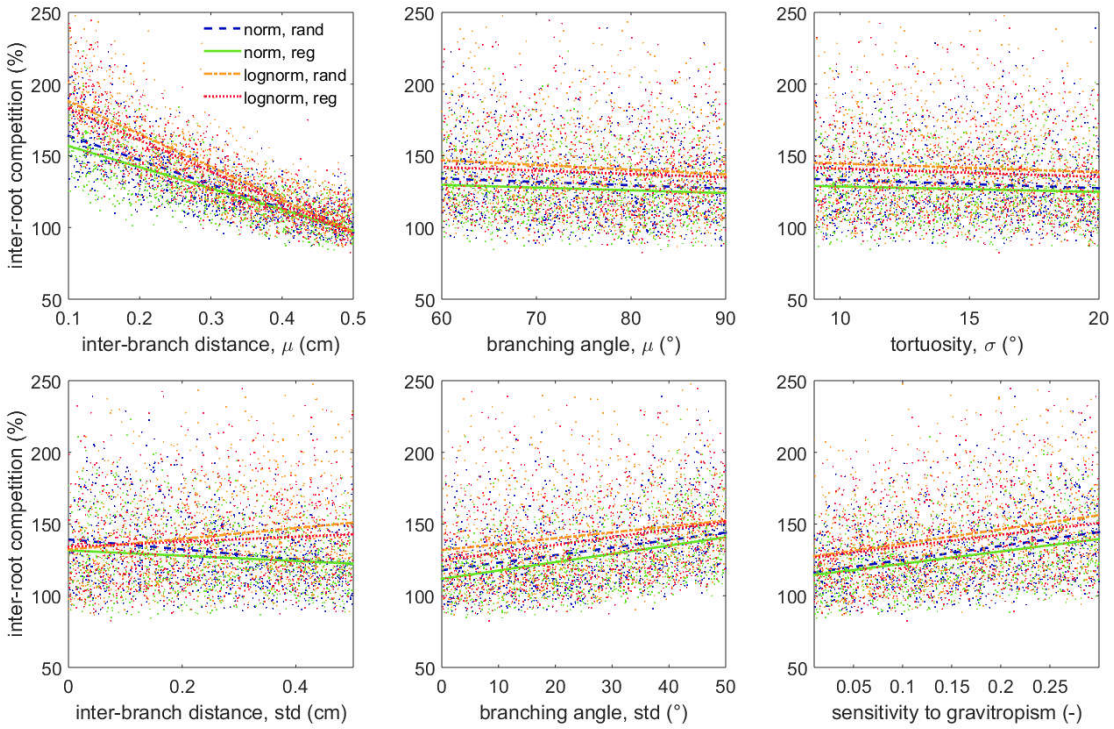

Fig. 3.16: Scatter plots with linear regression lines illustrating the relationships between inter-root competition and different parametrization factors for D_e = 10^{-8} cm^2s^{-1}; μ…mean value, std… standard deviation, norm / lognorm… normally / lognormally distributed inter-branch distances, rand / reg… random / regular alignment of 1st order laterals around the root axis

Table 3-6: Correlation coefficients between inter-root competition and parametrization factors, bold characters represent significant values at p<0.05

		ibd, μ (cm)	ibd, std (cm)	θ, μ (°)	θ, std (°)	σ (°)	sg (-)
$D_e = 10^{-8}$ cm²s^{-1}	norm, rand	**-0.78**	**-0.20**	**-0.08**	**0.30**	**-0.07**	**0.32**
	norm, reg	**-0.76**	**-0.12**	**-0.07**	**0.36**	-0.05	**0.32**
	lognorm, rand	**-0.81**	**0.17**	**-0.09**	**0.18**	-0.06	**0.26**
	lognorm, reg	**-0.83**	**0.08**	**-0.07**	**0.25**	-0.06	**0.22**
$D_e = 10^{-7}$ cm²s^{-1}	norm, rand	**-0.81**	**-0.25**	-0.02	**0.16**	**-0.07**	**0.32**
	norm, reg	**-0.80**	**-0.17**	0.01	**0.20**	-0.06	**0.32**
	lognorm, rand	**-0.82**	**0.12**	-0.03	**0.09**	-0.05	**0.27**
	lognorm, reg	**-0.85**	0.03	0.00	**0.13**	**-0.08**	**0.24**
$D_e = 2x10^{-6}$ cm²s^{-1}	norm, rand	**-0.73**	**-0.24**	0.00	0.04	**-0.09**	**0.49**
	norm, reg	**-0.72**	**-0.17**	0.06	0.04	**-0.10**	**0.49**
	lognorm, rand	**-0.70**	0.04	0.01	0.01	**-0.07**	**0.45**
	lognorm, reg	**-0.72**	**-0.06**	0.02	0.01	**-0.12**	**0.43**

ibd… inter-branch distance, θ… branching angle, σ… tortuosity, sg … sensitivity to gravitropism, μ…mean value, std… standard deviation, norm / lognorm… normally / lognormally distributed inter-branch distances, rand / reg… random / regular alignment of 1st order laterals around the root axis

3.4. Discussion

2D image analysis is a simple and fast way to retrieve information on root system architectures for the parameterization of 3D root architecture models. The systematic analysis of root images from three different sources (root drawings, rhizotron images, images of roots grown on germination paper) allowed us to identify universally occurring parameter patterns of wheat roots.

Observed patterns of root architecture parameters contrast common model assumptions

Inter-branch distance along axial roots predominantly increased with increasing distance from the base of the branched zone. But in some cases, it also remained constant or decreased. These results are in line with published data: While inter-branch distance along the axial roots was frequently observed to

increase with increasing distance from the base of the branched zone (e.g. maize by Ito et al. (2006), Pagès and Pellerin (1994), Postma et al. (2014) and pea by (Tricot et al. 1997)), other studies found constant or no identifiable pattern of inter-branch distance along axial roots (e.g. wheat by Ito et al. (2006) and banana by Draye (2002)). Studies have proposed that soil compaction (Pagès and Pellerin 1994), oxygen gradients (Liang et al. 1996) or water availability in the vicinity of the root (Bao et al. 2014) may alter branching density and thus inter-branch distances. In 3D root architecture models, the phenomenon of varying inter-branch distances along axial roots could be considered by a coefficient that is linked to these processes. Our findings suggest that the global distribution of inter-branch distances of wheat roots follows a lognormal distribution, which is in line with observations by Pagès et al. (2014) on roots of various species of the Poaceae family and Le Bot et al. (2010) on the root system of a tomato plant. This contrasts common assumptions of 3D root architecture models where inter-branch distances are either set to a fixed value or drawn from a normal distribution (see Table 3-1).

The branching angle of lateral roots relative to their parent axis is a standard parameter that is included in all 3D root architecture models (Table 3-1) and defines the initial direction of the first segment of a lateral root at the point of emergence. Our findings suggest that branching angles of 1st order laterals of wheat root systems are significantly smaller than 90° with a variance that depends on the growth medium. This contrasts common model assumptions where branching angles are frequently set to a constant value of 90° relative to the parent root for reasons of simplicity (Clausnitzer and Hopmans 1994; Pagès et al. 2004; Wu et al. 2005) or as a general model condition (Diggle 1988).

More horizontally growing roots reoriented stronger towards the vertical than more vertically growing roots with reorientation angles approaching 0 ° as the roots turn to the vertical. These findings are in line with observations by Wu et al. (2015) on axial maize root trajectories. A number of axial root trajectories derived from root drawings did not follow a continuous gravitropic growth path, but changed their slope abruptly to the vertical after growing in relatively constant direction. Similar observations were reported by Tardieu and Pellerin (1990) who suggest that earthworm channels that can be used by roots as preferential growth paths might be responsible for this effect. Levels of root tortuosity showed a relatively clear ranking with tortuosity of root systems grown in structured soil > tortuosity of roots grown in sieved soil > tortuosity of roots grown on filter paper. While root age seems to have an influence, this effect is probably also caused by differences in the penetration resistance of the growth

medium as proposed by Popova et al. (2016). A simulation study showed good agreement between simulated and observed curvature and tortuosity of axial wheat root trajectories. We developed characteristic curves that relate model input parameters with downwards reorientation and segment angles of axial trajectories. These characteristic curves can be used to calibrate the model parameters gravitropism and tortuosity from 2D root trajectories, which is a step forward in the realistic parameterization of 3D root architecture models.

Root system projection leads to overestimation of the variance of branching angles

The use of two-dimensional root drawings or rhizotron images for the parameterization of 3D root architecture models is common practice (Delory et al. 2016; Doussan et al. 2006; Leitner et al. 2014; Pagès et al. 2004). To our knowledge, the effects of root system projection or deflection on size and distribution of 3D root architecture parameters, however, has not yet been analyzed. We showed that projection greatly affects branching angles by overestimating their variance. Effects of projection and deflection, respectively, on tortuosity and gravitropism parameters were shown to be negligible.

Root foraging performance depends strongly on parameter distribution and parameter variance

The influence of the main determinants of root architecture (e.g. mean inter-branch distance, mean branching angle) on root foraging performance is well documented in literature (Bingham and Wu 2011; Postma et al. 2014). The influence of parameter variance and distribution, however, which describes the degree to which stochasticity affects developmental processes, is much less explored (Forde 2009). In most 3D root architecture models, parameter stochasticity is not used or only used to a limited extent (Table 3-1). We could demonstrate the significant impact of variance in both inter-branch distance and branching angle on foraging performance of a root system. Also, the use of different distributions of inter-branch distance (normal, lognormal) led to significant differences in effective rhizosphere volume around a root system. Interestingly, differences in radial alignment of lateral roots around the root axis, i.e. random or acropetal branching, only led to minor differences in root foraging performance.

We chose the model approach by Nye and Tinker (1977) to compute the rhizosphere volume around a root system. This purely physical model assumes continuous nutrient uptake by individual root segments. Gao et al. (1998) and Bouma et al. (2001), however, showed that root segment age is

inversely related to nutrient uptake capacity and that young roots therefore take up more nutrients than old roots. Inter-root competition is mainly caused by rhizosphere zone overlap of neighboring laterals, which are usually of similar age. Taking into account root segment age-dependent nutrient uptake rates would therefore alter absolute values of root foraging performance, but not our described qualitative relationships and trends.

This study improves the capacity of modelers to simulate realistic root systems, which can be used to investigate root-soil interaction processes. Further investigations could include research on parameters that were not the focus of this study, but also greatly influence root foraging performance such as number of axial roots, axial insertion angle and length and distribution of lateral roots. More information on root architecture parameters for a range of plant species would also be desirable. Increased knowledge on plastic root response to soil heterogeneity and environmental changes would further improve 3D root architecture modeling.

Chapter IV

Modeling the impact of biopores on root growth and root water uptake

This chapter is based on a journal article published as:

Landl, M., A. Schnepf, D. Uteau, S. Peth, M. Athmann, T. Kautz, U. Perkons, H. Vereecken, and J. Vanderborght. 2019. Modeling the Impact of Biopores on Root Growth and Root Water Uptake. Vadose Zone J. 18:180196. doi:10.2136/vzj2018.11.0196

4.1. Introduction

The ability of plants to extract water from the soil is referred to as 'plant water accessibility' and is determined by the architecture of the root system as well as by various interaction processes in the soil-plant continuum (Colombi et al. 2018). One of the most important constraints limiting plant water accessibility is soil penetration resistance with its direct impact on root elongation (Bengough et al. 2011). Soil penetration resistance is positively correlated with soil bulk density and the absolute value of the soil matric potential (Gao et al. 2012; Whalley et al. 2007). Higher soil penetration resistance leads to lower root growth rates and in consequence to less extended root systems with reduced ability to take up water from deeper soil layers (Bengough et al. 2011; Chen et al. 2014; Colombi et al. 2018; Tracy et al. 2012; Valentine et al. 2012). This is an issue in particular during prolonged dry spells when the upper soil layers are water-depleted and when subsoil water supply is of high potential value for plant transpiration (Gaiser et al. 2013; Kirkegaard et al. 2007).

An opportunity for roots to overcome compact soil layers and to grow into greater depths is the use of large-sized biopores (diameters >2 mm) as preferential growth pathways (Kautz 2015; McKenzie et al. 2009; Stirzaker et al. 1996). Biopores are generally vertically oriented, tubular shaped cavities in the soil formed by decayed plant roots or earthworm burrowing (Kautz 2015; Naveed et al. 2016). Their abundance depends on soil management and cropping sequence (Han et al. 2015; Kautz et al. 2010) and they can persist over many years in subsoil horizons below the plough layer (Edwards et al. 1988; Shipitalo et al. 2004). Higher soil compaction was found to increase the amount of roots growing in biopores (Gaiser et al. 2013; Hirth et al. 2005) and these roots were shown to elongate faster and deeper (Hirth et al. 2005; Stirzaker et al. 1996).

The probability of roots to remain within biopores and to continue growing along them was demonstrated to be higher if biopores were aligned more vertically (Dexter and Hewitt 1978; Hirth et al. 2005; Stirzaker et al. 1996) and if pore walls were smooth (Hirth et al. 2005; Stirzaker et al. 1996). Large-sized biopores are usually air-filled (Fredlund and Xing 1994) and root water uptake is thus limited to the contact area between root and biopore wall. In a field study, Athmann et al. (2013) observed that 85 % of barley and oilseed rape roots found in biopores maintained direct contact with the pore wall. Using analytical solutions, de Willigen et al. (2018) showed that incomplete radial root-soil contact (i.e. root

growing in pre-existing pore with larger diameter) hardly reduced root water uptake capacity due to compensatory root water uptake, while incomplete axial root-soil contact (i.e. entire axial root parts without soil contact) led to a significant decrease in root water uptake potential.

Direct measurements of the impact of biopores on root growth and root water uptake are difficult. Laboratory experiments (e.g. Hirth et al. 2005; Stirzaker et al. 1996) can give valuable information on the influence of soil structure on both root growth and root water uptake, but are limited to young plants, small pot sizes and short measurement intervals. Field experiments (e.g. Colombi et al. 2017; Kautz et al. 2013; White and Kirkegaard 2010) provide important insights on the dynamics of root growth in soil with biopores over entire cropping periods, but do not allow direct investigation of the influence of soil structure on root water uptake. Simulation models can thereby help to explain relations between experimental data (e.g. link water use efficiency with soil water content and bioporosity) and to test scenarios of different environmental and soil physical conditions. In recent years, significant progress has been made in the development of crop models, which are used to analyze the performance of cropping systems under variable climate and soil management conditions (Vereecken et al. 2016; Wöhling at al. 2013). These models, however, are usually based on simplifying assumptions such as uniform root distribution and homogeneous root water uptake in lateral soil horizons. The effect of soil structure is thereby at best taken into account indirectly via stress functions on root elongation (e.g. de Moraes et al. 2018, Gaiser et al. 2013). If the impact of biopores on model input parameters such as root length density development, root system hydraulic conductance and relative distribution of root water uptake is known, the effects of structured soil can be taken into account more accurately. We recently developed a new model approach for the simulation of root growth in structured soil. In this approach, the structure of the biopore network as well as the root architecture are considered in a spatially explicit way and the growth of individual root tips is described as a function of local soil penetration resistance. In test simulations, this model realistically reproduced root growth in artificial macropores on both the single root and the plant root system scale (Landl et al. 2017). Our model approach was incorporated in the three dimensional numerical R-SWMS model (Root soil water movement and solute transport) (Javaux et al. 2008) and is, to our knowledge, the first explicit 3D simulation model for root architecture development and root water uptake in soil with biopores.

Experimental studies showed that root growth in artificial macropores and naturally created biopores differs significantly: While Stirzaker et al. (1996) found roots to be trapped in straight vertical macropores created with steel rods, Kautz et al. (2013) observed field-grown roots to leave biopores when entering less compact soil layers. An explanation for this discrepancy is the wide range of geometries and orientations covered by naturally created biopores, which contrasts the generally straight and smooth appearance of artificial pores (Pagenkemper et al. 2015; Pagenkemper et al. 2013). For realistic simulations of root growth and root water uptake in structured soil, it is thus necessary to use realistic biopore networks. A possibility to non-invasively reproduce soil structure in three dimensions is X-ray computed tomography (X-ray CT) (Luo et al. 2008; Pagenkemper et al. 2015; Pagenkemper et al. 2013; Peth et al. 2008). A simplified reconstruction of the pore space geometry of X-ray CT-images can serve as a realistic description of the pore network in simulation models.

In the present study, we evaluated the impact of subsoil biopores on root growth, root water uptake, and root soil exploration in a simulation study using R-SWMS. Our model approach for root growth in structured soil is calibrated with extensive experimental field data. A natural biopore system is created using X-ray CT imaging of intact soil columns from the field site. We use the calibrated model to simulate scenarios in which we evaluate the impact of subsoil biopores on root growth and root water uptake under different soil physical and environmental conditions. To compute root water uptake, we use the model approach developed by Couvreur et al. (2012), which provides realistic parameters describing root system hydraulic conductance and relative distribution of root water uptake that can directly be used in 1D crop-scale models such as Hydrus (Cai et al. 2018; Šimůnek et al. 2016).

4.2. Material and Methods

4.2.1. Field experiment

The model setup is based on a field experiment, which was performed at the study site Klein Altendorf (University of Bonn, Germany, 50°62’ N, 6°98’ E) in 2010. In this experiment, the effect of varying biopore densities on root growth of spring wheat was investigated. The soil at the field site was classified as Haplic Luvisol (FAO-UN, 2014), which is characterized by a silt clay loam texture (4-7 % sand, 67-76 % silt, 17-29 % clay, 2.6-10 g kg^{-1} organic carbon). Below a plough horizon of 30 cm depth, the soil was well

structured with pronounced biopore networks originating from decayed plant roots as well as from earthworm activity (Kautz et al. 2014; Kautz et al. 2010).

After ploughing to a depth of 30 cm, spring wheat (*Triticum aestivum* L. 'Scirocco') was sown with a density of 400 grains m^{-2} and a row width of 10 cm on 8 April 2010. Root length densities (RLD) in both bulk soil and biopores were measured on 5 occasions with the profile wall method for both alfalfa and fescue pre-crop treatment (Boehm and Koepke 1977; Gaiser et al. 2013) (Table 4-1) down to a soil depth of 80 cm (first four occasions) respectively 160 cm (last occasion). It is well known that RLDs measured with the profile wall method underestimate actual RLDs (Gaiser et al. 2013). Using the calibration equation established by Gaiser et al. (2013) for this very same field experiment from reference measurements with auger samples, RLDs obtained with the profile wall method were converted to absolute RLDs:

$$RLD = RLD_{pw} \times (3.0092 + 13.5 \times e^{-7.2969 \times RLD_{pw}}), \quad (4.1)$$

where RLD is the absolute root length density (L L^{-3}) and RLD_{pw} (L L^{-3}) is the root length density measured with the profile wall method.

Leaf area index (LAI), which was needed to partition potential crop evapotranspiration into evaporation and transpiration, was measured with a LI-3100C Area Meter (LI-COR, Lincoln, USA) in the year 2010 on three occasions between seeding and mid-season as indicated in Table 4-1. To obtain the entire development of leaf area index from seeding to harvest, we additionally used measurements from the year 2012 when a second field trial adjacent to the first one with identical design was also cultivated with spring wheat.

To investigate the biopore system, eight intact soil columns (18 cm Ø, 55 cm height, 4 from alfalfa and 4 from fescue pre-crop treatment) were excavated from the subsoil (35-90 cm depth) with a lysimeter driller (UGT GmbH, Müncheberg Germany). They were scanned with an industrial X-ray CT scanner (v tome x 240, Phoenix X-ray, GE Sensing and Inspection Technologies GmbH, Wunstorf, Germany) and processed as described by Pagenkemper et al. (2015): Via segmentation, the obtained grey-scale images were transformed into highly resolved binary image stacks with a resolution of 231 µm displaying only biopore and soil matrix voxels. Using volume thresholding, disconnected pore volumes <0.2 cm^3 were

then eliminated to set the focus on the continuous biopore network. The upper parts of all binary image stacks showed unrealistic high bioporosities. This fault, which was also observed in other studies (e.g., Luo et al., 2008; Pagenkemper et al., 2013), is a result of the rotary cutting process used to cut the soil columns from the soil matrix during the excavation process. To obtain realistic biopore networks we thus eliminated the upper 15 cm of each image stack, thereby reducing the height to 40 cm. Due to the cylindrical shape of the excavated soil columns, the corner regions of the cubic image stacks did not contain biopores. We therefore cropped the outer edges of each image stack in both x- and y-direction from 18 cm to 12 cm.

In general, it is expected that taproot plants such as alfalfa generate large continuous biopore networks, while fibrous root systems such as fescue do not produce large biopores in the subsoil (Pagenkemper et al. 2015). Due to the presence of older biopore systems at our study site, however, differences in biopore networks between the two pre-crop treatments were not as pronounced as could be expected if the preceding crops were planted in homogenized soil (Pagenkemper et al. 2013). The similarity between biopore networks of different origin was also reflected in root length density measurements of spring wheat where we could not observe large differences between the different pre-crop treatments: A two-sample t-test showed that RLD in bulk soil after fescue pre-crop observed at different times and depths was in 9 % of all measurements significantly larger, in 35 % significantly lower and in 50 % not significantly different to RLD in bulk soil after alfalfa pre-crop. RLD in biopores was significantly different in only 4 % of all measurements after different pre-crop treatments. For modeling purposes, these differences were not sufficiently pronounced. For both biopore network reconstruction and RLD measurement data we therefore did not distinguish between different pre-crop treatments, but used them as replicates.

Table 4-1: Dates of RLD and LAI measurements of spring wheat in 2010 and 2012, days after sowing (DAS) and- if known- growth stages according to the BBCH scale (Lancashire et al. 1991)

Measurement no.	RLD measurements		LAI measurements			
	Date	DAS/BBCH	Date	DAS/BBCH	Date	DAS/BBCH
1	31/05-02/06/2010	53–55/ 33	31/05/2010	53/ 33	28/05/2012	50/-
2	14/06–17/06/2010	67–70/ 55-58	15/06/2010	68/ 56	13/06/2012	65/-
3	28/06-30/06/2010	81–83/ 68	30/06/2010	83/ 68	26/06/2012	78/-
4	13/07–16/07/2010	96–99/ 83			09/07/2012	91/-
5	27/07–30/07/2010	110-113/ 89			30/07/2012	112/-

4.2.2. Modeling theory

We used the three-dimensional numerical R-SWMS model (Root-Soil Water Movement and Solute Transport) developed by Javaux et al. (2008) to simulate the impact of biopores on root growth, soil water flow and root water uptake. The equations and assumptions underlying this mechanistic model as well as the used sub-models are presented in the following section.

Simulation of root system development

Root system development is explicitly represented in three dimensions using the model approach by Clausnitzer and Hopmans (1994). In this approach, the root system is described by a set of user-defined input parameters that determine plant-specific properties such as unimpeded growth speed, branching angles, root trajectory development and distance between two successive lateral roots. In addition to these root system-inherent parameters, environmental impact factors on root system development were considered.

The influence of varying soil strength as well as biopores on root system development is taken into account with the approach by Landl et al. (2017). In this approach, biopores are regarded as an additional soil material with very low penetration resistance. Soil mechanical resistance is expressed by its inverse, soil mechanical conductance, and is handled in analogy to hydraulic conductivity in Darcy's law. Differences in soil strength between the biopore and the soil matrix lead to anisotropic or direction dependent soil mechanical conductance, which is larger in the direction of the main axis of the biopore

and smaller in the radial direction. This anisotropy influences both the direction of root growth and the root growth rate. The orientation of an individual root segment *d* is computed as

$$d = k \times F, \tag{4.2}$$

where *k* is the three-dimensional soil mechanical conductance tensor that represents the ease with which a root can penetrate the soil and *F* is a driving force, which is determined by the orientation of the previous root segment, a random deflection angle and a tropic component.

It is generally assumed that root elongation *E* (L T^{-1}) is at its maximum at zero soil penetration resistance and stops completely when a maximum soil penetration resistance R_{max} (P) is reached (Bengough and Mullins, 1990). We use the empirical equation developed by Veen and Boone (1990) to calculate R_{max} as a function of soil matric potential ψ_m as:

$$R_{max} = 4exp^4 + 2.33\psi_m. \tag{4.3}$$

where R_{max} and ψ_m are expressed in hPa. It must be noted that this equation was originally developed for maize root growth on sandy loam. However, considering that wheat and maize show similar root growth pressures (Clark et al. 2003) and that the computed values of R_{max} fall well within the range of measured values of R_{max} specified by Ehlers et al. (1983) for silt loam, we consider this equation valid for our modeling purposes.

Experimental studies on the evolution of root elongation between zero and maximum soil penetration resistance frequently observed a strong initial decrease that was followed by a lower reduction rate when approaching maximum soil penetration resistance (Bengough et al. 2011; Bengough and Mullins 1990; Taylor and Ratliff 1969). We described this relationship between elongation rate and soil penetration resistance with the inverse of a polynomial relation as

$$E = E_{max} \times \left(1 - (R/R_{max})^{\frac{1}{2}}\right), \tag{4.4}$$

where E and E_{max} are actual and maximum elongation rate (L T^{-1}) and R and R_{max} are actual and maximum soil penetration resistance (P). Soil penetration resistance R (hPa) was computed as a function of bulk density ρ_b (g cm^{-3}), soil matric potential ψ_m (hPa) and effective saturation S_e (-) using the empirical pedotransfer function developed by Whalley et al. (2007) as

$$\log_{10}(R \times 10^{-1}) = 0.35 \times \log_{10}(|\psi_m \times 10^{-1}| \times S_e) + 0.93 \times \rho_b + 1.26. \quad (4.5)$$

This pedotransfer function was developed for 12 different, undisturbed soils with diverse matric potentials as well as with varying texture, organic carbon content and bulk density (1.2-1.65 g cm^{-3}) and can thus be considered valid for a wide range of different soils. It must be noted that soil texture is considered indirectly via effective saturation in this equation.

In addition to soil strength, also soil temperature is considered to limit root elongation. It was shown that root growth only occurs if soil temperature lies within a plant and genotype specific interval and reaches a maximum at a defined optimum soil temperature (Koevoets et al. 2016; Porter and Gawith 1999). In our model, reduced root elongation due to sub- or supra-optimal soil temperature is described by a sine-wave shaped impedance function, which equals zero at the lower (2 °C) and upper (25 °C) limit and one at the optimum (15 °C) soil temperature (Somma et al. 1998). Minimum, maximum and optimum soil temperature values for spring wheat root growth were derived from Porter and Gawith (1999).

Simulation of water flow in the soil and root water uptake

Water flow in the soil is driven by gradients of soil water potential and described by the Richards' equation (Richards 1931):

$$\frac{\partial \theta}{\partial t} = \nabla[K \nabla \psi] - S, \quad (4.6)$$

where θ is the volumetric water content (L^3 L^{-3}), t is the time (T), K is the unsaturated hydraulic conductivity (L^2 P^{-1} T^{-1}), ψ is the total soil water potential (matric + gravitational) (P) and S is a sink term (L^3 L^{-3} T^{-1}), which is defined positive for root water uptake and negative for root water release.

The relationships between soil water content θ ($L^3\ L^{-3}$), matric potential ψ_m (P) and hydraulic conductivity K ($L^2\ P^{-1}\ T^{-1}$) are calculated from soil hydraulic properties via the closed-form expression established by Mualem (1976) and Van Genuchten (1980) as

$$\theta(\psi) = \theta_r + \frac{\theta_s - \theta_r}{(1+(\alpha|\psi_m|)^n)^m}, \tag{4.7}$$

and

$$K(\psi) = K_s \frac{\left\{1-(\alpha|\psi_m|)^{n-1}[1+(\alpha|\psi_m|)^n]^{-m}\right\}^2}{[1+(\alpha|\psi_m|)^n]^{\frac{m}{2}}}, \tag{4.8}$$

where θ_r ($L^3\ L^{-3}$) is the residual water content, θ_s ($L^3\ L^{-3}$) is the saturated water content, α is related to the inverse of the air entry suction (P^{-1}), n and m are shape parameters with $m=1-1/n$ and K_s is the saturated hydraulic conductivity ($L\ T^{-1}$).

Due to the large size of our root system (>50,000 root segments), it was computationally not feasible to compute water flow between soil and root system on the root segment level as proposed by Doussan et al. (1998). We therefore used the implicit approach by Couvreur et al. (2012), where root water uptake is computed on the soil element level, which drastically reduces computation time. In this approach, hydraulic conductances of individual roots are summarized to a single equivalent root system hydraulic conductance, while spatially heterogeneous soil-root interface water potentials are combined to a single equivalent soil water potential (SWP) sensed by the plant. The sink term of an individual soil element is computed as

$$S_k \times V_k = K_{rs} \times \left(\psi_{s,eq} - \psi_{col}\right) \times SSF_k + K_{comp} \times \left(\psi_{s,k} - \psi_{s,eq}\right) \times SSF_k, \tag{4.9}$$

where S_k ($L^3\ L^{-3}\ T^{-1}$) is the sink term in the k^{th} soil element, V_k (L^3) is the volume of the k^{th} soil element, K_{rs} ($L^3\ P^{-1}\ T^{-1}$) is the equivalent conductance of the root system, $\psi_{s,eq}$ (P) is the equivalent total (matric + gravitational) SWP sensed by the plant, ψ_{col} (P) is the total (matric + gravitational) water potential at the root collar, SSF_k (-) is the standard sink fraction of the k^{th} soil element, K_{comp} ($L^3\ P^{-1}\ T^{-1}$) is the compensatory root water uptake conductance, and $\psi_{s,k}$ (P) is the SWP of the k^{th} soil element. While the

first term of the equation describes the standard root water uptake under homogeneous SWP distribution, the second term accounts for SWP heterogeneity. The parameters *SSF*, K_{rs} and K_{comp} were introduced by Couvreur et al. (2012) as the three macroscopic parameters, which describe the hydraulic architecture of a root system: *SSF* specifies for each soil element the amount of water taken up by the root segments located within this soil element as a fraction of the total plant water uptake under homogeneously distributed SWP, K_{rs} describes the water flow per unit of water potential difference between root collar and soil and K_{comp} defines the extent of compensatory root water uptake within individual soil elements due to water potential heterogeneity within the soil domain. These macroscopic parameters remain constant for root systems with static architecture and constant hydraulic properties. The parameters *SSF* and K_{rs} were determined from the numerical solution of the hydraulic tree approach by Doussan et al. (1998), which was run for one single time step. K_{comp} was assumed to equal K_{rs}. This is a valid assumption if root axial hydraulic conductances substantially exceed root radial hydraulic conductances (Couvreur et al. 2012), which is the case for cereal root systems (Meunier et al. 2018).

The equivalent SWP sensed by the plant, $\psi_{s,eq}$, is computed as a function of the distribution of local SWPs as well as standard sink fractions as

$$\psi_{s,eq} = \sum_{k=1}^{M} \psi_{s,k} SSF_k, \tag{4.10}$$

where *k* is the index of soil elements ranging from 1 to M. For soil elements that do not contain any root segments, SSF_k equals zero. It must be noted that equation (4.9-4.10) rely on the assumptions that SWP within one soil element is constant and that root radial conductances are much smaller than root axial conductances.

The water potential at the root collar ψ_{col} (P) is assumed to be equal to the leaf water potential and the flux at the root collar is set to the actual transpiration rate T_{act} ($L^3\ T^{-1}$). When no water stress is present, i.e. when the water potential at the collar is above a specified threshold value ψ_{lim}, T_{act} is equal to the potential transpiration rate T_{pot} ($L^3\ T^{-1}$). Under water stress, T_{act} falls below T_{pot} and is computed as

$$T_{act} = K_{rs} \times \left(\psi_{s\,eq} - \psi_{lim}\right), \tag{4.11}$$

where ψ_{lim} (P) is the minimal water potential at the root collar, which triggers stomatal closure due to water stress and which was set to the constant value of -15,000 hPa (permanent wilting point).

4.2.3. Numerical solution of the R-SWMS model

For the numerical solution of the water flow equation in R-SWMS, the soil domain is discretized in a regular cubic grid of nodes. Soil hydraulic state variables (e.g. soil water potential and soil water content) as well as parameters that describe local soil properties (e.g. bulk density) are specified explicitly for each soil node. Eight adjacent soil nodes then define one soil element whose average state variables and parameters are calculated from the nodal values. The root system, which consists of a multitude of straight root segments that are connected with each other, develops within this soil grid. Length and orientation of newly emerging root segments are influenced by the properties of the soil element in which the root tip is located. The resolution of the soil grid is chosen according to the size of the soil domain as well as the length of the simulation period, the required preciseness of the results and the available computation time. For simulations on the root system-scale, the solution of water flow in the soil is computationally expensive due to large soil domains (>1m depth) and the long periods that are simulated (up to several months). This makes it necessary to choose a relatively coarse grid resolution (cm scale). For simulations of root system development in response to small-scale soil structures such as biopores, however, a finer grid resolution must be used (mm scale). We reconciled these opposing needs by introducing two soil grids: a fine soil grid in which biopores were represented and which was used for the simulation of root system development and its architectural response to environmental impact factors and a coarse grid, which was used to compute soil water flow, but did not represent biopores. It must be noted that the influence of biopores on soil water flow was therefore neglected. Different soil layers as well as all further soil properties were represented in both grids. Soil water potential distribution, which was computed in the coarse grid, was transferred to the fine grid, where it influenced root system development via its effect on soil penetration resistance.

Coupling root growth and root water uptake

Root water uptake is computed using root hydraulic architecture parameters (K_{rs}, K_{comp} and *SSF*) that are defined initially for a root system with specific root architecture and root segment hydraulic parameters. If the root system changes, these root hydraulic architecture parameters need to be updated. Root

system development is computed dynamically at each time step as a function of local soil properties such as soil penetration resistance, which is a function of soil matric potential (equation (4.5)) and thus also of root water uptake. We took these interdependencies into account by coupling root growth with root water uptake: After specified time intervals, the root growth model was given the updated soil water potential distributions within the soil domain, while root hydraulic architecture parameters were recalculated for the updated root system.

Assumptions in the simulation of root growth and root water uptake in soil with biopores

A root segment was considered to be located within a biopore if a minimum of one node of its surrounding grid nodes had biopore properties. Considering that root length units in the profile wall method had an equivalent length of 0.5 cm (Perkons et al. 2014), lateral roots in biopores were only counted if more than 0.5 cm of their length was located within a biopore. We neglected water flow in biopores, which were thus assumed to be air-filled at all times. Partial root-soil contact in biopores was assumed to inhibit water flow between soil and root and thus to decrease root radial hydraulic conductivity. Root radial hydraulic conductivity was therefore considered proportional to the part of the root in contact with bulk soil i.e. the number of surrounding grid nodes with bulk soil properties. Bulk density of biopore nodes was set equal to zero.

4.2.4. Model setup

The basic model setup was based on and calibrated with data from the experimental field study i.e. root length densities, soil properties, climate data and leaf area index.

Soil parametrization

We used a rectangular shaped soil domain with dimensions of 3 x 10 x 160 cm. The dimensions in x and y direction corresponded to inter-plant and inter-row distances, respectively, the dimension in z-direction to the maximum measured rooting depth (Perkons et al. 2014). The soil domain was discretized into two regular cubic grids of nodes with resolutions of 1 cm and 0.5 cm for the coarse and fine soil grid, respectively. Our simulated biopores therefore had rather large diameters >0.5 cm. The soil domain was divided horizontally into five different soil layers (1 topsoil layer, a mixing zone between top- and subsoil and 3 subsoil layers) whose extents and soil properties were derived from the reference field site profile

described in Barej et al. (2014). Using the information on soil texture and bulk density, we estimated soil hydraulic properties by means of the pedotransfer functions developed by Tóth et al. (2015) that were established for continental-scale applications in Europe (Table 4-2).

Table 4-2: Soil properties used in the model setup

			Texture				Soil hydraulic parameters according to Van Genuchten (1980)†				
	Horizon	Depth	Sand	Silt	Clay	Bulk density	Θr	Θs	α	n	Ks
		(cm)	——— (%) ———			(g cm^{-3})	(-)	(-)	(hPa^{-1})	(-)	(cm d^{-1})
Topsoil	Ap	0-30	7	76	17	1.29	0.041	0.4857	0.0103	1.2767	5.08
Mixing zone	E/B	31-40	5	75	20	1.32	0.041	0.4778	0.0056	1.2990	1.56
subsoil	Bt1	41-75	5	68	27	1.42	0.041	0.4502	0.0047	1.2691	1.31
	Bt2	76-115	4	67	29	1.52	0.041	0.4223	0.0041	1.2468	1.20
	Bw	116-160	6	74	20	1.46	0.041	0.4381	0.0050	1.2732	1.62

Ap…distinct topsoil disturbed by ploughing, E/B…eluviated mineral horizon, Bt…argillic horizon, Bw…weathered B-horizon, †θr, residual water content; θs, saturated water content;α and n, shape parameters; Ks, saturated hydraulic conductivity

From an earlier study by Kautz et al. (2010) we obtained soil penetration resistance measurements that were determined on 10 sampling points on the same field site in Klein-Altendorf on plots grown with sugar beet, winter wheat and winter barley down to a depth of 80 cm with a penetrologger when the soil was at field capacity. In Fig. 4.1, we compared these measurements with soil penetration resistance values predicted with equation (4.5) for the top four soil layers defined in Table 4-2. It was not possible to predict the exact measured values; the general evolution of soil penetration resistance with depth, however, could be well reproduced and we thus consider equation (4.5) to be suitable for our modeling purposes.

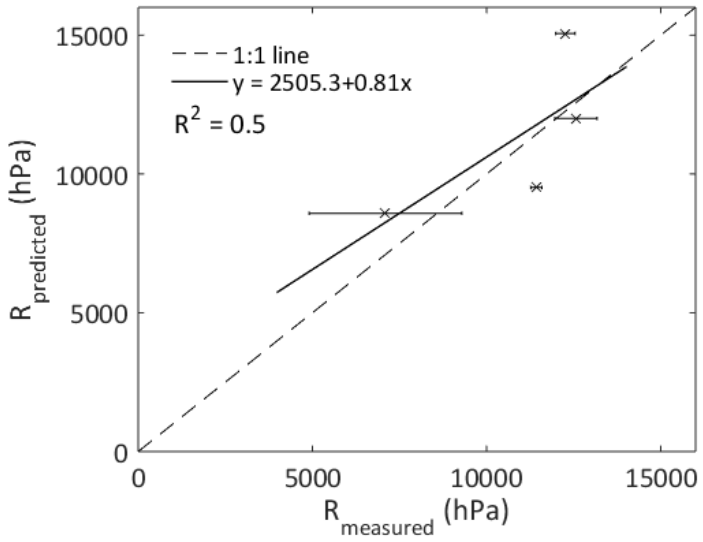

Fig. 4.1: Measured versus predicted soil penetration resistance for the individual soil layers of our study site (Table 4-2) at field capacity, error bars represent the standard deviation of measurements within one soil layer

Setup of the biopore network

The biopore networks used in our simulation study were created with the help of the highly resolved binary image stacks. Before using these high-resolution image stacks to set up our simulation biopore network, they had to be up-scaled to 0.5 cm, which was the discretization of our fine soil grid. Considering that a significant amount of biopores in the original image stacks had diameters smaller than the resolution of our fine soil grid, simple up-scaling would have resulted in a strong overestimation of the biopore volume. To satisfy our priority objective of conserving biopore network connectivity, while keeping the overestimation of biopore volume at a minimum, we applied the following technique: In a first step, we skeletonized the 8 binary image stacks with the help of the open source software ImageJ, which allowed iterative and symmetric eroding of the biopore surface around its center line. Examples of original and skeletonized images are shown in Fig. 4.2a and Fig. 4.2b. In a second step, we reduced the resolution of the 8 skeletonized images from 231 µm to 0.5 cm (discretization of the simulation domain). If at least one of the original voxels located within the sphere of influence of an up-scaled voxel had

biopore properties, the up-scaled voxel was also assigned biopore properties; an example is given in Fig. 4.2c. From these 8 image stacks, we then cut 12 sub-stacks with 40 cm depth and a cross-sectional area of 3 x 10 cm to obtain images whose size corresponds to the dimensions of our soil domain (example in Fig. 4.2d). The number of sub-stacks cut from each image stack as well as the location of the cuts was determined with the objective of obtaining clear, continuous biopore networks.

To quantify the modifications of the biopore systems that occurred due to up-scaling and image cutting, we determined for the different process steps the pore network parameters bioporosity and biopore length density. Bioporosity ($L^3\ L^{-3}$) is defined as the volume of biopores per volume of bulk soil; biopore length density ($L\ L^{-3}$) is determined as the total length of biopores in a unit soil volume (Luo et al. 2008; Pagenkemper et al. 2013). The up-scaling process combined with the assignment of biopore properties to up-scaled voxels with at least one original voxel with biopore properties within their vicinity led to an increase in bioporosity from approximately 1.4 to 5 % (Image state 1-2; Table 4-3). Bioporosity then again increased to 10 % from the up-scaled image stacks to the cut sub-stacks (Image state 2-3; Table 4-3). This increase, however, was not caused by any image processing, but by preserving those parts of the image stacks that contained clear, continuous biopore networks. In contrast to bioporosities, biopore length densities could be kept fairly constant throughout all process steps: While the up-scaling process led to a small decrease in biopore length density from 0.064 to 0.038 cm cm^{-3}, the cropping of the sub-stacks again increased it to 0.086 cm cm^{-3}. These values correspond well to the range of 0.06 to 0.09 cm cm^{-3} that was found by Pagenkemper et al. (2013) for biopore networks of soil monoliths taken from the same field site with the same pre-crops. It must be noted that the number of biopores remained the same throughout the image processing.

In a last step, we translated the information from the image stacks to 3D coordinate grids by assigning biopore properties to each grid node corresponding to a biopore voxel. Observations from the field experiment showed that root growth in biopores mainly occurred in the subsoil in depths >30 cm. This can be explained by the topsoil cultivation with a plough, which leads to a reduction in the number of large-sized biopores with simultaneous soil loosening, which again facilitates root proliferation in the bulk soil (Dal Ferro et al. 2014; Edwards et al. 1988; Golabi et al. 1995; Holland 2004). In our simulations, we therefore only considered biopores in the subsoil. Considering that anecic earthworms can burrow as deep as 2.5 m under favorable conditions (Kobel-Lamparski and Lamparski, 1987), biopores were

considered to exist in the complete subsoil profile. To obtain biopores over the entire subsoil depth of 130 cm (Table 4-2), we inserted each biopore coordinate system 3.25 times one below the other into the soil grid, which resulted in 12 soil domains with individual biopore networks. Continuity of the biopore network across the connection of two biopore coordinate systems was obtained by vertically flipping one of the coordinate systems so that always either two top or two bottom ends were connected to each other (example in Fig. 4.3).

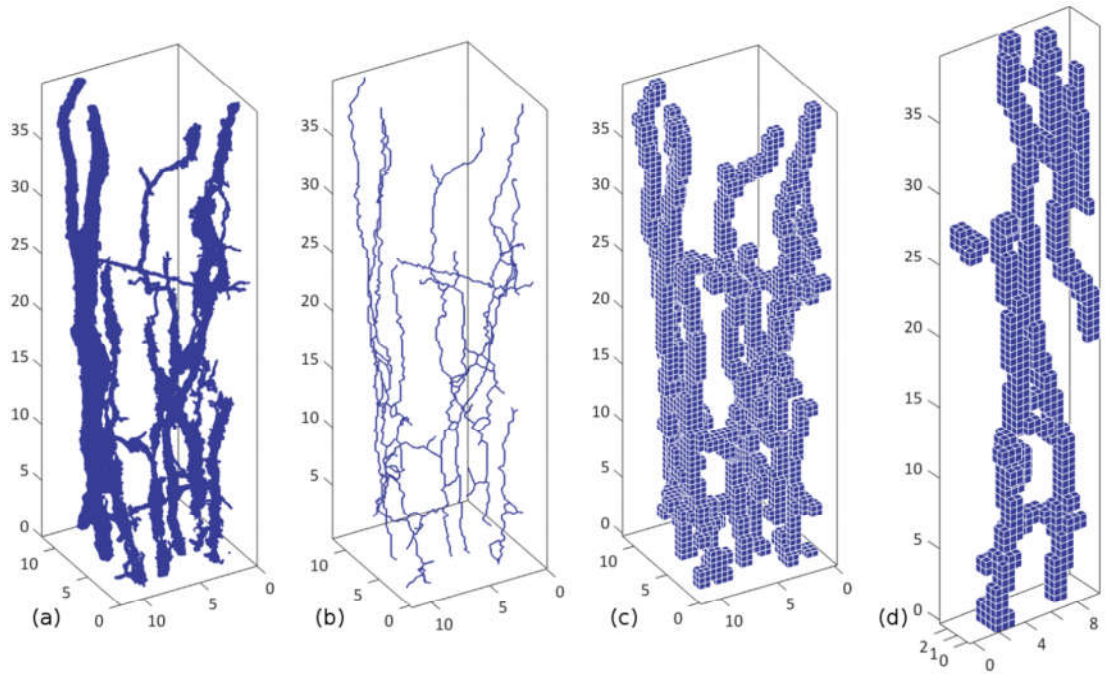

Fig. 4.2: Examples for binary image stack with a resolution of 231 µm (a), skeletonized image stack (b), image stack with a resolution of 0.5 cm (c), sub-stack with cross-sectional dimensions of soil domain (d)

Table 4-3: mean and standard deviations (std) of bioporosities (bps) as well as biopore length densities (BPLDs) for images of different processing steps

Image state	Image description	Mean bps	Std of bps	Mean BPLDs	Std of BPLDs
		——— (%) ———		——— (cm cm^{-3}) ———	
1	Binary image stacks with resolution of 231µm	1.42	0.54	0.064	0.016
2	Up-scaled image stacks with resolution of 0.5cm	5.04	2.05	0.038	0.016
3	Sub-stacks with resolution of 0.5cm cropped to cross-sectional dimensions of soil domain	10.21	2.76	0.086	0.022

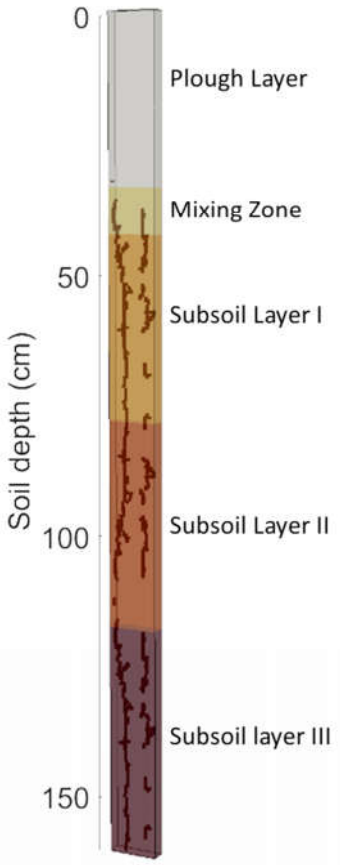

Fig. 4.3: Soil domain with 5 different soil layers (Table 4-2) and subsoil biopore system

Root hydraulic properties

We used the values of root hydraulic properties of wheat specified by Couvreur et al. (2014a), which are based on experimental measurements by Bramley et al. (2007), Sanderson et al. (1988), Tazawa et al. (1997) and Watt et al. (2008). Values for different root types as well as their variations with root age are represented in Fig. 4.4a and Fig. 4.4b for axial and lateral roots, respectively. Root hydraulic properties are key drivers of root water uptake by controlling the amount of water that can be transported from the soil to the root collar at a given time. They thus also substantially influence the model parameters root system hydraulic conductance and relative distribution of root water uptake, which are used in the model approach by Couvreur et al. (2012).

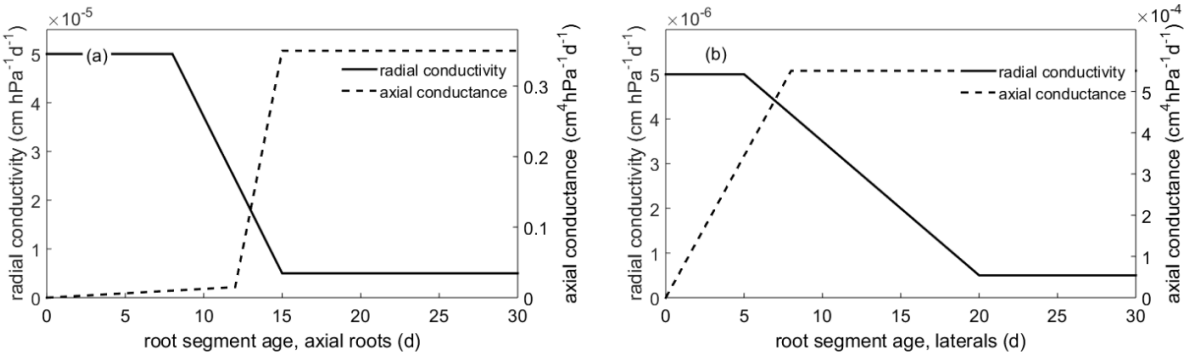

Fig. 4.4: Root hydraulic properties of spring wheat for (a) axial and (b) lateral root segments

Boundary conditions for the simulation of soil water flow, root system development and root water uptake

The boundary conditions at the top and bottom of the soil domain were set to time variable flux and unit hydraulic gradient, respectively. The time variable flux at the top boundary was calculated from the daily climatic water balance, which is defined as the difference between precipitation and evaporation. Additionally, we considered transpiration from the root collar. The simulation runtime was set to 112 days i.e. the whole cropping cycle of spring wheat. Daily precipitation measurements were obtained from the climate station Klein Altendorf; daily potential reference evapotranspiration ET_0 was estimated with the Penman-Monteith equation (Allen et al. 1998) from temperature, wind speed, relative humidity

and radiation measurements that were also obtained from the climate station Klein-Altendorf. Potential crop evapotranspiration ETc_{pot} (L T^{-1}) was estimated from ET_0 (L T^{-1}) using the single crop coefficient approach (Allen et al. 1998):

$$ETc_{pot} = k_c \times ET_0, \tag{4.12}$$

where k_c (-) is the crop coefficient. Crop coefficient values for spring wheat were derived for each crop stage (initial stage, mid-season, late stage) from Allen et al. (1998) and are 0.3 for the initial period (8 Apr.-14 May 2010), 1.15 for midseason (9 June-15 July 2010), and 0.25 for the late stage (16-31 July 2010). Potential crop evapotranspiration was partitioned into evaporation and transpiration based on Beer's law, which uses canopy interception to separate solar radiation from the total energy budget (Ritchie et al. 1997; Klosterhalfen et al. 2017):

$$T_{pot,daily} = ETc_{pot} \times \left(1 - e^{-k\,LAI}\right), \tag{4.13}$$

$$E_{pot,daily} = ETc_{pot} \times e^{-k\,LAI}, \tag{4.14}$$

where $T_{pot,daily}$ and $E_{pot,daily}$ are daily potential transpiration and evaporation fluxes (LT^{-1}), respectively, LAI is the leaf area index, which was measured in the field experiment (Table 4-1) and k is a constant governing the radiation extinction by the canopy (-) as a function of sun angle respectively plant and leaf distribution (following Mo and Liu (2001) we used k=0.6). Fig. 4.5a shows precipitation, potential evaporation and transpiration as well as LAI over the whole simulation period 2010. To obtain transpiration from the root collar, daily potential transpiration was multiplied with the surface area of the soil domain (30 cm²). Following the approach by Couvreur et al. (2014a), we considered daily sinusoidal variations in $T_{pot,daily}$ using the expression

$$T_{pot}(t) = T_{pot,daily}\left(sin\left(\frac{2\pi t}{24} - \frac{\pi}{2}\right) + 1\right), \tag{4.15}$$

where t (h) is the time after midnight.

As mentioned above, root growth was considered to be a function of soil temperature. Daily soil temperature values in five different depths (0 cm, 5 cm, 10 cm, 20 cm and 50 cm) were obtained from the German weather service (DWD 2017) as well as from the climate station Klein-Altendorf; soil temperature patterns over the simulation period are shown in Fig. 4.5b.

To mimic field conditions, we assumed periodic boundaries in horizontal direction for root growth, soil water flow and root system fluxes. In that way, simulated roots respectively water fluxes that exit the soil domain on one side simultaneously enter it on the opposite side. The computation time step of the root growth model is constant and was set to 0.16 d, which is just small enough so that the maximum possible size of a root segment does not exceed one grid side length. The computation time step of the soil water flow model was set to 10^{-1} d. This time step, however, is adjustable and can be reduced to a minimum value of 10^{-5} d if no convergence is reached. Root growth and root water uptake models were provided with updated root systems respectively SWP distributions within the soil domain every day during the first 10 days of simulation when root systems changed rapidly due to large initial elongation rates and every 5 days from day 11 to day 112, the last day of simulation. As initial conditions, the matric potential in the soil domain was set to hydrostatic equilibrium with -400 hPa at the top boundary.

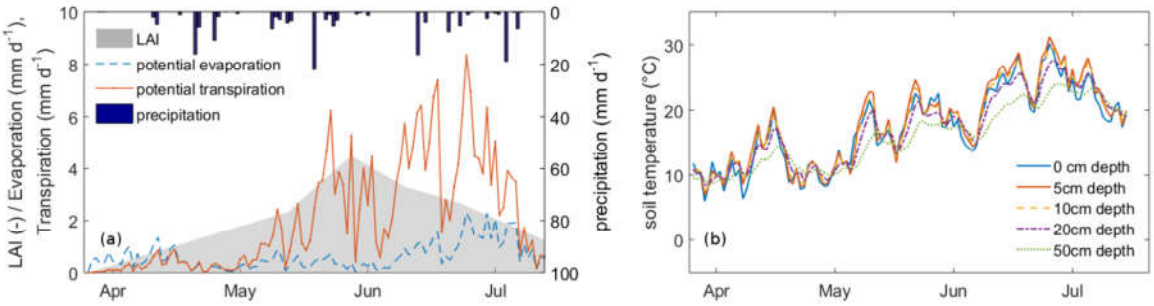

Fig. 4.5: (a) Leaf area index (LAI) for spring wheat, potential evaporation, potential transpiration, precipitation and (b) soil temperature at five different depths over the whole simulation period from 8 April 2010 to 30 July 2010

4.2.5. Model calibration

We used the model set-up derived from the experimental field measurements as well as our 12 different biopore networks to simulate root systems over the entire cropping season of 112 days from 8 April 2010 to 30 July 2010. To obtain realistic root system architectures, we optimized our root growth model input parameters so that simulated and experimentally observed RLDs in both bulk soil and biopores corresponded to each other. To indicate the quality of fit between observed and simulated RLDs, we computed Pearson's correlation coefficient R as well as the relative root mean square error (rRSME). While R is a measure of the statistical relationship between observed and simulated RLD, rRMSE defines the relative differences between observed and simulated RLD values (Loague and Green 1991). The parameter rRMSE was computed as

$$rRSME = \left[\frac{1}{n}\sum_{i=1}^{n}\left(RLD_{sim,i} - RLD_{obs,i}\right)^2\right]^{1/2} \times \frac{100}{\overline{RLD_{obs}}}, \quad (4.16)$$

where n is the number of RLD measurements in depth and RLD_{sim} and RLD_{obs} are simulated and observed RLDs, respectively. For the optimization procedure, we selected those five input parameters, which had the greatest impact on root length density variation: While number, emergence time and initial growth rate of axial roots are the major determinants of total root length density, sensitivity to gravitropism as

well as root tortuosity define the distribution of root length density within the soil profile. Additionally, we optimized the parameter 'conductance in the macropore', which defines the degree of anisotropy of penetration resistance in the soil elements containing biopore walls and affects the probability of a root to continue growing within a biopore or to re-enter the bulk soil (Landl et al. 2017). The values of the optimized parameters were in the same orders of magnitude as standard values found in literature. All remaining root growth model input parameters were derived from literature. Parameter values, literature sources and literature-derived ranges for optimized parameters are indicated in the appendix in Table 6-1.

4.2.6. Setup of simulation scenarios

The initial model setup was based on measurements from the field experiment. For a more general evaluation of the impact of subsoil biopores on root growth and root water uptake under varying environmental and soil physical conditions, we additionally set up 5 different simulation scenarios:

Scenario I, Presence of subsoil biopores: To get a better understanding of the impact of biopores on root system development and root water uptake, we performed simulations with and without subsoil biopores.

Scenario II, Subsoil bulk density: The importance of biopores as root growth pathways typically increases with soil compaction. We therefore additionally performed simulations with subsoil bulk density that was increased to 1.65 g cm^{-3}.

Scenario III, Influence of partial root-soil contact on radial root hydraulic conductivity: It was suggested that root hairs may bridge the gap between soil and roots in biopores so that partial root soil contact does not reduce root radial hydraulic conductivity (Carminati et al. 2013; Wasson et al. 2012). This aspect was taken into account by additional simulations with unlimited root radial hydraulic conductivity in biopores.

Scenario IV, Soil type: Typically, roots use biopores as preferential growth pathways to reach water resources in greater depths. Subsoil water availability, however, depends on the soil type. Apart from the original silt loam, we therefore also performed simulations with sandy loam. While silt loam is characterized by a relatively high water holding capacity and hydraulic conductivity for a wide range of

soil matric potentials, sandy loam is highly conductive close to saturation, but rapidly becomes resistive to water flow when soil water potential decreases. These differences in soil hydraulic properties also lead to differences in SWP distributions in the soil domain, which in turn affect root system development. Water retention curves and soil hydraulic parameters used in our simulations are shown in the appendix in Fig. 6.1, Table 6-2 and Table 6-3.

Scenario V, Climate conditions: We performed additional simulations with climate data from the year 2012 measured at the same reference field site in Klein-Altendorf, Germany. Like in 2010, the field plots were planted with spring wheat and we used measured LAI values to partition evapotranspiration into evaporation and transpiration. We used the crop coefficient values from the basic setup from the year 2010. As compared to 2010, the year 2012 was less dry, especially towards the end of the cropping season.

Using the optimized root architecture parameters, we simulated root growth and root water uptake for all possible combinations of soil physical and environmental conditions. Altogether, we carried out simulations with 24 different setups, which is the factorial combination of 3 types of soil structure (BPs with limited hydraulic conductivity, no BPs and BPs with unlimited hydraulic conductivity), 2 different soil bulk densities, 2 soil types and climate data of 2 different seasons. For each of these setups we ran simulations with all 12 different biopore systems; for combinations without biopores, 12 replicate simulations were performed. Altogether we therefore carried out 24x12=288 different simulations.

4.3. Results

4.3.1. Comparison of observed and simulated root systems

Simulated root length density (RLD) profiles could be well fitted to measured ones for all five observation dates via optimization of root growth model input parameters (Fig. 4.6). While the agreement between simulated and measured RLD profiles was quite good for root growth in bulk soil (R=0.84-0.94, rRMSE=30-53 %), less consistency was reached for the highly variable RLD profiles of root growth in biopores where R was partly negative and rRMSE values were larger (R=-1-0.86, rRMSE=43-142 %). On the last measurement date, 46 % of observed and 41 % of simulated spring wheat RLD was accumulated in the topsoil and thus 54 % and 59 % in the subsoil. The share of subsoil RLD in biopores relative to total

subsoil RLD at the last day of measurement amounted to approximately 10 % in observations and 9 % in simulations. Considering that mean subsoil bioporosities in the simulation domain amount to approximately 10 % (Table 4-3), this value appears very low; however, it must be noted that simulated lateral roots, which constitute the largest part of RLD, are generally not located within biopores due to plagiotropism (tendency to bend horizontally). If only axial roots are considered, the simulated share of subsoil RLD in biopores relative to total subsoil RLD amounts to 24 %, which shows that simulated roots predominantly did use biopores as preferential growth paths. Observed and simulated maximum RLD in biopores within one soil layer of 10 cm depth was similar with values of 0.28 and 0.26 cm cm^{-3} that were recorded at DAS 68 and DAS 112. The maximum share of RLD in biopores relative to total RLD within one soil layer of 10 cm depth amounted to 25 % and 13 % for observations and simulations, respectively; if only axial roots are considered, the simulated share increases to 40 %.

Experimentally observed RLD profiles show that topsoil layers also contain a low share of roots growing in biopores. Our simulations could not reproduce these observations because biopores were only considered in the subsoil. Between two-node and dough stage (DAS 54–DAS 97), simulated rooting depths were larger than experimentally observed ones because root length densities were only measured down to a depth of 80 cm. At the first four measurement dates, experimentally observed RLDs in biopores were substantially larger than simulated RLDs in biopores. This is due to inconsistencies in observed biopore RLDs: Summed up over all depths, observed RLDs in biopores were larger at DAS 68 than 6 weeks later at DAS 112, even though RLDs in bulk soil increased with time. In our simulations, however, RLDs in biopores obviously increased with increasing RLDs in the bulk soil. Considering that for each point in time a new soil profile is used to count roots with the profile wall method, these inconsistencies in observed RLDs can be regarded as the natural variability of root growth in biopores.

Simulated roots generally showed lower RLD in the uppermost topsoil layer. This is a model artefact, which is caused by our assumption of constant gravitropism for axial roots. Axial roots that emerge from the seed therefore immediately start bending towards the vertical and do not spread out horizontally. Our simulations also failed to reproduce the observed increase in topsoil RLD until flowering (DAS 82) and the decrease thereafter because our root architecture model does not take into account root decay. However, considering that our main interest was root growth behavior in the subsoil, these deviations can be regarded as negligible.

The optimized values of root growth model input parameters, which were used for further root architecture simulations, were all within the range of values found in literature and are listed together with reference sources in the appendix.

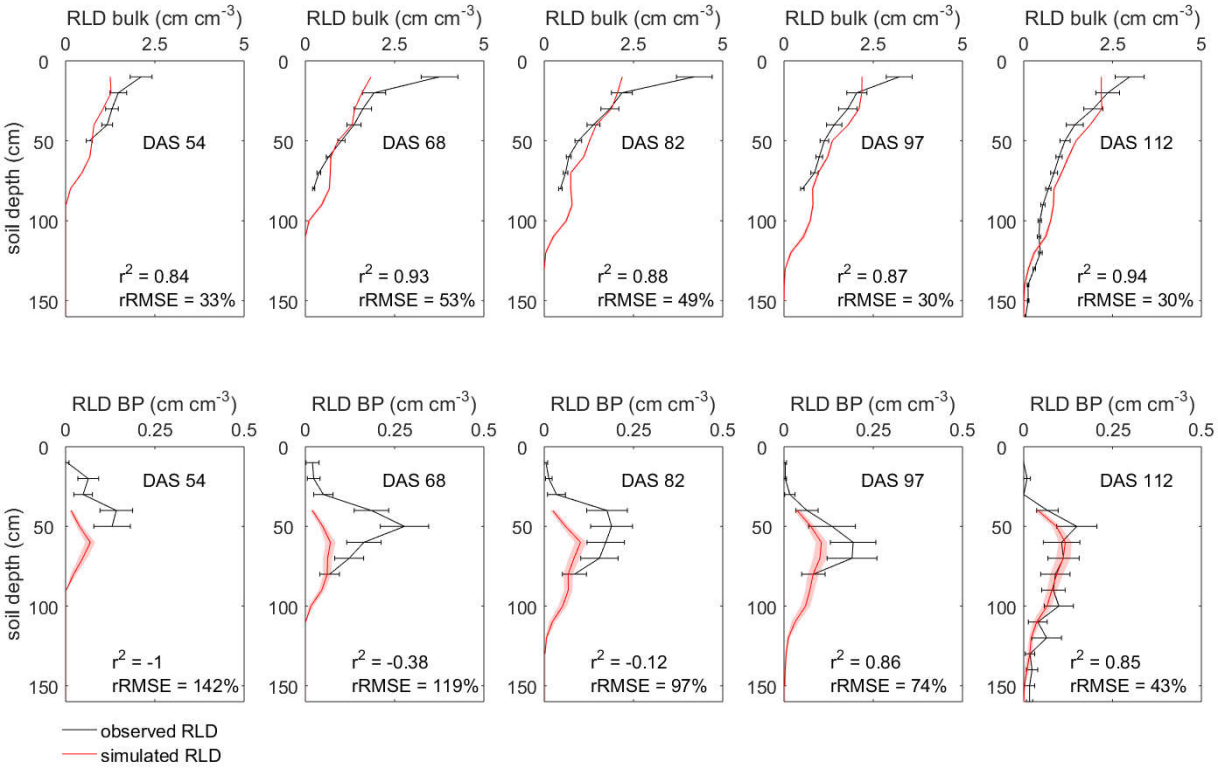

Fig. 4.6: Measured and simulated root length density (RLD) in bulk soil and biopores (BP) at five different points in time, error bars respectively shaded areas (partly invisible due to low variance) represent the standard error of the mean (measured RLD: n=280, simulated RLD: n=12)

4.3.2. Influence of biopores on simulated root length density under different soil physical and environmental conditions

Fig. 4.7 shows maximum rooting depths as well as total RLD (total root length scaled with the volume of the soil domain) on the last day of simulation (DAS 112) averaged over 12 individual simulation runs with different biopore networks respectively without biopores for scenario combinations with low and high soil bulk density, silt and sandy loam and climate conditions of the years 2010 and 2012.

For all different environmental and soil physical conditions, biopores led to an increase in rooting depth (between 13 and 35 % respectively 16 and 27 cm) and total RLD (between 10 and 14 % respectively 0.06 and 0.12 cm cm^{-3}). The increase in rooting depth was stronger for high than for low soil bulk density (both in relative and absolute numbers). This is caused by the stronger difference between bulk soil and biopore penetration resistance in more compact soil, which causes more axial roots to remain within biopores and to grow along them. Different soil types respectively climate conditions did not lead to substantially different increases in rooting depth. In contrast to rooting depth, the biopore-affected increase in total RLD was larger for low than for high soil bulk density because lateral roots, which generally left the biopore and re-entered the bulk soil due to their tendency to bend horizontally, developed faster in loose than in hard bulk soil. In more compact soil, biopores mainly facilitated axial root growth, while laterals that re-entered the bulk soil needed longer time to fully develop. Different soil types respectively climate conditions did not lead to substantially different increases in total RLD.

Increased soil bulk density led to lower maximum rooting depths and lower total RLDs due to increased mechanical stress. Interestingly, both maximum rooting depth and total RLD were larger in sandy loam than in silt loam. This is caused by the different hydraulic properties of the two soils leading to differences in SWP and thus soil penetration resistance. SWP heterogeneity was more pronounced in sandy loam than in silt loam due to the sandy loam's larger hydraulic resistivity under the prevailing soil water contents. SWP in sandy loam was therefore more negative in upper soil layers and less negative in deeper soil layers as compared to silt loam. SWP-triggered impedance of root tip elongation in deeper soil layers was then stronger in silt loam than in sandy loam. It must also be noted that water contents are higher in silt loam than in sandy loam in case of equal SWP. Despite the silt loam's larger saturated water content, this leads to a higher degree of saturation and thus to larger soil penetration resistance values and lower root elongation rates in silt loam than in sandy loam at equal SWP (equation (4.5)). Differences in climate conditions between the years 2010 and 2012, which mostly appeared in the second half of the growing period, were not large enough to substantially influence maximum rooting depths or total RLDs.

It must be noted that despite the presence of biopores, maximum rooting depth in dense soil was lower than maximum rooting depth in loose soil, which indicates that roots did not grow within biopores over

the entire subsoil depth. Reasons are biopore discontinuities over the soil depth and the tendency of roots to leave non-vertically oriented biopores.

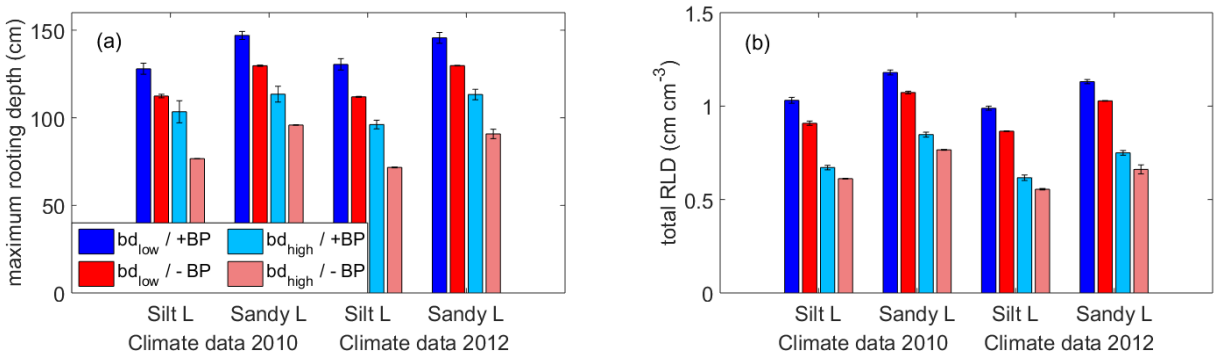

Fig. 4.7: Maximum rooting depth (a) and total RLD (b) on the last day of simulation DAS 112 for root growth in soil with and without biopores (+/- BP) at different levels of bulk density (bd_{low}/bd_{high} …low/high subsoil bulk density), in silt loam or sandy loam under climate conditions of the years 2010 and 2012; error bars represent the standard error of the mean for 12 individual simulation runs

4.3.3. Influence of biopores on root hydraulic architecture parameters

We computed root hydraulic architecture parameters for all possible combinations of soil physical and environmental conditions and the various biopore systems. Mean root system conductance K_{rs}, which describes the water flow per unit of water potential difference between root collar and soil, is a function of root system size and root hydraulic parameters (radial and axial root conductance, Fig. 4.4). Under the assumption of limited hydraulic conductivity (HC) of the root-soil interface in biopores, mean root system conductance is furthermore a function of root-soil contact. When assuming limited HC in biopores, the increase in root system conductance due to increased root system size was partly cancelled out by its decrease due to incomplete root-soil contact. When assuming unlimited HC in biopores, root system conductance was naturally higher than in simulations without biopores due to increased root system size. These relationships persisted for simulation scenarios with different soil types and climate conditions and are represented for scenario combinations with silt loam and climate conditions of 2010 in Fig. 4.8a. Absolute values of root system conductance were higher for sandy loam than for silt loam due to larger root systems.

The standard sink fraction SSF defines the location from which a root takes up water. To explore the influence of biopores on SSF, we use the measure 'mean depth of the standard sink fraction' (zSSF), which is defined as the product of SSF and the depth of the respective root segment summed up over all segments. Biopores led to an increase in rooting depth in both low and high soil bulk density and therefore also to an increase in zSSF. When assuming limited HC in biopores, the increase in zSSF was less pronounced (Fig. 4.8b). This was true for all simulation scenarios with different soil types and climate conditions and is represented for scenario combinations with silt loam and climate conditions of 2010 in Fig. 4.8b. Absolute values of zSSF were higher in sandy loam than in silt loam due to deeper reaching root systems.

An important physiological parameter is the carbon cost of the root biomass. Root water uptake efficiency can thus be described by the ability of a plant to take up water per gram of carbon spent in the root system. We found varying results for the influence of biopores on root water uptake efficiency (Fig. 4.8c): Up to certain root system volume (corresponding to a certain root system age), root water uptake efficiency was similar for simulations with and without biopores. For larger root system volumes (older root systems), however, biopores led to larger water uptake efficiency in simulations with unlimited and – to a lesser extent – also with limited HC in biopores. These relationships persisted for simulation scenarios with different soil types and climate conditions and are represented for scenario combinations with silt loam and climate conditions of 2010 in Fig. 4.8c.

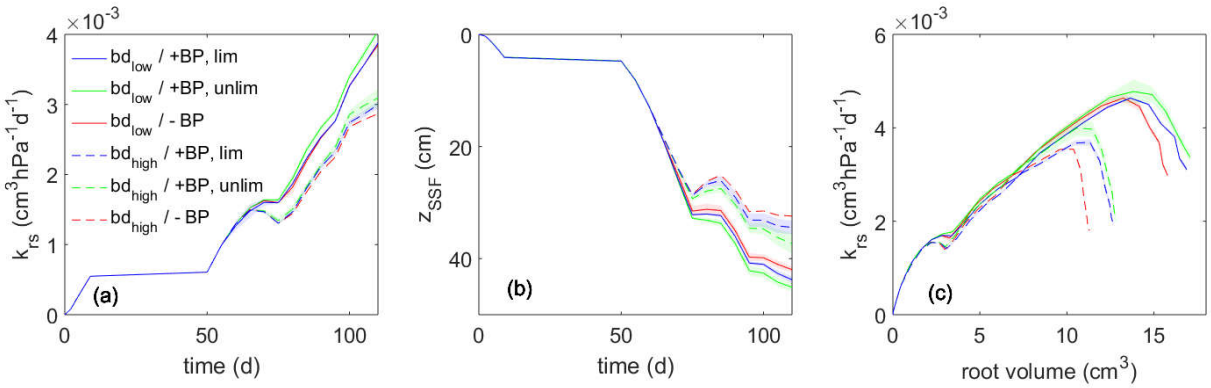

Fig. 4.8: Evolution of mean root system conductance (k_{rs}) (a) and depth of the standard sink fraction (zSSF) over time; relationship between mean root system conductance (k_{rs}) and root volume (c), (+/- BP …with/without biopores, bd_{low}/bd_{high} …low/high subsoil bulk density, unlim/lim… unlimited/limited radial

root hydraulic conductivity); each line is the average of 12 individual simulation runs, the shaded bands (partly invisible due to low variance) represent the 95 % confidence interval; scenario: silt loam, climate conditions 2010

4.3.4. Influence of biopores on root water uptake

Daily cumulated transpiration (Fig. 4.9) as well as mean daily equivalent SWP sensed by the plant (Fig. 4.10) was computed for all possible combinations of soil physical and environmental conditions and the various biopore systems. During the second part of the reference season 2010 (mid-May to mid-July), a pronounced dry period led to significant plant drought stress and transpiration demands could no longer be satisfied (Fig. 4.9a-b, Fig. 4.10a-b). Under these conditions, simulations with biopores led to higher actual transpiration rates than simulations without biopores and thus to a better plant water supply in both loose and dense soil. Interestingly, at the beginning of the dry period, simulations with limited HC showed lower transpiration rates than simulations with unlimited HC; towards the end of the dry period, however, the situation changed and simulations with limited HC revealed equal or even slightly higher transpiration rates as compared to simulations with unlimited HC (Fig. 4.9a-b). Unlimited HC in biopores and thus higher root system conductance is therefore only an advantage for plant water uptake as long as soil water availability is high enough. This phenomenon is also reflected in the plant-sensed SWPs, which differ at the beginning, but are similar at the end of the dry period for simulations with limited and unlimited HC (Fig. 4.10a-b). Despite larger root systems and thus larger root system conductances, actual transpiration rates were lower in loose sandy loam than in loose silt loam. This is caused by the sandy loam's more negative SWP in the medium to upper soil layers (~0-80cm) where root water uptake predominantly takes place due to higher RLD in this soil region (cf. zSSF, Fig. 4.8b) and is also reflected in the plant-sensed SWPs, which are more negative for loose sandy loam than for loose silt loam (Fig. 4.10a-b). In dense soil, silt loam and sandy loam showed similar transpiration rates because SWPs in the upper soil layers where root water uptake took place were equally negative for both soil types (Fig. 4.10a-b). Simulations with climate conditions of spring 2012 led to optimal root water uptake in loose soil throughout the entire growing season and to less drought stress for plants growing in dense soil. Simulations with biopores again led to less negative equivalent SWP sensed by the plant and thus to larger actual transpiration rates as compared to simulations without biopores. Actual transpiration rates

were slightly higher for silt loam than for sandy loam due to slightly less negative SWPs in the uppermost soil layers (Fig. 4.9c-d, Fig. 4.10c-d).

To better understand the impact of biopores on total root water uptake over the entire growing season, we evaluated cumulated transpiration deficits (Fig. 4.11). Simulations with biopores led to lower transpiration deficits than simulations without biopores for any climate and soil physical condition and for limited and unlimited HC in biopores. The impact of biopores on transpiration deficits was larger in dense soil than in loose soil: This is a result of both the generally larger transpiration deficits produced by smaller root systems and the larger effect of biopores on rooting depth. Biopores also had a larger effect on transpiration deficits in sandy loam than in silt loam: This is caused by the larger SWP variation with depth in sandy loam, which increases the importance of root water uptake from deeper, wetter soil layers to satisfy transpiration demands. In loose soil, transpiration deficits were reduced by up to 14 mm (season 2010, sandy loam), which represented 7 % of the seasonal transpiration demand. In dense soil, transpiration deficits were reduced by up to 24 mm (season 2010, sandy loam), which represented 11 % of the seasonal transpiration demand.

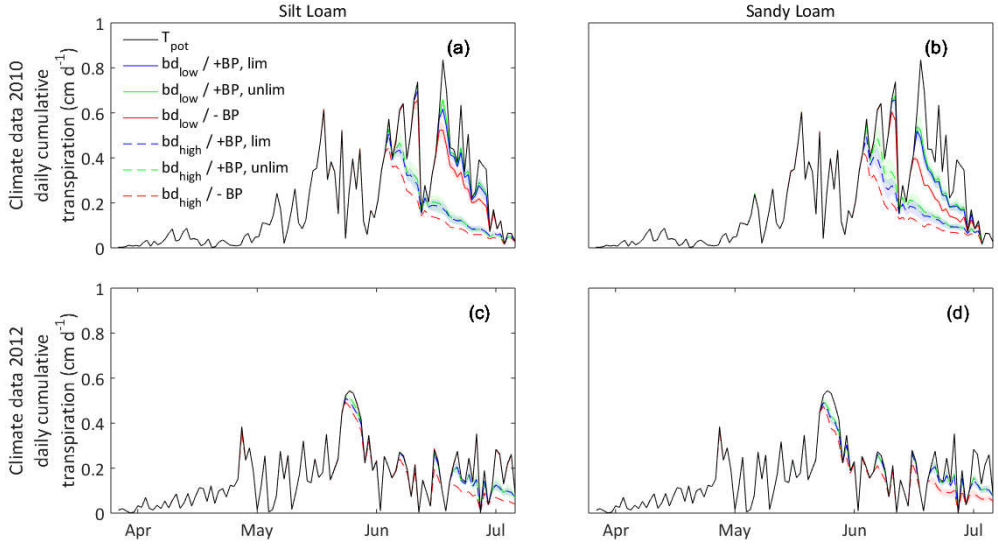

Fig. 4.9: Daily potential and actual transpiration rates over the entire growing period for (a) climate data 2010 and silt loam, (b) climate data 2010 and sandy loam, (c) climate data 2012 and silt loam and (d) climate data 2012 and sandy loam, (+/- BP …with/without biopores, bd_{low}/bd_{high} …low/high subsoil bulk density, lim/unlim… limited/ unlimited radial root hydraulic conductivity); each line is the average of 12

individual simulation runs, the shaded bands (partly invisible due to low variance) represent the 95 % confidence interval

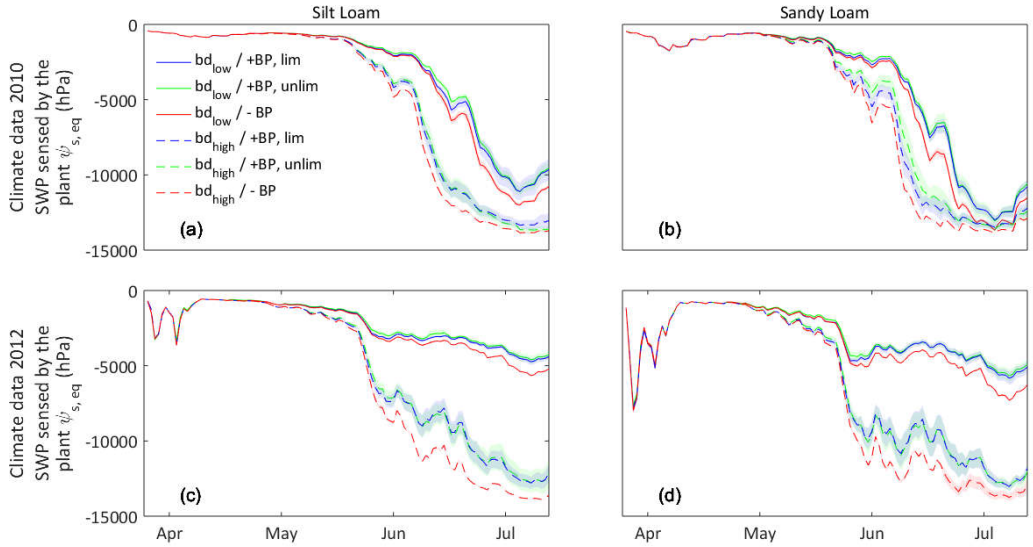

Fig. 4.10: Mean soil water potential sensed by the plant at each day of the growing period for (a) climate data 2010 and silt loam, (b) climate data 2010 and sandy loam, (c) climate data 2012 and silt loam and (d) climate data 2012 and sandy loam, (+/- BP …with/without biopores, bd_{low}/bd_{high} …low/high subsoil bulk density, lim/unlim… limited/ unlimited radial root hydraulic conductivity); each line is the average of 12 individual simulation runs, the shaded bands (partly invisible due to low variance) represent the 95 % confidence interval

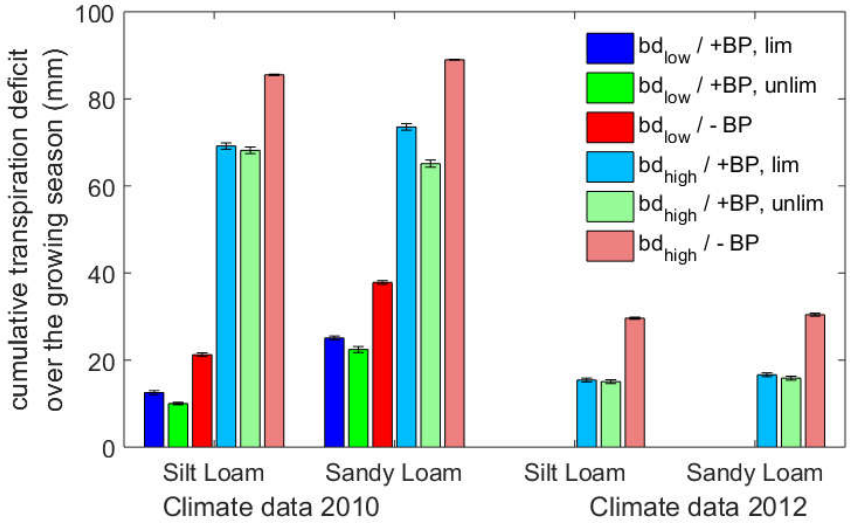

Fig. 4.11: Transpiration deficit cumulated over the entire growing season (+/- BP …with/without biopores, bd_{low}/bd_{high} …low/high subsoil bulk density, lim/unlim… limited/ unlimited radial root hydraulic conductivity); error bars represent the standard error of the mean for 12 individual simulation runs

4.4. Discussion

Modeling root growth in soil with biopores

Via optimization of root growth model input parameters, we were able to simulate root length density profiles in bulk soil and biopores that corresponded well to experimentally observed ones. All optimized model input parameters were in the range of values found in literature (Appendix, Table 6-1). Our parameterized simulation model was able to reproduce the impacts of biopores on root system development as described in literature (Hirth et al. 2005; Stirzaker et al. 1996): Biopores led to substantial increases in both total root length and rooting depth and the latter phenomenon increased for more compact soil. These results suggest that our simulated root systems represent a valid basis for further analysis of root water uptake under different soil physical and environmental conditions. To improve model simulation of root development in biopores for different soils as well as under varying environmental conditions, however, more quantitative information from both field and laboratory experiments will be necessary.

At our study site, the abundance of subsoil biopores was observed to decrease with soil depth (Athmann et al. 2013; Perkons et al. 2014), which is in line with most studies from literature (e.g. White and Kirkegaard 2010; Pitkänen and Nuutinen 1997). However, other studies (e.g. Silva et al. 2016) report constant or increasing numbers of subsoil biopores with soil depth or a homogeneous distribution of biopores in a soil depth of 125-150 cm (Nielsen et al. 2010). In the present study, we used a homogeneous biopore network over the entire subsoil profile, which we considered to be justified for a general evaluation of the impact of biopores on root growth and root water uptake. For a more detailed evaluation, however, differences in subsoil biopore density with depth need to be taken into account. The abundance of biopores in the topsoil is known to largely depend on the tillage practice: While conventional tillage leads to soft topsoil with only few biopores, no-tillage results in more compact topsoil with a large number of biopores (Dal Ferro et al. 2014; Golabi et al. 1995; Holland 2004). Crop development simulation under no-tillage practice thus further requires the consideration of topsoil biopores, which can be expected to yet again increase the impact of biopores on root growth and root water uptake.

For reasons of simplicity and a lack of accurate values, we assumed regular branch spacing and constant lateral root length under any soil physical condition. Bao et al. (2014), however, observed that lateral root formation depends on the availability of water in the vicinity of the root, which might be of importance for root branching within biopores due to the prevailing limited root-soil contact. Lateral root length, on the other hand, was observed to decrease under soil compaction (Grzesiak 2009; Konôpka et al. 2009), which can be expected to result in different lengths of laterals that develop within a biopore and those that grow back into the bulk soil.

The mean share of subsoil RLD in biopores relative to total subsoil RLD observed in the field experiment amounted to 10 % on the last day of measurement, which is rather low compared to values from literature where shares of 14 to 100 % are reported (Ehlers et al. 1983; Gaiser et al. 2013; Nakamoto 2000; White and Kirkegaard 2010). The reasons for this large variability in biopore RLD observed in different studies are manifold and include crop species, soil structure and texture, but above all diverging definitions of biopores with regard to diameter as well as different methods to assess root distribution within bulk soil and biopores (e.g. profile wall method, Boehm and Koepke 1977; core-break method, Kirkegaard et al. 2007). In our simulations, the low share of subsoil RLD in biopores relative to total

subsoil RLD is mainly due to the fact that in our model, lateral roots are hardly ever located within biopores: Based on findings by Cuesta et al. (2013) and Rosquete et al. (2013), we considered lateral roots to be influenced by plagiotropism and to predominantly grow in horizontal direction. Simulated lateral roots therefore left the generally vertically oriented pores by re-entering the bulk soil and hence did not contribute to the share of subsoil biopore RLD. If only axial roots were considered, the simulated share of subsoil RLD in biopores relative to total subsoil RLD would increase from 9 to 24 % in loose soil and from 9 to 26 % in dense soil. In the field, Athmann et al. (2013) observed that the growth behavior of lateral roots in biopores depends on the crop root architecture. The share of laterals re-entering the bulk soil, however, could not be quantified in these field experiments. An interesting question is whether lateral roots in biopores premeditatedly grow towards the bulk soil to gain better access to water and nutrient resources. Such feedforward mechanisms, where plants are able to 'sense' their physical environment, have been observed in several studies (e.g. Colombi et al. 2017; Passioura 2002; Stirzaker et al. 1996).

Our model was well capable to reproduce experimental observations of root system development in soil with biopores, but it also showed limitations. The assumption of lateral periodic boundaries allowed us to mimic field conditions with regard to root growth and water flow, however, the biopore system was not periodic in lateral direction. A root that grew along a biopore and reached the border of the soil domain was therefore obliged to grow out of the biopore and to re-enter the bulk soil (Fig. 4.12-1). Another limitation was posed by the cubic grid cell structure of the biopore system: Root growth direction is computed in accordance with equation (4.2) as the product of the soil mechanical conductance tensor and a driving force, which is influenced by the previous growth direction, a random deflection angle and gravitropism. To grow around the corner of a cubic grid cell, a root has to endure large direction changes, i.e. the direction of the mechanical conductance tensor must dominate the direction of the driving force. If the bulk soil is not entirely impenetrable, roots therefore frequently re-enter the bulk soil instead of continuing to grow along biopores (Fig. 4.12-2). Furthermore, we know from experimental studies that biopore walls are generally more compact than the surrounding bulk soil (Stirzaker et al. 1996; Young 1998), which means that roots are less likely to leave a pore when already inside. Our model, though, does not take into account biopore wall compaction. The greatest model limitation, however, was implied by the spatial resolution of the model: The relatively coarse resolution, which was necessary to meet computational requirements, led to bioporosities that were much larger

than those observed in the field. By adjusting root growth model parameters, we were able to simulate root length densities in biopores that were comparable to observed ones. However, this implies that model parameterization is sensitive to spatial model resolution. To solve this issue, further research and model development, but also computing power is needed.

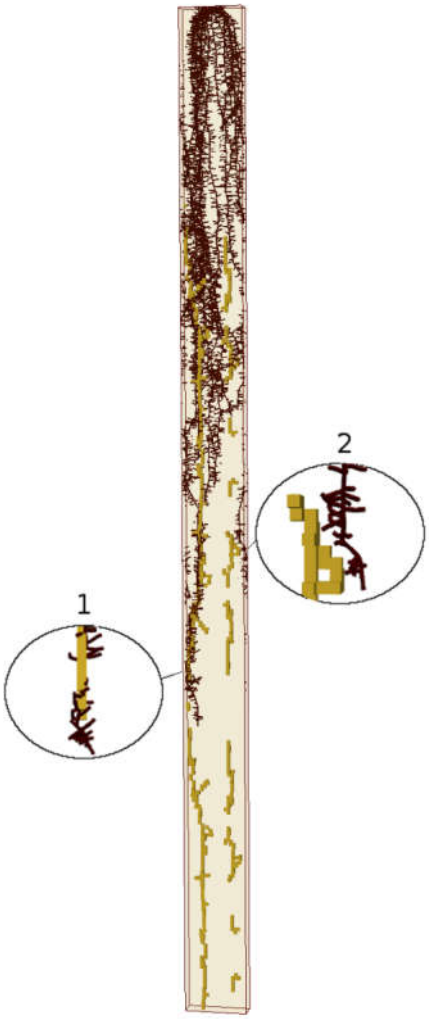

Fig. 4.12: Simulated root system (brown) in soil with biopores (yellow): (1) root growing out of discontinuous biopore, (2) root leaving biopore that is not vertically aligned

Several studies showed that biopores play an important role with regard to soil aeration (Tracy et al. 2011; Bengough et al. 2011). Uteau et al. (2013) reported for the site in Klein-Altendorf that alfalfa increased air capacity, air permeability and diffusion coefficients in the subsoil, while fescue, with its shallower root system, did not affect subsoil structure and hence soil aeration. In other studies, compacted soils with poor pore structure were found to be prone to waterlogging, which causes hypoxia and in consequence limits root elongation (Bengough et al. 2011). The beneficial effect of biopores for root growth can thus be assumed to be even greater if poor soil aeration respectively hypoxia was additionally considered as a limiting factor for root system development.

Legumes were shown to be more sensitive to soil compaction than cereals (Arvidsson and Håkansson 2014) and soybean, maize and barley roots were observed to colonize biopores more frequently than wheat roots when grown on the same field site (Colombi et al. 2017; Perkons et al. 2014). The significance of biopores as root growth pathways to greater soil depths may thus be even higher for plants other than wheat.

Modeling root water uptake in soil with biopores

In times of drought, our simulations showed a beneficial impact of biopores on root water uptake. Biopores could thereby reduce transpiration deficit by up to 24 mm, which represented 11 % of the seasonal transpiration demand of spring wheat in our study area. This positive effect was primarily caused by the increased rooting depth in structured soil, which allowed roots to take up water from deeper and wetter soil regions.

The impact of biopores on hydraulic root architecture parameters depended on the water uptake ability of roots with limited root-soil contact. When unlimited hydraulic conductivity at the root-biopore wall interface was assumed, mean root water uptake took place deeper in the soil domain and root system conductance increased. When limited hydraulic conductivity at the root-biopore wall interface was assumed, roots were also able to take up water from deeper soil layers, root system conductance, however, remained fairly constant. These findings may be important for simulations of root water uptake in structured soil using 1D models (e.g. Hydrus, Šimůnek et al. 2016) where the impact of biopores on plant transpiration can only be taken into account implicitly via root hydraulic architecture parameters and root length density profiles.

Many studies (e.g. Stirzaker et al. 1996; White and Kirkegaard 2010; Passioura 2002) emphasize the problem of poor root-soil contact in biopores and its adverse effect on root water uptake and plant development. However, simulations with limited hydraulic conductivity (HC) at the root–soil interface in biopores performed better in meeting plant transpiration demands than simulations without biopores under any soil physical and environmental condition. Furthermore, towards the end of dry periods when the soil was already water depleted, simulations with limited HC in biopores led to equal or even slightly higher actual transpiration rates than simulations with unlimited HC in biopores. Similar results were found by Meunier et al. (2016) and Couvreur et al. (2014b), who showed that root systems with low radial conductance can maintain higher transpiration rates towards the end of a dry period.

Our simulation results suggest that the influence of biopores on root water uptake differs for different soil densities as well as soil types: Due to the larger increase in rooting depth, biopores had a more beneficial effect on root water uptake in more compact soil. Furthermore, the effect of biopores was stronger in sandy loam than in silt loam due to the sandy loam's higher soil hydraulic resistivity and soil water potential heterogeneity. When evaluating the impact of biopores on crop performance, it is therefore necessary to take into account not only characteristics that are directly related to biopores (e.g. number of biopores per unit surface area, abundance and spatial distribution of roots in biopores), but also properties whose connection to biopores is less evident such as soil type and soil bulk density.

In the present study, we considered biopores to be air-filled at all times. Under natural conditions, however, rain events can lead to preferential flow in biopores, which significantly influences water content distribution in the soil profile (Jarvis et al. 2016). Preferential flow allows water to quickly infiltrate and drain into deeper soil layers and thereby reduces the amount of water that can be stored in the topsoil (Good et al. 2015). This difference in water distribution within the soil profile is encountered by larger rooting depths due to biopores.

4.5. Conclusions

In this simulation study, we combined extensive experimental field data with an explicit 3D model for the simulation of water flow, root system development and root water uptake in soil with biopores. Our model helps to better understand plant physiological responses to structured soil under different soil physical and environmental conditions. Our simulation results confirmed the beneficial impact of

biopores for root penetration into greater soil depths as well as for plant transpiration under drought conditions. The positive influence of biopores persisted even under the assumption of reduced root water uptake in biopores due to limited root-soil contact and was larger for dense soil than for loose soil as well as for sandy loam than for silt loam. We furthermore evaluated the influence of biopores on root hydraulic architecture parameters. These relationships may be of use for larger scale simulations with 1D-models that can only implicitly take into account the effect of biopores on root growth and root water uptake via root length density profiles and root hydraulic architecture parameters.

Chapter V

Conclusions and Outlook

5.1. Conclusions

The objective of this thesis was to get a better understanding of the interaction processes between biopores, root growth and root water uptake and to evaluate the relevance of biopores for overall plant performance with the help of 3D model simulation. We also aimed to improve the parameterization of 3D root architecture models and to evaluate the importance of correct model parameterization on simulation results.

In the first paper discussed in this thesis, we developed a new approach to model root growth in soil with macropores. The drawn analogy between root growth and water flow in porous media represents a paradigm change in modelling the orientation of growing root segments in response to soil mechanical resistance. The good agreement between experimentally observed and simulated root growth patterns in structured soil confirmed the usefulness of our new approach.

Our results from the second paper of this thesis contribute to build trust in the use of widely available 2D root images for the parameterization of 3D root architecture models. The effect of root system projection in 2D (hand-drawings) or deflection in quasi-2D containers (rhizotrons) was found to be significant with regard to parameter variance. Irrespective of the image source, inter-branch distances demonstrated to follow a log-normal distribution. This should be accounted for in root architectural models, considering the impact of inter-branch distances on rhizosphere overlap and thus root foraging performance.

In the third paper of the thesis we combined our newly developed model approach with extensive experimental field data to evaluate root-biopore interactions on the plot scale under different climatic

and soil physical conditions. Comparisons of simulated and experimentally observed root length densities in bulk soil and biopores showed reasonable agreement. A difficulty was thereby the large natural variability of root growth in biopores that reflected in the measured data. The new model approach allowed us to simulate root systems whose response to biopores in the soil corresponded well to experimental observations described in literature such as increased total root length and increased maximum rooting depth. The simulated ratio of roots growing in biopores relative to roots growing in bulk soil, however, was relatively low. This was partly due to the cubic grid cell structure of our model, which encouraged roots to leave a biopore and to re-enter the bulk soil. Simulations of root water uptake confirmed that biopores substantially mitigate transpiration deficits in times of water scarcity by allowing roots to take up water from deeper, less dry soil regions. Intriguingly, this effect persisted even when assuming reduced root water uptake in biopores due to limited root-soil contact and was stronger more compact soil and soil with low hydraulic conductivity at low soil water potential. We could furthermore evaluate the impact of biopores on root hydraulic architecture parameters used in the root water uptake model by Couvreur et al. (2012). These findings may be of use for larger scale simulations with 1D or 2D models that can only implicitly take into account the effect of biopores on root water uptake via root hydraulic architecture parameters.

5.2. Outlook

The experiments from literature, which we used to test our new model approach for root growth in soil with macropores, were not designed to calibrate or validate our simulation model. For future simulation studies on root growth and root water uptake in macropores, it would be beneficial to explicitly design experiments that provide customized data for a better determination of model parameters and finally more reliable simulation results. A promising tool for such experiments are non-invasive methods including X-ray computed tomography (Tracy et al. 2010) or magnetic resonance imaging (Pohlmeier et al. 2013) that allow determining both root growth in macropores and distributions of soil water content in three dimensions. Considering the importance of biopores for plant nutrient supply (Athmann et al. 2014; Kautz et al. 2013a), it would be interesting to further extend the new model approach by a sub-model for root nutrient acquisition and uptake.

Root trait analysis showed the importance of correct parameterization of root growth models for the simulation of realistic root systems that can be used to investigate root-soil interaction processes. The creation of a database containing root architecture parameters of different plant species would be desirable. More research on root plasticity responses to soil heterogeneity and varying environmental conditions would further improve 3D root architecture modeling.

The impact of biopores on plant water uptake largely depends on the water uptake ability of roots with limited root-soil contact. So far, this aspect has rarely been investigated. Using analytical equations, de Willigen et al. (2018) stated the importance of the type of contact area between root and soil (partial radial or partial longitudinal contact) on the amount of water that can be taken up by the root. To confirm these findings and to make an attempt of quantifying the impact of limited root-soil contact on plant water uptake, it could be useful to experimentally investigate root water uptake in biopores using non-invasive imaging methods such as X-ray computed tomography (Koebernick et al. 2015) or magnetic resonance imaging (Pohlmeier et al. 2013). Furthermore, the impact of biopores on root water uptake largely depends on radial and axial root hydraulic conductances and their variation with root age. However, due to the difficult experimental determination of root hydraulic conductances, exact values for different plants are scarce. A better understanding of root hydraulic architecture is a key factor to a better estimation of the influence of biopores on root water uptake. Furthermore, it is not yet clear how biopores influence root branching patterns. Considering the importance of lateral roots for water and nutrient uptake, more information on lateral root development in biopores would improve simulation results significantly.

Appendix

Table 6-1: Root growth model input parameters: Parameter description, parameter values, literature sources and literature-derived ranges for optimized parameters; optimized values are shown in bold font

Symbol	Description	Dimension	Unit	Values for axial roots	Values for lateral roots	Literature source	Literature-derived ranges for optimized parameters
k_r	Radial conductivity	$LP^{-1}T^{-1}$	cm hPa^{-1} d^{-1}	$5x10^{-6}$-$5x10^{-5}$	$5x10^{-6}$-$5x10^{-5}$	Couvreur et al. (2014a)	
k_x	Axial conductance	$L^4P^{-1}T^{-1}$	cm^4 hPa^{-1} d^{-1}	0 – 0.35	0-$5.5x10^{-4}$	Couvreur et al. (2014a)	
n_{ax}	Number of axial roots	-	-	**16**	-	Ping et al. (2011)	6-8
						Colombi and Walter (2017)	4-16
						Finch et al. (2017)	5-9
r	Initial unimpeded elongation rate	LT^{-1}	cm d^{-1}	**3.5**	3.5	Colombi et al. (2017)	2.27*
						Materechera et al. (1991)	12
a	Root radius	L	cm	0.041	0.027	Watt et al. (2006)	
l_b	Basal root zone	L	cm	2	-	Bingham and Wu (2011)	
ln	Inter-branch distance	L	cm	0.4	-	Landl et al. (2018)	
l_{max}	Maximum root length	L	cm	**10-161**	1	Kutschera and Lichtenegger (2010)	15-175**
t_{newax}	Emergence time of axial	T	d (DAS)	**0-65**	-	No literature sources found	-

	roots						
θ	Branching angle		°	80	-	Landl et al. (2018)	
σ	Unit standard deviation of the random angle deviation		°	**10**	10	Landl et al. (2018)	8-26
	Tropism		-	gravitropism	plagiotropism	Roychoudhry et al. (2013)	
sg	Tropism sensitivity		-	**0.7**	0.3	Landl et al. (2018)	0.01-0.4
						Bingham and Wu (2011)	0.5-1.5
condMP	Conductance in the macropore	P^{-1}	MPa^{-1}	**200**	200	Landl et al. (2017)	10-200

*at a soil bulk density of 1.3 g cm^{-3}, **derived via 2D image analysis using the root tracking tool Root System Analyzer (Leitner et al. 2014)

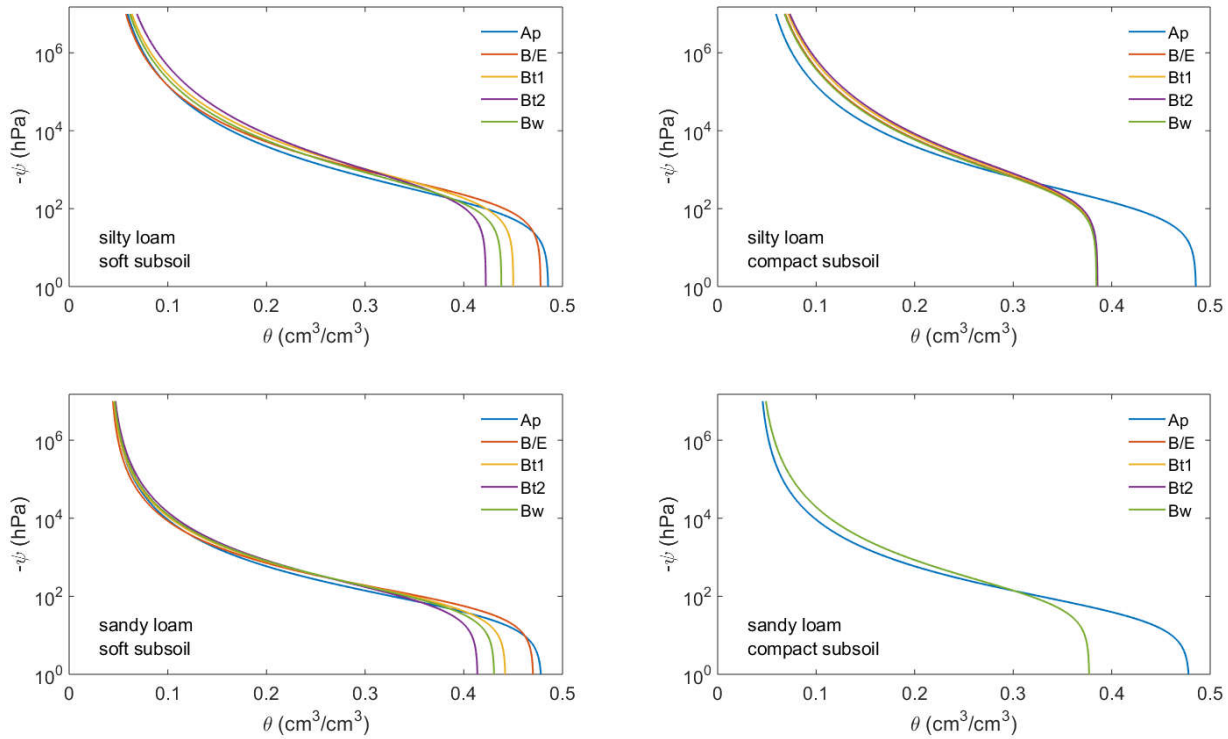

Fig. 6.1: Water retention curves of soils used in the different simulation scenarios (ψ… water potential, θ… water content)

Table 6-2: Texture of compacted silty loam with bulk density and soil hydraulic values used in the different simulation scenarios

			Texture				Soil hydraulic parameters according to Van Genuchten (1980)*				
	Horizon	Depth (cm)	Sand	Silt	Clay	Bulk density (g cm^{-3})	Θr (-)	Θs (-)	α (hPa^{-1})	n (-)	Ks (cm d^{-1})
			——— (%) ———								
Topsoil	Ap	0-30	7	76	17	1.29	0.041	0.4857	0.0103	1.2767	5.08
Mixing zone	E/B	31-40	5	75	20	1.65	0.041	0.3847	0.0041	1.2377	1.56
Subsoil	Bt1	41-75	5	68	27	1.65	0.041	0.3853	0.0038	1.2294	1.31
	Bt2	76-115	4	67	29	1.65	0.041	0.3857	0.0037	1.2254	1.20
	Bw	116-160	6	74	20	1.65	0.041	0.3845	0.0042	1.2394	1.62

*θr, residual water content; θs, saturated water content;α and n, shape parameters; Ks, saturated hydraulic conductivity

Table 6-3: Texture of sandy loam with bulk density and soil hydraulic values used in the different simulation scenarios

			Texture			Bulk density (g cm^{-3})	Soil hydraulic parameters according to Van Genuchten (1980)*				
	Horizon	Depth (cm)	Sand	Silt	Clay		Θr (-)	Θs (-)	α (hPa^{-1})	n (-)	Ks (cm d^{-1})
			——— (%) ———								
Topsoil	Ap	0-30	40	50	10	1.29	0.041	0.4789	0.0027	1.3625	23.34
Mixing zone	E/B	31-40	40	50	10	1.32	0.041	0.4704	0.0016	1.4035	8.38
Subsoil	Bt1	41-75	40	50	10	1.42	0.041	0.4422	0.0015	1.3764	8.38
	Bt2	76-115	40	50	10	1.52	0.041	0.4140	0.0013	1.3512	8.38
	Bw	116-160	40	50	10	1.46	0.041	0.4309	0.0014	1.3661	8.38
Different subsoil horizons		31-160	40	50	10	1.65	0.041	0.3773	0.0117	1.3208	8.38

*θr, residual water content; θs, saturated water content;α and n, shape parameters; Ks, saturated hydraulic conductivity

Acknowledgements

Particular thanks go to my two supervisors Andrea Schnepf and Jan Vanderborght for all the given support and guidance throughout this thesis. Thanks a lot for always taking time to think through my problems, for getting me back on the right track when I had lost my way and especially for the constant encouragement throughout this more than $3^1/_2$ years.

Furthermore, I want to thank Harry Vereecken for the great working environment as well as for the motivating structure of the doctoral program at IBG3.

Great thanks to Glyn Bengough for having me at the James Hutton Institute in Dundee for 3 months and for making this stay so enjoyable; many thanks also to all colleagues there.

I also want to thank

- The project group DFG-PAK888 for motivating discussions in the project meetings
- Daniel Uteau, Sarah Bauke, Miriam Athmann, Timo Kautz, Sabine Seidel and Guillaume Lobet for providing me with lots of experimental data sets
- Katrin Huber for all the patience and explanations when introducing me to programming in general and to R-SWMS in particular
- The root group – Helena, Mirjam, Shehan, Xiaoran, Sheng, Mai, Emil, Guillaume, Andreas – for all the helpful comments and discussions during our weekly meetings
- Mathieu Javaux as well as the rest of the group in Louvain-la-Neuve for helping me finding a way into and through R-SWMS
- Horst Hardelauf and Thomas Schuster for all the help with my various cluster and computer problems

Special thanks go to Asta for spending the first time of PhD together, to Asta and Pascha for the great time in Neusserstraße as well as to all the other friends and colleagues at IBG3, who made life in Jülich so enjoyable: Manuela, Anne(s), Cosimo, Michael, Maria, Igor, Mirjam, Emil, Helena, Anneli, Lutz, Sean, Markus, Daniela, Sheng, Axelle, Luka, Dorina, Roland, Kathrina, Inge, Sebastian, Anja, Yu Yi, Xiaoran…

Ganz besonders möchte ich mich bei meinen Wiener Freunden, bei meinen Geschwistern, beim Michael sowie vor allem bei meinen Eltern bedanken fürs Immer-da-Sein und die unbedingte Unterstützung bei eh allem.

Bibliography

Abadia-Fenoll F, Casero P, Lloret P, Vidal M 1986 Development of lateral primordia in decapitated adventitious roots of Allium cepa. Annals of botany 58: 103-107.

Alcamo J, Henrichs T, Rösch T 2017 World water in 2025: Global modeling and scenario analysis for the world commission on water for the 21st century. Kassel.

Allen RG, Pereira LS, Raes D, Smith M 1998 Crop evapotranspiration-Guidelines for computing crop water requirements-FAO Irrigation and drainage paper. FAO, Rome.

Alm DM, Cavelier J, Nobel PS 1992 A finite-element model of radial and axial conductivities for individual roots: development and validation for two desert succulents. Annals of Botany 69: 87-92.

Arvidsson J, Håkansson I 2014. Response of different crops to soil compaction—Short-term effects in Swedish field experiments. Soil Tillage Res 138: 56-63.

Asare S, Rudra R, Dickinson W, Fenster A 1999 Quantification of soil macroporosity and its relationship with soil properties. Canadian Agricultural Engineering 41: 23-34.

Athmann M, Huang N, Kautz T, Köpke U 2014 Biopore characterization with in situ endoscopy: Influence of earthworms on carbon and nitrogen contents. In: RGA U (ed) 4th ISOFAR Scientific Conference, Istanbul.

Athmann M, Kautz T, Pude R, Köpke U 2013 Root growth in biopores—evaluation with in situ endoscopy. Plant and Soil 371: 179-190.

Atkinson JA, Lobet G, Noll M, Meyer PE, Griffiths M, Wells DM 2017 Combining semi-automated image analysis techniques with machine learning algorithms to accelerate large scale genetic studies. GigaScience 6: 1-7.

Atkinson JA, Wingen LU, Griffiths M, Pound MP, Gaju O, Foulkes MJ, Le Gouis J, Griffiths S, Bennett MJ, King J 2015 Phenotyping pipeline reveals major seedling root growth QTL in hexaploid wheat. J Exp Bot, doi: erv006.

Bao Y, Aggarwal P, Robbins NE, Sturrock CJ, Thompson MC, Tan HQ, Tham C, Duan L, Rodriguez PL, Vernoux T 2014 Plant roots use a patterning mechanism to position lateral root branches toward available water. Proceedings of the National Academy of Sciences 111: 9319-9324.

Barej JAM, Pätzold S, Perkons U, Amelung W 2014 Phosphorus fractions in bulk subsoil and its biopore system. European Journal of Soil Science 65: 553-561.

Barlow P, Adam J 1988 The position and growth of lateral roots on cultured root axes of tomato, Lycopersicon esculentum (Solanaceae). Plant Systematics and Evolution 158: 141-154.

Bauke SL, Landl M, Koch M, Hofmann D, Nagel KA, Siebers N, Schnepf A, Amelung W 2017 Macropore effects on phosphorus acquisition by wheat roots – a rhizotron study. Plant and Soil 416: 67-82.

Bear J 2013 Dynamics of fluids in porous media. Elsevier, N.Y.

Bengough A, McKenzie B, Hallett P, Valentine T 2011 Root elongation, water stress, and mechanical impedance: a review of limiting stresses and beneficial root tip traits. J Exp Bot 62: 59-68.

Bengough AG, Mullins CE 1990 Mechanical impedance to root growth: a review of experimental techniques and root growth responses. European Journal of Soil Science 41: 341-358.

Bingham IJ, Wu L 2011 Simulation of wheat growth using the 3D root architecture model SPACSYS: validation and sensitivity analysis. European Journal of Agronomy 34: 181-189.

Boehm W, Koepke U 1977 Comparative root investigations with two profile wall methods [Oats]. Z Acker Pflanzenbau doi: 297-303.

Bouma TJ, Yanai RD, Elkin AD, Hartmond U, Flores-Alva DE, Eissenstat DM 2001 Estimating age-dependent costs and benefits of roots with contrasting life span: comparing apples and oranges. New Phytologist 150: 685-695.

Cahn M, Zobel R, Bouldin D 1989 Relationship between root elongation rate and diameter and duration of growth of lateral roots of maize. Plant and Soil 119: 271-279.

Cai G, Vanderborght J, Couvreur V, Mboh CM, Vereecken H 2018 Parameterization of Root Water Uptake Models Considering Dynamic Root Distributions and Water Uptake Compensation. Vadose Zone Journal, doi: 10.2136/vzj2016.12.0125.

Carminati A, Vetterlein D, Koebernick N, Blaser S, Weller U, Vogel H-J 2013 Do roots mind the gap? Plant and Soil 367: 651-661.

Chen YL, Palta J, Clements J, Buirchell B, Siddique KH, Rengel Z 2014 Root architecture alteration of narrow-leafed lupin and wheat in response to soil compaction. Field Crops Research 165: 61-70.

Clark RT, MacCurdy RB, Jung JK, Shaff JE, McCouch SR, Aneshansley DJ, Kochian LV 2011 3-dimensional root phenotyping with a novel imaging and software platform. Plant Physiology 156: 455-465.

Clausnitzer V, Hopmans J 1994 Simultaneous modeling of transient three-dimensional root growth and soil water flow. Plant and Soil 164: 299-314.

Colombi T, Kirchgessner N, Walter A, Keller T 2017 Root Tip Shape Governs Root Elongation Rate under Increased Soil Strength. Plant Physiology 174: 2289-2301.

Colombi T, Torres LC, Walter A, Keller T 2018 Feedbacks between soil penetration resistance, root architecture and water uptake limit water accessibility and crop growth–A vicious circle. Science of The Total Environment 626: 1026-1035.

Colombi T, Walter A 2017 Genetic diversity under soil compaction in wheat: Root number as a promising trait for early plant vigor. Frontiers in plant science, doi: 10.3389/fpls.2017.00420.

Couvreur V, Beff L, Javaux M 2014a Horizontal soil water potential heterogeneity: simplifying approaches for crop water dynamics models. Hydrology and Earth System Sciences 18: 1723-1743.

Couvreur V, Vanderborght J, Draye X, Javaux M 2014b Dynamic aspects of soil water availability for isohydric plants: Focus on root hydraulic resistances. Water Resources Research 50: 8891-8906.

Couvreur V, Vanderborght J, Javaux M 2012 A simple three-dimensional macroscopic root water uptake model based on the hydraulic architecture approach. Hydrology and Earth System Sciences 16: 2957-2971.

Cuesta C, Wabnik K, Benková E 2013 Systems approaches to study root architecture dynamics. Frontiers in Plant Science, doi: 10.3389/fpls.2013.00537.

Dal Ferro N, Sartori L, Simonetti G, Berti A, Morari F 2014 Soil macro-and microstructure as affected by different tillage systems and their effects on maize root growth. Soil and Tillage Research 140: 55-65.

Daly KR, Tracy SR, Crout NM, Mairhofer S, Pridmore TP, Mooney SJ, Roose T 2018 Quantification of root water uptake in soil using X-ray computed tomography and image-based modelling. Plant, cell & environment 41: 121-133.

de Moraes MT, Bengough AG, Debiasi H, Franchini JC, Levien R, Schnepf A, Leitner D 2018 Mechanistic framework to link root growth models with weather and soil physical properties, including example applications to soybean growth in Brazil. Plant and Soil, doi: 10.1007/s11104-018-3656-z.

de Willigen P, Heinen M, van Noordwijk M 2018 Roots partially in contact with soil: Analytical solutions and approximation in models of nutrient and water uptake. Vadose Zone Journal, doi: 10.2136/vzj2017.03.0060.

Delory BM, Baudson C, Brostaux Y, Lobet G, Du Jardin P, Pagès L, Delaplace P 2016 archiDART: an R package for the automated computation of plant root architectural traits. Plant and Soil 398: 351-365.

Dexter A 1986 Model experiments on the behaviour of roots at the interface between a tilled seed-bed and a compacted subsoil. Plant and Soil, doi: 149-161.

Dexter A, Hewitt J 1978 The deflection of plant roots. Journal of agricultural Engineering Resources 23: 17-22.

Diggle AJ 1988 ROOTMAP - a model in three-dimensional coordinates of the growth and structure of fibrous root systems. Plant and Soil 105: 169-178.

Doussan C, Pierret A, Garrigues E, Pagès L 2006 Water uptake by plant roots: II-Modelling of water transfer int he soil root-system with explicit accoutn of flow within the root system - Comparison with experiments. Plant and Soil 283: 99-117.

Doussan C, Vercambre G, Pagès L 1998 Modelling of the Hydraulic Architecture of Root Systems: An integrated Approach to Water Absorption - Distribution of Axial and Radial Conductances in Maize. Annals of Botany 81: 225-232.

Draye X 2002 Consequences of root growth kinetics and vascular structure on the distribution of lateral roots. Plant, Cell & Environment 25: 1463-1474.

Dunbabin V, Diggle AJ, Rengel Z, van Hugten R 2002 Modelling the interactions between water and nutrient uptake and root growth. Plant and Soil 239: 19-38.

Dunbabin VM, Postma JA, Schnepf A, Pagès L, Javaux M, Wu L, Leitner D, Chen YL, Rengel Z, Diggle AJ 2013 Modelling root–soil interactions using three–dimensional models of root growth, architecture and function. Plant and Soil 372: 93-124.

Durner W 1994 Hydraulic conductivity estimation for soils with heterogeneous pore structure. Water resources research 30: 211-223.

DWD 2017 CDC (Climate Data Center). Offenbach.

Edwards W, Norton L, Redmond C 1988 Characterizing macropores that affect infiltration into nontilled soil. Soil Science Society of America Journal 52: 483-487.

Ehlers W, Köpke U, Hesse E, Böhm W 1983 Penetration resistance and root growth of oats in tilles and untilled Loess soil. Soil & Tillage Research 3: 261-275.

FAO-UNESCO 1974 Soil map of the world. UNESCO, Paris.

Feddes RA, Hoff H, Bruen M, Dawson T, de Rosnay P, Dirmeyer P, Jackson RB, Kabat P, Kleidon A, Lilly A 2001 Modeling root water uptake in hydrological and climate models. Bulletin of the American meteorological society 82: 2797-2809.

Finch JA, Guillaume G, French SA, Colaço RD, Davies JM, Swarbreck SM 2017 Wheat root length and not branching is altered in the presence of neighbours, including blackgrass. PloS one 12: e0178176.

Fitter A, Stickland T, Harvey M, Wilson G 1991 Architectural analysis of plant root systems 1. Architectural correlates of exploitation efficiency. New Phytologist 118: 375-382.

Forde BG 2009 Is it good noise? The role of developmental instability in the shaping of a root system. J Exp Bot 60: 3989-4002.

Fredlund DG, Xing A 1994 Equations for the soil-water characteristic curve. Canadian geotechnical journal 31: 521-532.

Gaiser T, Perkons U, Küpper PM, Kautz T, Uteau-Puschmann D, Ewert F, Enders A, Krauss G 2013 Modeling biopore effects on root growth and biomass production on soils with pronounced sub-soil clay accumulation. Ecological Modelling 256: 6-15.

Gao S, Pan WL, Koenig RT 1998 Integrated root system age in relation to plant nutrient uptake activity. Agronomy Journal 90: 505-510.

Gao W, Watts C, Ren T, Whalley W 2012 The effects of compaction and soil drying on penetrometer resistance. Soil and Tillage Research 125: 14-22.

Ge Z, Rubio G, Lynch JP 2000 The importance of root gravitropism for inter-root competition and phosphorus acquisition efficiency: results from a geometric simulation model. Plant and Soil 218: 159-171.

Good SP, Noone D, Bowen G 2015 Hydrologic connectivity constrains partitioning of global terrestrial water fluxes. Science 349: 175-177.

Gregory P, McGowan M, Biscoe P, Hunter B 1978 Water relations of winter wheat: 1. Growth of the root system. The Journal of Agricultural Science 91: 91-102.

Gregory PJ 2008 Plant roots: growth, activity and interactions with the soil. John Wiley & Sons.

Gruwel ML 2014 In situ magnetic resonance imaging of plant roots. Vadose Zone Journal 13: 1539-1663.

Grzesiak MT 2009 Impact of soil compaction on root architecture, leaf water status, gas exchange and growth of maize and triticale seedlings. Plant Root 3: 10-16.

Han E, Kautz T, Perkons U, Uteau D, Peth S, Huang N, Horn R, Köpke U 2015 Root growth dynamics inside and outside of soil biopores as affected by crop sequence determined with the profile wall method. Biol Fertil Soils 51: 847-856.

Hargreaves CE, Gregory PJ, Bengough AG 2009 Measuring root traits in barley (Hordeum vulgare ssp. vulgare and ssp. spontaneum) seedlings using gel chambers, soil sacs and X-ray microtomography. Plant and Soil 316: 285-297.

Hatano R, Iwanaga K, Okajima H, Sakuma T 1988 Relationship between the distribution of soil macropores and root elongation. Soil Science and Plant Nutrition 34: 535-546.

Hillel D 2013 Fundamentals of soil physics. Academic press.

Hirth J, McKenzie B, Tisdall J 2005 Ability of seedling roots of Lolium perenne L. to penetrate soil from artificial biopores is modified by soil bulk density, biopore angle and biopore relief. Plant and Soil 272: 327-336.

Ito K, Tanakamaru K, Morita S, Abe J, Inanaga S 2006 Lateral root development, including responses to soil drying, of maize (Zea mays) and wheat (Triticum aestivum) seminal roots. Physiologia Plantarum 127: 260-267.

Jakobsen B, Dexter A 1988 Influence of biopores on root-growth, water-uptake and grain-yield of wheat (triticum-aestivum) based on predictions from a computer-model. Biol Fertil Soils 6: 315-321.

Jarvis N 1989 A simple empirical model of root water uptake. Journal of Hydrology 107: 57-72.

Jarvis N, Koestel J, Larsbo M 2016 Understanding Preferential Flow in the Vadose Zone: Recent Advances and Future Prospects. Vadose Zone Journal, doi: 10.2136/vzj2016.09.0075.

Javaux M, Schröder T, Vanderborght J, Vereecken H 2008 Use of a Three-Dimensional Detailed Modeling Approach for Predicting Root Water Uptake. Vadose Zone Journal 7: 1079-1079.

Jiménez JJ, Cepeda A, Decaëns T, Oberson A, Friesen DK 2003 Phosphorus fractions and dynamics in surface earthworm casts under native and improved grasslands in a Colombian savanna Oxisol. Soil Biology and Biochemistry 35: 715-727.

Jones CA, W.L. B, Ritchie JT, J.R. W 1991 Simulation fo root growth. Modeling Plant and Soil Systems - Agronomy Monograph, Madison, Wisconsin.

Judd LA, Jackson BE, Fonteno WC 2015 Advancements in root growth measurement technologies and observation capabilities for container-grown plants. Plants 4: 369-392.

Kautz T 2015 Research on subsoil biopores and their functions in organically managed soils: A review. Renewable Agriculture and Food Systems 30: 318-327.

Kautz T, Amelung W, Ewert F, Gaiser T, Horn R, Jahn R, Javaux M, Kemna A, Kuzyakov Y, Munch J, Patzold S, Peth S, Scherer H, Schloter M, Schneider H, Vanderborght J, Vetterlein D, Walter A, Wiesenberg G, Kopke U 2013a Nutrient acquisition from arable subsoils in temperate climates: A review. Soil Biol Biochem 57: 1003-1022.

Kautz T, Köpke U 2009 Assessing the root-soil contact in biopores. International Symposium 'Root Research and Applications', Vienna, Austria.

Kautz T, Luesebrink M, Paetzold S, Vetterlein D, Pude R, Athmann M, Kuepper PM, Perkons U, Köpke U 2014 Contribution of anecic earthworms to biopore formation during cultivation of perennial ley crops. Pedobiologia 57: 47-52.

Kautz T, Perkons U, Athmann M, Pude R, Köpke U 2013b Barley roots are not constrained to large-sized biopores in the subsoil of a deep Haplic Luvisol. Biol Fertil Soils 49: 959-963.

Kautz T, Stumm C, Kösters R, Köpke U 2010 Effects of perennial fodder crops on soil structure in agricultural headlands. Journal of Plant Nutrition and Soil Science 173: 490-501.

Keller C, Rizwan M, Davidian J-C, Pokrovsky O, Bovet N, Chaurand P, Meunier J-D 2015 Effect of silicon on wheat seedlings (Triticum turgidum L.) grown in hydroponics and exposed to 0 to 30 µM Cu. Planta 241: 847-860.

Kirkegaard J, Lilley J, Howe G, Graham J 2007 Impact of subsoil water use on wheat yield. Aust J Agric Res 58: 303-315.

Koebernick N, Huber K, Kerkhofs E, Vanderborght J, Javaux M, Vereecken H, Vetterlein D 2015 Unraveling the hydrodynamics of split root water uptake experiments using CT scanned root architectures and three dimensional flow simulations. Frontiers in plant science 6: 370.

Koevoets IT, Venema JH, Elzenga JTM, Testerink C 2016 Roots withstanding their environment: exploiting root system architecture responses to abiotic stress to improve crop tolerance. Frontiers in plant science 7.

Kolb E, Hartmann C, Genet P 2012 Radial force development during root growth measured by phytoplasticity. . Plant and Soil 360: 19-35.

Konôpka B, Pages L, Doussan C 2009 Soil compaction modifies morphological characteristics of seminal maize roots. Plant Soil Environ 55: 1-10.

Kuchenbuch R, Ingram K 2002 Image analysis for non-destructive and non-invasive quantification of root growth and soilw ater content in rhizotrons. Journal of Plant Nutrition and Soil Science 165: 573-581.

Kuhlmann H, Baumgärtel G 1991 Potential importance of the subsoil for the P and Mg nutrition of wheat. Plant and Soil 137: 259-266.

Kuijken RC, van Eeuwijk FA, Marcelis LF, Bouwmeester HJ 2015 Root phenotyping: from component trait in the lab to breeding. J Exp Bot 66: 5389-5401.

Kutschera L 1960 Wurzelatlas mitteleuropäischer Ackerunkräuter und Kulturpflanzen. DLG-Verlag, Frankfurt/Main.

Kutschera L, Lichtenegger E 2010 Wurzelatlas mitteleuropäischer Ackerunkräuter und Kulturpflanzen. DLG-Verlag.

Laloy E, Weynants M, Bielders C, Vanclooster M, Javaux M 2010 How efficient are one-dimensional models to reproduce the hydrodynamic behavior of structured soils subjected to multi-step outflow experiments? Journal of Hydrology 393: 37-52.

Lancashire PD, Bleiholder H, Boom TVD, Langelüddeke P, Stauss R, Weber E, Witzenberger A 1991 A uniform decimal code for growth stages of crops and weeds. Annals of Applied Biology 119: 561-601.

Landl M, Huber K, Schnepf A, Vanderborght J, Javaux M, Bengough AG, Vereecken H 2017 A new model for root growth in soil with macropores. Plant and Soil 415: 99-116.

Landl M, Schnepf A, Vanderborght J, Bengough AG, Bauke SL, Lobet G, Bol R, Vereecken H 2018 Measuring root system traits of wheat in 2D images to parameterize 3D root architecture models. Plant and Soil 425: 457-477.

Landl, M, Schnepf A, Uteau D, Peth S, Athmann M, Kautz T, Perkons U, Vereecken H, Vanderborght J 2019 Modeling the Impact of Biopores on Root Growth and Root Water Uptake. Vadose Zone J. 18:180196. doi:10.2136/vzj2018.11.0196

Le Bot J, Serra V, Fabre J, Draye X, Adamowicz S, Pagès L 2010 DART: a software to analyse root system architecture and development from captured images. Plant and Soil 326: 261-273.

Le Marié C, Kirchgessner N, Marschall D, Walter A, Hund A 2014 Rhizoslides: paper-based growth system for non-destructive, high throughput phenotyping of root development by means of image analysis. Plant Methods 10: 1746-4811.

Leitner D, Felderer B, Vontobel P, Schnepf A 2014 Recovering root system traits using image analysis exemplified by two-dimensional neutron radiography images of lupine. Plant Physiology 164: 24-35.

Leitner D, Klepsch S, Bodner G, Schnepf A 2010a A dynamic root system growth model based on L-Systems. Plant and Soil 332: 177-192.

Leitner D, Schnepf A, Klepsch S, Roose T 2010b Comparison of nutrient uptake between three-dimensional simulation and an averaged root system model. Plant Biosystems 144: 443-447.

Leue M, Gerke HH 2016 Roughness of biopores and cracks in Bt-horizons assessed by confocal laser scanning microscopy. Journal of Plant Nutrition and Soil Science 179: 529-536.

Liang J, Zhang J, Wong M 1996 Effects of air-filled soil porosity and aeration on the initiation and growth of secondary roots of maize (Zea mays). Plant and Soil 186: 245-254.

Loague K, Green RE 1991 Statistical and graphical methods for evaluating solute transport models: Overview and application. Journal of Contaminant Hydrology 7: 51-73.

Lobet G, Couvreur V, Meunier F, Javaux M, Draye X 2014 Plant Water Uptake in Drying Soils. Plant Physiology 164: 1619-1627.

Luo L, Lin H, Halleck P 2008 Quantifying Soil Structure and Preferential Flow in Intact Soil Using X-ray Computed Tomography. Soil Science Society of America Journal 72: 1058-1069.

Lust M 2001 Quaternionen- mathematischer Hintergrund und ihre Interpretation als Rotationen. In: U Koblenz-Landau (ed).

Lynch J 1995 Root architecture and plant productivity. Plant physiology 109: 7-13.

Lynch JP 2007 Roots of the second green revolution. Australian Journal of Botany 55: 493-512.

Lynch JP 2013 Steep, cheap and deep: an ideotype to optimize water and N acquisition by maize root systems. Annals of botany 112: 347-357.

Lynch JP, Nielsen KL, Davis RD, Jablokow AG 1997 SimRoot: modelling and visualization of root systems. Plant and Soil 188: 139-151.

Mairhofer S, Zappala S, Tracy SR, Sturrock C, Bennett M, Mooney SJ, Pridmore T 2012 RooTrak: automated recovery of three-dimensional plant root architecture in soil from X-ray microcomputed tomography images using visual tracking. Plant Physiology 158: 561-569.

Malamy J 2005 Intrinsic and environmental response pathways that regulate root system architecture. Plant, cell & environment 28: 67-77.

Manschadi AM, Hammer GL, Christopher JT, P. d 2008 Genotypic variation in seedling root architectural traits and implications for drought adaptation in wheat (Triticum aestivum L.). Plant Soil 303: 115-129.

Materechera S, Dexter A, Alston A 1991 Penetration of very strong soils by seedling roots of different plant species. Plant and Soil 135: 31-34.

McKenzie B, Bengough A, Hallett P, Thomas W, Forster B, McNicol J 2009 Deep rooting and drought screening of cereal crops: A novel field-based method and its application. Field crops research 112: 165-171.

Meunier F, Javaux M, Couvreur V, Draye X, Vanderborght J 2016 A new model for optimizing the water acquisition of root hydraulic architectures over full crop cycles. Functional-Structural Plant Growth Modeling, Simulation, Visualization and Applications (FSPMA), International Conference on. IEEE.

Meunier F, Rothfuss Y, Bariac T, Biron P, Richard P, Durand J-L, Couvreur V, Vanderborght J, Javaux M 2017 Measuring and modeling hydraulic lift of Lolium multiflorum using stable water isotopes. Vadose Zone Journal, doi: 10.2136/vzj2016.12.0134.

Meunier F, Zarebanadkouki M, Ahmed MA, Carminati A, Couvreur V, Javaux M 2018 Hydraulic conductivity of soil-grown lupine and maize unbranched roots and maize root-shoot junctions. Journal of Plant Physiology, doi: 10.1016/j.jplph.2017.12.019.

Mo X, Liu S 2001 Simulating evapotranspiration and photosynthesis of winter wheat over the growing season. Agricultural and Forest Meteorology 109: 203-222.

Mooney SJ, Pridmore TP, Helliwell J, Bennett MJ 2012 Developing X-ray computed tomography to non-invasively image 3-D root systems architecture in soil. Plant and soil 352: 1-22.

Mualem Y 1976 A new model for predicting the hydraulic conductivity of unsaturated porous media. Water resources research 12: 513-522.

Nagel K, Putz A, Gilmer F, Heinz K, Fischbach A, Pfeifer J, Faget M, Bloßfeld S, Ernst M, Dimaki C, Kastenholz B, Kleinert A, Galinski A, Scharr H, Fiorani F, Schurr U 2012 GROWSCREEN-Rhizo is a novel phenotyping robot enablign simultaneous measruements of root and shoot growth for pkants grown in soil-filled rhizotrons. Functional Plant Biology 39: 891-904.

Nagel KA, Bonnett D, Furbank R, Walter A, Schurr U, Watt M 2015 Simultaneous effects of leaf irradiance and soil moisture on growth and root system architecture of novel wheat genotypes: implications for phenotyping. J Exp Bot 66: 5441-5452.

Nakamoto T 1994 Plagiogravitropism of maize roots. Plant and Soil 165: 327-332.

Nakamoto T 2000 The Distribution of Wheat and Maize Roots as Influenced by Biopores in a Subsoil of the Kanto Loam Type. Plant Production Science 3: 140-144.

Naveed M, Moldrup P, Schaap MG, Tuller M, Kulkarni R, Vogel H-J, de Jonge LW 2016 Prediction of biopore-and matrix-dominated flow from X-ray CT-derived macropore network characteristics. Hydrology and Earth System Sciences 20: 4017-4030.

Nielsen D, Biggar J 1986 Water flow and solute transport processes in the unsaturated zone. Water resources research 22: 89S-108S.

Nielsen MH, Styczen M, Ernstsen V, Petersen CT, Hansen S 2010 Field Study of Preferential Flow Pathways in and between Drain Trenches All rights reserved. No part of this periodical may be reproduced or transmitted in any form or by any means, electronic or mechanical, including photocopying, recording, or any information storage and retrieval system, without permission in writing from the publisher. Vadose Zone Journal 9: 1073-1079.

Nye PH, Tinker PB 1977 Solute movement in the soil-root system. Univ of California Press.

Pagenkemper SK, Athmann M, Uteau D, Kautz T, Peth S, Horn R 2015 The effect of earthworm activity on soil bioporosity–Investigated with X-ray computed tomography and endoscopy. Soil and Tillage Research 146: 79-88.

Pagenkemper SK, Peth S, Puschmann DU, Horn R 2013 Effects of root-induced biopores on pore space architecture investigated with industrial X-Ray computed tomography. Soil–Water–Root Processes: Advances in Tomography and Imaging, doi: 69-96.

Pagès L 2002 Modeling root system architecture. In: Y Waisel, A Eshel, U Kafkafi (eds) Plant roots - The hidden half. Marcel Dekker Inc., New York.

Pagès L 2011 Links between root developmental traits and foraging performancepce_2371 1749.. 1760. Plant, Cell and Environment 34: 1749-1760.

Pages L, Asseng S, Pellerin S, Diggle A 2000 Modelling root system growth and architecture. Root Methods. Springer.

Pagès L, Bécel C, Boukcim H, Moreau D, Nguyen C, Voisin A-S 2014 Calibration and evaluation of ArchiSimple, a simple model of root system architecture. Ecological Modelling 290: 76-84.

Pages L, Jordan M-O, Picard D 1989 A simulation model of the three-dimensional architecture of the maize root system. Plant and Soil 119: 147-154.

Pagès L, Pellerin S 1994 Evaluation of parameters describing the root system architecture of field grown maize plants (Zea mays L.),II. Plant and Soil 164: 169-176.

Pagès L, Vercambre G, Drouet J-L, Lecompte F, Collet C, Le Bot J 2004 Root Typ: a generic model to depict and analyse the root system architecture. Plant and Soil 258: 103-119.

Passioura JB 2002 'Soil conditions and plant growth'. Plant, Cell & Environment 25: 311-318.

Pellerin S, Pagès L 1994 Evaluation of parameters describing the root system architecture of field grown maize plants (Zea mays L.), I. Plant and Soil 164: 155-167.

Pellerin S, Tabourel F 1995 Length of the apical unbranched zone of maize axile roots: its relationship to root elongation rate. Environmental and Experimental Botany 35: 193-200.

Perkons U, Kautz T, Uteau D, Peth S, Geier V, Thomas K, Lütke Holz K, Athmann M, Pude R, Köpke U 2014 Root-length densities of various annual crops following crops with contrasting root systems. Soil and Tillage Research 137: 50-57.

Peth S, Horn R, Beckmann F, Donath T, Fischer J, Smucker A 2008 Three-dimensional quantification of intra-aggregate pore-space features using synchrotron-radiation-based microtomography. Soil Science Society of America Journal 72: 897-907.

Piñeros MA, Larson BG, Shaff JE, Schneider DJ, Falcão AX, Yuan L, Clark RT, Craft EJ, Davis TW, Pradier PL 2016 Evolving technologies for growing, imaging and analyzing 3D root system architecture of crop plants. Journal of integrative plant biology 58: 230-241.

Ping W, Wang Z-L, Cai R-G, Yong L, Chen X-G, Yin Y-P 2011 Physiological and molecular response of wheat roots to nitrate supply in seedling stage. Agricultural Sciences in China 10: 695-704.

Pitkänen J, Nuutinen V 1997 Distribution and abundance of burrows formed by Lumbricus terrestris L. and Aporrectodea caliginosa Sav. in the soil profile. Soil Biology and Biochemistry 29: 463-467.

Pohlmeier A, Javaux M, Vereecken H, Haber-Pohlmeier S 2013 Magnetic resonance imaging techniques for visualization of root growth and root water uptake processes. Soil–Water–Root Processes: Advances in Tomography and Imaging, doi: 10.2136/sssaspecpub61.c7: 137-156.

Popova L, van Dusschoten D, Nagel KA, Fiorani F, Mazzolai B 2016 Plant root tortuosity: an indicator of root path formation in soil with different composition and density. Annals of Botany 118: 685-698.

Porter JR, Gawith M 1999 Temperatures and the growth and development of wheat: a review. European Journal of Agronomy 10: 23-36.

Postma JA, Dathe A, Lynch JP 2014 The optimal lateral root branching density for maize depends on nitrogen and phosphorus availability. Plant Physiology 166: 590-602.

Postma JA, Kuppe C, Owen MR, Mellor N, Griffiths M, Bennett MJ, Lynch JP, Watt M 2017 OpenSimRoot: widening the scope and application of root architectural models. New Phytologist 215: 1274-1286.

Potocka I, Szymanowska-Pułka J 2018 Morphological responses of plant roots to mechanical stress. Annals of Botany, doi: 10.1093/aob/mcy010: 0305-7364.

Rab M, Haling R, Aarons S, Hannah M, Young I, Gibson D 2014 Evaluation of X-ray computed tomography for quantifying macroporosity of loamy pasture soils. Geoderma 213: 460-470.

Rascher U, Blossfeld S, Fiorani F, Jahnke S, Jansen M, Kuhn AJ, Matsubara S, Märtin LL, Merchant A, Metzner R 2011 Non-invasive approaches for phenotyping of enhanced performance traits in bean. Functional Plant Biology 38: 968-983.

Rich S, Watt M 2013 Soil conditions and cereal root system architecture: review and considerations for linking Darwin and Weaver. J Exp Bot 64: 1193-1208.

Richards L 1931 Capillary conduction of liquids through porous medium. Physics 1: 318-333.

Ritchie JT 1972 Model for predicting evaporation from a row crop with incomplete cover. Water resources research 8: 1204-1213.

Roose T, Fowler A 2004 A model for water uptake by plant roots. Journal of Theoretical Biology 228: 155-171.

Roose T, Schnepf A 2008 Mathematical models of plant–soil interaction. Philosophical Transactions of the Royal Society of London A: Mathematical, Physical and Engineering Sciences 366: 4597-4611.

Rose D 1983 The description of teh growth of root systems. Plant and Soil 75: 405-415.

Rosquete MR, von Wangenheim D, Marhavý P, Barbez E, Stelzer EH, Benková E, Maizel A, Kleine-Vehn J 2013 An auxin transport mechanism restricts positive orthogravitropism in lateral roots. Current biology 23: 817-822.

Roychoudhry S, Del Bianco M, Kieffer M, Kepinski S 2013 Auxin controls gravitropic setpoint angle in higher plant lateral branches. Current Biology 23: 1497-1504.

Sammartino S, Lissy A-S, Bogner C, Van Den Bogaert R, Capowiez Y, Ruy S, Cornu S 2015 Identifying the functional macropore network related to preferential flow in structured soils. Vadose Zone Journal 14.

Schenk M, Barber S 1979 Phosphate uptake by corn as affected by soil characteristics and root morphology. Soil Science Society of America Journal 43: 880-883.

Schlaepfer DR, Bradford JB, Lauenroth WK, Munson SM, Tietjen B, Hall SA, Wilson SD, Duniway MC, Jia G, Pyke DA 2017 Climate change reduces extent of temperate drylands and intensifies drought in deep soils. Nature communications 8: 14196.

Schnepf A, Leitner D, Klepsch S 2012 Modeling Phosphorus Uptake by a Growing and Exuding Root System. Vadose Zone Journal 11.

Schnepf A, Leitner D, Landl M, Lobet G, Mai TH, Morandage S, Sheng C, Zoerner M, Vanderborght J, Vereecken H 2018 CRootBox: A Structural-Functional Modelling Framework For Root Systems. Annals of Botany 121: 1033-1053.

Shipitalo MJ, Nuutinen V, Butt KR 2004 Interaction of earthworm burrows and cracks in a clayey, subsurface-drained, soil. Applied Soil Ecology 26: 209-217.

Shkolnik D, Krieger G, Nuriel R, Fromm H 2016 Hydrotropism: root bending does not require auxin redistribution. Molecular plant 9: 757-759.

Šimůnek J, Van Genuchten MT, Sejna M 2005 The HYDRUS-1D software package for simulating the one-dimensional movement of water, heat, and multiple solutes in variably-saturated media. University of California-Riverside Research Reports 3: 1-240.

Šimůnek J, Van Genuchten MT, Šejna M 2016 Recent Developments and Applications of the HYDRUS Computer Software Packages. Vadose Zone Journal 15: vzj2016.2004.0033-vzj2016.2004.0033.

Sinha RK 2004 Modern plant physiology. CRC Press.

Smith S, De Smet I 2012 Root system architecture: insights from Arabidopsis and cereal crops. Philosophical Transactions of the Royal Society 367: 1441-1452.

Somma F, Clausnitzer V, Hopmans JW 1998 An algorithm for three-dimensional, simultaneous modeling of root growth, transient soil water flow and solute transport and uptake. Plant and Soil 202.

Steudle E 2000 Water uptake by plant roots: an integration of views. Plant and Soil 226: 45-56.

Stewart J, Moran C, Wood J 1999 Macropore sheath: quantification of plant root and soil macropore association. Plant and Soil 211: 59-67.

Stingaciu L, Schulz H, Pohlmeier A, Behnke S, Zilken H, Javaux M, Vereecken H 2013 In situ root system architecture extraction from magnetic resonance imaging for water uptake modeling. Vadose zone journal 12.

Stirzaker R, Passioura J, Wilms Y 1996 Soil structure and plant growth: Impact of bulk density and biopores. Plant and soil 185: 151-162.

Tardieu F, Pellerin S 1990 Trajectory of the nodal roots of maize in fields with low mechanical constraints. Plant and Soil 124: 39-45.

Taylor HM, Ratliff LF 1969 Root elongation rates of cotton and peanuts as a function of soil strength and soil water content. Soil Science 108: 113-119.

Thiel H 1865 De radicum plantarum quarundam ab agricolis praecipue cultarum directione et extensione. Formis Caroli Georgi.

Topp CN 2016 Hope in change: the role of root plasticity in crop yield stability. Plant physiology 172: 5-6.

Tóth B, Weynants M, Nemes A, Makó A, Bilas G, Tóth G 2015 New generation of hydraulic pedotransfer functions for Europe. European Journal of Soil Science 66: 226-238.

Toyota M, Gilroy S 2013 Gravitropism and mechanical signaling in plants. American journal of botany 100: 111.

Tracy S 2013 The response of root system architecture to soil compaction. Philosophy. Nottingham.

Tracy SR, Black CR, Roberts JA, Dodd IC, Mooney SJ 2015 Using X-ray computed tomography to explore the role of abscisic acid in moderating the impact of soil compaction on root system architecture. Environmental and Experimental Botany 110: 11-18.

Tracy SR, Black CR, Roberts JA, Sturrock C, Mairhofer S, Craigon J, Mooney SJ 2012 Quantifying the impact of soil compaction on root system architecture in tomato (Solanum lycopersicum) by X-ray micro-computed tomography. Annals of Botany 110: 511-519.

Tracy SR, Roberts JA, Black CR, McNeill A, Davidson R, Mooney SJ 2010 The X-factor: visualizing undisturbed root architecture in soils using X-ray computed tomography. J Exp Bot 61: 311-313.

Tricot F, Crozat Y, Pellerin S 1997 Root system growth and nodule establishment on pea (Pisum sativum L.). J Exp Bot 48: 1935-1941.

Tsutsumi D, Kosugi K, Mizuyama T 2003 Root-system development and water-extraction model considering hydrotropism. Soil Science Society of America Journal 67: 387-401.

Valentine T, Hallet P, Binnie K, Young M, Squire G, Bengough G 2012 Soil strength and macropore volume limit root elongation rates in many UK agricultural soils. Annals of Botany 110: 259-270.

Van Genuchten MT 1980 A closed-form equation for predicting the hydraulic conductivity of unsaturated soils. Soil science society of America journal 44: 892-898.

Van Keulen H, Seligman N 1987 Simulation of water use, nitrogen nutrition and growth of a spring wheat crop, Pudoc, Wageningen.

Van Laar H, Goudriaan J, Van Keulen H 1992 Simulation of crop growth for potential and water-limited production situations: as applied to spring wheat. CABO-DLO.

Vereecken H, Schnepf A, Hopmans JW, Javaux M, Or D, Roose T, Vanderborght J, Young M, Amelung W, Aitkenhead M, Allison SD, Assouline S, Baveye P, Berli M, Brüggemann N, Finke P, Flury M, Gaiser T, Govers G, Ghezzehei T, Hallett PD, Hendricks Franssen HJ, Heppel J, Horn R, Huisman J, Jacques D, Jonard F, Kollet S, Lafolie F, Lamorski K, Leitner D, Mc Bratney A, Minasny B, Montzka C, Nowak W, Pachepsky Y, Padarian J, Romano N, Roth K, Rothfuss Y, Rowe E, Schwen A, Simunek J, Tiktak A, Van Dam J, van der Zee S, Vogel H, Vrugt J, Wöhling T, Young I 2016 Modeling Soil Processes: Review, Key Challenges, and New Perspectives. Vadose Zone Journal 15.

Volder A, Smart DR, Bloom AJ, Eissenstat DM 2005 Rapid decline in nitrate uptake and respiration with age in fine lateral roots of grape: implications for root efficiency and competitive effectiveness. New Phytologist 165: 493-502.

Waisel Y, Eshel A, Beeckman T, Kafkafi U 2002 Plant roots: the hidden half. CRC Press.

Wang E, Smith CJ 2004 Modelling the growth and water uptake function of plant root systems: a review. Australian journal of agricultural research 55: 501-523.

Wasson AP, Richards RA, Chatrath R, Misra SC, Prasad SVS, Rebetzke GJ, Kirkegaard JA, Christopher J, Watt M 2012 Traits and selection strategies to improve root systems and water uptake in water-limited wheat crops. J Exp Bot 63: 3485-3498.

Watt M, Silk W, Passioura J 2006 Rates of root and organism growth, soil conditions, and temporal and spatial developement of the Rhizosphere. Annals of Botany 97: 839-855.

Weaver JE, Jean FC, Crist JW 1922 Development and activities of roots of crop plants: a study in crop ecology. Carnegie Institution of Washington, United States.

Weaver JE, Kramer J, Reed M 1924 Development of Root and Shoot of Winter Wheat Under Field Environment. Ecology 5: 26-50.

Wenzel WW, Wieshammer G, Fitz WJ, Puschenreiter M 2001 Novel rhizobox design to assess rhizosphere characteristics at high spatial resolution. Plant and Soil 237: 37-45.

Whalley W, To J, Kay B, Whitmore A 2007 Prediction of the penetrometer resistance of soils with models with few parameters Geoderma 137: 370-377.

White R, Kirkegaard J 2010 The distribution and abundance of wheat roots in a dense, structured subsoil - implications for water uptake. Plant Cell Environ 33: 133-148.

Wiekenkamp I, Huisman J, Bogena H, Lin H, Vereecken H 2016 Spatial and temporal occurrence of preferential flow in a forested headwater catchment. Journal of hydrology 534: 139-149.

Wu J, Pagès L, Wu Q, Yang B, Guo Y 2015 Three-dimensional architecture of axile roots of field-grown maize. Plant and soil 387: 363-377.

Wu L, McGechan M, McRoberts N, Baddeley J, Watson C 2007 SPACSYS: integration of a 3D root architecture component to carbon, nitrogen and water cycling—model description. Ecological Modelling 200: 343-359.

Young I 1998 Biophysical interactions at the root–soil interface: a review. The Journal of Agricultural Science 130: 1-7.

Yu P, Gutjahr C, Li C, Hochholdinger F 2016 Genetic control of lateral root formation in cereals. Trends in plant science 21: 951-961.

Zobel R, Waisel Y 2010 A plant root system architectural taxonomy: a framework for root nomenclature. Plant Biosystems 144: 507-512.

List of Figures

List of Tables